The Use of Mechanical Foaming for Development of Bioinks and Bioprinting Techniques

by

Elias MADADIAN

MANUSCRIPT-BASED THESIS PRESENTED TO ÉCOLE DE TECHNOLOGIE SUPÉRIEURE IN PARTIAL FULFILLMENT FOR A MASTER'S DEGREE WITH THESIS IN MECHANICAL ENGINEERING
M.A.Sc.

MONTREAL, AUGUST 17, 2023

ÉCOLE DE TECHNOLOGIE SUPÉRIEURE
UNIVERSITÉ DU QUÉBEC

BOARD OF EXAMINERS

THIS THESIS HAS BEEN EVALUATED

BY THE FOLLOWING BOARD OF EXAMINERS

Mr. Ali Ahmadi, Thesis Supervisor
Department of Mechanical Engineering, École de technologie supérieure

Mr. Ricardo Zednik, President of the Board of Examiners
Department of Mechanical Engineering, École de technologie supérieure

Ms. Elmira Moosavi, Member of the jury
Department of Mechanical Engineering, École de technologie supérieure

THIS THESIS WAS PRENSENTED AND DEFENDED

IN THE PRESENCE OF A BOARD OF EXAMINERS AND PUBLIC

AUGUST 16, 2023

AT ÉCOLE DE TECHNOLOGIE SUPÉRIEURE

DEDICATION

To my mother and my sister,
for everything they have done to help me get where I am today.

ACKNOWLEDGMENTS

First and foremost, I want to begin by expressing my utmost appreciation to my supervisor, Dr. Ali Ahmadi, for his guidance, encouragement, and support during my graduate studies and research journey. Your distinctive mentorship allowed me to pursue my interests and research goals with more flexibility. It significantly influenced my research and personal life and has been crucial in enabling me to attain my objectives.

My heartfelt gratitude goes out to my collaborators and lab mates at the Atlantic biofabrication lab and biomaterials and biofabrication lab for their constant support and encouragement throughout my master's degree program. Their assistance provided a supportive and friendly environment that helped me navigate the many challenges I faced, particularly being far from my home country. I want to specifically thank Sara Badr and Sydney Wheatley. Without their support, I would not have been able to overcome the obstacles that I encountered during my journey.

Finally, I would like to thank my mother, Robabeh, and my sister, Marzieh, for their boundless love and support. Their encouragement and belief in my abilities have been an endless source of motivation, and I am deeply grateful for their presence in my life.

L'utilisation de la mousse mécanique pour le développement de bioinks et de techniques de bio-impression

Elias MADADIAN

RÉSUMÉ

La bio-impression tridimensionnelle est un sous-ensemble unique de la fabrication additive dans lequel le dépôt précis de bioink donne lieu à des structures 3D complexes composées de cellules vivantes intégrées dans des hydrogels. Pour les applications biologiques, les structures bio-imprimées en 3D doivent présenter un degré élevé de porosité afin favoriser la croissance et la fonction cellulaires. Cependant, la faible porosité intrinsèque des bioinks ne permet pas toujours de créer un environnement idéal pour les cellules. En outre, de nombreux hydrogels biocompatibles n'ont pas les propriétés mécaniques et rhéologiques suffisantes pour la bio-impression 3D. Lorsque ces propriétés ne répondent pas aux exigences d'imprimabilité, la bio-impression échoue en raison d'une mauvaise fidélité de la forme et d'autres complications. C'est pourquoi il est nécessaire d'accorder plus d'attention à la mise au point de méthodes permettant de remédier aux limitations susmentionnées.

Ce mémoire porte sur le développement de méthodes basées sur la mousse pour la bio-impression 3D de structures supermacroporeuses, ainsi que sur la bio-impression 3D d'hydrogels à faible viscosité/réticulation lente. L'albumine, un agent moussant bien connu, est utilisée pour produire des bioinks hybrides hautement poreux et imprimables en 3D. En outre, la mousse d'albumine est utilisée comme matériau sacrificiel pour fabriquer des fibres creuses, et est également utilisée comme matériau de support à base de mousse dans la bio-impression intégrée comme alternative aux bains de support à base de gel.

Pour l'étude d'un bioink poreux imprimable en 3D, des solutions hybrides d'albumine et d'alginate avec différentes concentrations d'albumine et d'alginate de sodium sont préparées et mélangées mécaniquement. La mousse obtenue est imprimée en 3D et réticulée avec une solution ou une brume de chlorure de calcium. Les échafaudages fabriqués sont caractérisés par l'analyse de l'imprimabilité, des propriétés mécaniques, de la porosité, de l'absorption d'eau, de la dégradation et des tests de libération de médicaments. Ces études indiquent que les échafaudages réticulés par la brume présentent des propriétés mécaniques supérieures et offrent des profils de libération de médicaments relativement plus longs.

Pour l'étude sur la bio-impression de fibres creuses, un matériau sacrificiel à base de mousse est développé pour être utilisé comme flux central. Cette méthode implique l'incorporation de l'agent de réticulation (chlorure de calcium) dans une mousse d'albumine. Les effets des débits de mousse et d'alginate sur le diamètre des fibres et l'épaisseur des parois sont étudiés. La

résolution d'impression est quantifiée en déterminant l'indice d'imprimabilité. Les propriétés mécaniques sont évaluées en analysant la déformation à la rupture et l'effondrement du filament. En outre, la viabilité des cellules Neuro-2a co-incubées avec les structures imprimées est examinée et ne montre aucun impact négatif sur la viabilité des cellules.

Pour l'étude de la bio-impression intégrée, une mousse d'albumine enrichie de milieu de culture cellulaire est utilisée comme bain de support pour bio-imprimer des structures complexes avec des hydrogels à faible viscosité et à réticulation lente. Les conditions optimales du bain à base de mousse sont déterminées en testant différentes concentrations d'albumine et différents temps de moussage. Un avantage unique de l'utilisation de bains de support à base de mousse dans la bio-impression intégrée est la coalescence des bulles au fil du temps, ce qui conduit à la formation d'un bain de support sacrificiel. L'utilisation de la mousse comme matériau de support présente d'autres avantages, notamment un meilleur accès à l'oxygène gazeux environnant, ainsi qu'un accès immédiat aux nutriments présents dans la mousse. Un hydrogel thermosensible à base de chitosane de diverses structures complexes a été bio-imprimé avec succès en utilisant le matériau de support à base de mousse. En outre, la biocompatibilité du processus est démontrée en déterminant la viabilité cellulaire des fibroblastes L929 incorporés dans un bioink de chitosane-collagène après 7 jours de culture.

Les méthodes à base de mousse développées dans ce mémoire exploitent les avantages des techniques de bio-impression, tout en permettant l'impression 3D directe de structures très poreuses, ainsi que d'hydrogels à faible viscosité et à réticulation lente. L'utilisation de matériaux de support innovants à base de mousse s'avère être une excellente alternative aux matériaux de support conventionnels dans les systèmes de bio-impression coaxiale et de bio-impression intégrée pour les applications d'ingénierie tissulaire.

Mots-clés: Bio-impression 3D, bio-impression intégrée, bio-impression coaxiale, alginate de sodium, albumine

The use of mechanical foaming for development of bioinks and bioprinting techniques

Elias MADADIAN

ABSTRACT

Three-dimensional bioprinting is a unique subset of additive manufacturing in which the precise deposition of bioink gives yield to complex 3D structures made up of living cells embedded within hydrogels. For biological applications, 3D bioprinted structures are required to have a high degree of porosity to promote cellular growth and function. However, the low intrinsic porosity of bioinks often falls short in providing an ideal environment for cells. Moreover, many biocompatible hydrogels lack sufficient mechanical and rheological properties for 3D bioprinting. When these properties do not meet the requirements for printability, bioprinting fails due to poor shape fidelity and other complications. Therefore, further attention is required to develop methods to address the aforementioned limitations.

This thesis addresses the development of foam-based methods for the 3D bioprinting of supermacroporous structures, as well as the 3D bioprinting of low-viscosity/slow-crosslinking hydrogels. Albumin, a well-known foaming agent, is used to produce highly porous and 3D-printable hybrid bioinks. Moreover, albumin foam is utilized as a sacrificial material to fabricate hollow fibers, and also is used as a foam-based support material in embedded bioprinting as an alternative to gel-based support baths.

For the investigation of a porous 3D-printable bioink, hybrid albumin-alginate solutions with various concentrations of albumin and sodium alginate are prepared and mechanically mixed. The resulting foam is 3D printed and crosslinked with a calcium chloride solution or mist. The fabricated scaffolds are characterized through the analysis of the printability, mechanical properties, porosity, water absorption, degradation, and drug release tests. These studies indicate that the mist-crosslinked scaffolds show superior mechanical properties and provide relatively longer drug release profiles.

For the hollow fiber bioprinting study, a foam-based sacrificial material is developed to be used as a core flow. This method involves the incorporation of the crosslinker (calcium chloride) into an albumin foam. The effects of foam and alginate flow rates on fiber diameter and wall thickness are investigated. Printing resolution is quantified by determining the printability number. Mechanical properties are assessed by analyzing breaking strain and filament collapse. Moreover, the viability of Neuro-2a cells co-incubated with the printed structures are examined, showing no detrimental impact on cell viability.

For the embedded bioprinting study, albumin foam enriched with cell culture media are used as a support bath to bioprint complex structures with low-viscosity/slow-crosslinking hydrogels. The optimal conditions of the foam-based bath are determined by testing different albumin concentrations and foaming times. A unique benefit of utilizing foam-based support

baths in embedded bioprinting is the coalescence of bubbles over time, which leads to the formation of a sacrificial support bath. Additional benefits of utilizing foam as the supporting material include the enhanced access to surrounding gaseous oxygen, as well as immediate access to nutrients in the foam. A chitosan-based thermosensitive hydrogel of various complex structures are successfully bioprinted using the foam-based support material. Furthermore, the biocompatibility of the process is demonstrated by determining the cell viability over 7 days of L929 fibroblasts incorporated into a chitosan-collagen bioink.

The developed foam-based methods in this thesis leverage the advantages of the bioprinting techniques, while allowing direct 3D printing of highly porous structures, as well as low-viscosity/slow-crosslinking hydrogels. The use of innovative foam-based support materials is proved to be an excellent alternative to conventional support materials in coaxial bioprinting and embedded bioprinting systems for tissue engineering applications.

Keywords: 3D bioprinting, Embedded bioprinting, Coaxial bioprinting, Sodium Alginate, Albumin

PREFACE

This thesis is based on the research conducted in the Atlantic Biofabrication Lab at the University of Prince Edward Island, as well as the Biomaterials and BioFabrication Lab (BBF) at the University of Montreal Hospital Research Centre (CRCHUM) and École de technologie supérieure (ÉTS).

The contents of this thesis are under consideration for publication or have already been published in scientific journals. Chapter 2, development of 3D- printable albumin-alginate foam for wound dressing applications, is published in *3D Printing and Additive Manufacturing.* Emad Naseri assisted in performing drug release and mechanical properties tests, analyzing the data, and writing the manuscript. Ryan Legault assisted in freeze-drying the samples for SEM imaging. Chapter 3, development of foam-based support material for coaxial bioprinting of ionically crosslinking bioinks, is published in *Bioprinting.* Sara Badr assisted in performing mechanical properties, diameter and wall thickness control, and cell viability tests. She also analyzed the mechanical and wall diameter and thickness results, and drafted the cell viability section of the manuscript. Debra MacDonald and Andrew Tasker assisted with cell viability tests. Chapter 4, in-foam bioprinting: an embedded bioprinting technique with self-removeable support bath, is submitted for publication in *Advanced functional materials.* Hossein Ravanbakhsh is a co-first author on this paper. He assisted in performing all the tests, analyzing the data, and writing the manuscript. Francesco Touani Kameni assisted in performing the cell viability tests. Maedeh Rahimnejad designed the methodology for rheology tests and assisted in conducting the rheology tests. Following are lists of journal articles and conference proceedings published/submitted during the author's M.A.Sc. studies in chronological order.

Peer-reviewed journal articles

1. Badr, S., MacCallum, B., **Madadian, E.**, Kerr, G., Naseri, E., MacDonald, D., Tasker, R.A., & Ahmadi, A. (2022). Development of a mist-based printhead for droplet-based bioprinting of ionically crosslinking hydrogel bioinks. *Bioprinting*, 27, e00207.
   Contributions: E. Madadian conducted the droplet impact tests and analysis.
2. Wheatley, S. K., Cartmell, C., **Madadian, E.**, Badr, S., Haltli, B.A., Kerr, R.G., & Ahmadi, A. (2022). Microfabrication of a micron-scale microbial-domestication pod for in situ cultivation of marine bacteria. *RSC advances*, 12(43), 28123-28127.
   Contributions: E. Madadian conducted the finite element analysis.
3. **Madadian, E.**, Naseri, E., Legault, R., & Ahmadi, A. (2022). Development of 3D-Printable Albumin–Alginate Foam for Wound Dressing Applications. *3D Printing and Additive Manufacturing* (in-press), http://doi.org/10.1089/3dp.2022.0241.
4. **Madadian, E.**, Badr, S., MacDonald, D., Tasker, R.A. & Ahmadi, A. (2023). Development of a foam-based method for coaxial bioprinting of ionically crosslinking bioinks, *Bioprinting* (in-press), https://doi.org/10.1016/j.bprint.2023.e00281.
5. Badr, S., **Madadian, E.**, Naseri, E., MacDonald, D., Tasker, R.A., & Ahmadi, A. (2023). Development of a mist-based method for coaxial bioprinting of ionically crosslinking hydrogel bioinks, *bioprinting,* (under revision).
   Contributions: E. Madadian assisted in performing the cell viability tests.
6. Legault, R., Naseri, E., **Madadian, E.**, Villareal, G. & Ahmadi, A. (2023). Development of a Biodegradable Soft Bait Fishing Lure", *Fisheries Research*, 264, 106738.
   Contributions: E. Madadian assisted in SEM imaging of samples.
7. Navaei, T., **Madadian, E.**, Haltli, B.A., Cartmell, C., Kerr, R.G., & Ahmadi, A., (2023) Investigation of the impact of bacterial microencapsulation on natural product discovery, *Current Research in Biotechnology,* (under revision).
   Contributions: E. Madadian assisted in designing microbead fabrication methods.
8. **Madadian, E.**, Ravanbakhsh, H., Kameni, F.T., Rahimnejad, M., Lerouge, S., & Ahmadi, A., (2023) In-Foam Bioprinting: an Embedded Bioprinting Technique with Self-removeable Support Bath, *Advanced functional materials*, (submitted).

Conference presentations and proceedings

1. **Madadian, E.**, Badr, S., & Ahmadi, A. Investigation of impact dynamics of ionically crosslinking hydrogel droplets in mist-based 3D bioprinting applications. Proceedings of the Canadian Society for Mechanical Engineering International Congress (CSME 2021), Prince Edward Island, Canada. Abstract and oral presentation.
2. Badr, S., MacCallum, B., **Madadian, E.**, Naseri, E., MacDonald, Bodaghkhani, A., D., Tasker, R.A., & Ahmadi, A. Development of a mist-based printhead technology for extrusion-based, droplet-based and coaxial bioprinting, International Conference on Biofabrication (2021), Australia. Abstract and poster presentation.
3. **Madadian, E.**, Badr, S., MacDonald, D., Tasker, R.A., & Ahmadi, A. Development of a foam-based method for coaxial bioprinting of ionically crosslinking bioinks. International Conference on Biofabrication (2022), Pisa, Italy. Abstract and oral presentation.
4. Badr, S., **Madadian, E.**, MacCallum, B., Naseri, E., MacDonald, D., Tasker, R.A., & Ahmadi, A. Development of a mist-based printhead technology for extrusion-based, droplet-based and coaxial bioprinting, The 26th International Conference on Miniaturized systems for Chemistry and Life Sciences (MicroTAS 2022), Hanghzhou, China. Abstract and oral presentation.
5. **Madadian, E.,** Ravanbakhsh, H., Kameni, T.F., Rahimnejad, M., Lerouge, S., & Ahmadi, A. Development of an In-foam Embedded Bioprinting Method for Low-Viscosity Slow-Crosslinking Hydrogels, The 38th Canadian Biomaterials Society Annual Meeting (CBS 2023), Halifax, Canada. Abstract and oral presentation.

6. **Madadian, E.,** Ravanbakhsh, H., Kameni, F.T., Rahimnejad, M., Lerouge, S., & Ahmadi, A., International Conference on Biofabrication (2023), Development of a foam-based support bath for embedded bioprinting of bioinks, Saskatoon, Canada. Abstract and oral presentation.

TABLE OF CONTENTS

page

LIST OF TABLES

Page

LIST OF FIGURES

Page

LIST OF ABREVIATIONS

3D	three-dimensional
ANOVA	analysis of variance
DAPI	4’6-diamidino-2-phenylindole dihydrochloride
PI	propidium iodide
EBB	extrusion-based bioprinting
DMEM	Dulbecco’s Modified Eagle Medium
ECM	extracellular matrix
FBS	fetal bovine serum
PBS	phosphate-buffered saline
Pr	Printability number
SEM	scanning electron microscopy
SR	swelling ratio
TE	tissue engineering
UV	ultraviolet
PVA	poly(vinyl alcohol)
GelMA	Gelatin methacryloyl
PCL	polycaprolactone
PLGA	Polylactic-co-glycolic acid
CAD	computer-aided design
SA	sodium alginate
AL	albumin

LIST OF SYMBOLS AND UNITS OF MEASURE

µm	micrometer
mL	millilitre
cm	centimeter
°C	degree Celsius
kV	kilovolt
Å	angstrom
G	gauge
kPa	kilopascal
h	hour
ml/h	millilitre per hour
A	area
min	minute
mm	millimeter
mm/s	millilitre per second
Cm/s	centimeter per second
λ	wavelength (Lambda)
nm	nanometer
м	molar

INTRODUCTION

The field of tissue engineering aims to overcome one of the main challenges associated with traditional treatment methods, namely the limited availability of organs for transplantation, through the development and fabrication of implantable functional tissues. Among various fabrication techniques, three-dimensional (3D) bioprinting holds great promise as it is compatible with a wide range of biomaterials and offers precise control over the 3D deposition of the biomaterials. The printed structure serves as a framework to provide mechanical support and facilitate the growth of cells to form a tissue. Hydrogels, networks of crosslinked polymers, are widely used as biomaterials in tissue engineering due to their desirable properties, such as biocompatibility and high water absorption(Ullah, Othman, Javed, Ahmad, & Akil, 2015 ; Xu et al., 2022).

Hydrogels can be made from natural or synthetic polymers and can mimic biological tissues(Silva, Richard, Bessodes, Scherman, & Merten, 2009). Naturally derived hydrogels are inherently biocompatible and resemble extracellular matrix, which provides a biomimetic environment to supports cellular functions, including cell adhesion, migration, and proliferation(Lin & Metters, 2006). Synthetic hydrogels offer tunable mechanical properties, chemical versatility, and long-term stability but often have cytotoxic properties and limited biocompatibility(Madduma-Bandarage & Madihally, 2021). In order to mimic the biological tissues, hydrogels are desired to have a porous structure which is essential for cell growth and nutrient transportation(Bao et al., 2020). Moreover, they should exhibit proper mechanical and rheological properties to be 3D bioprinted(Askari et al., 2021). However, the intrinsic porosity of bioinks is usually not suitable for cell growth as small pore size can limit the cellular activities(Bao et al., 2020). Moreover, many biocompatible hydrogels lack the required mechanical and rheological properties, such as viscosity and gelation pace, for 3D bioprinting(Askari et al., 2021). Therefore, it is required to develop a method to fabricate porous structures and address issues with the bioprinting of low-viscosity/slow-crosslinking hydrogels.

The present thesis consists of four chapters. Chapter 1 articulates the motivations for studying the general problems that are the focus of this thesis and presents the specific objectives. The literature survey is divided into three sections providing a brief literature review for each of the three specific objectives. The literature review of objective one provides information on the importance of 3D printing of porous structures and reviews the current methods of fabricating porous constructs. The literature review of objective two reviews the various methods of fabricating hollow fibers and discusses the limitations of the current methods. The literature review of objective three focuses on 3D bioprinting of low-viscosity/slow-crosslinking hydrogels and reviews the advantages and disadvantages of embedded bioprinting. Each of the literature review sections also discusses the hypothesis to tackle the corresponding research objective.

Chapters 2, 3, and 4 present the three articles published/submitted during this M.A.Sc relating to the research objectives. Chapter 2 (the first article) reports the development of 3D-printable albumin-alginate foam for fabricating highly porous structures. The developed foam can be crosslinked with either calcium chloride solution or mist, and does not require additional post-processing steps, such as freeze-drying. The printed structures are characterized through printability, porosity, mechanical properties, and drug release properties. This article highlights the superiority of the developed method for wound dressing applications.

Chapter 3 (the second article) reports the development of foam-based support material for coaxial bioprinting of ionically crosslinking bioinks. In this chapter, albumin foam was utilized as a sacrificial material to provide temporary support for the hollow fiber while supplying calcium ions to the hydrogel for crosslinking.

Chapter 4 (the third article) reports the use of albumin foam as support material for embedded bioprinting. This work discusses the limitations of gel-based support baths and introduces

foam-based support baths as an alternative support material to address the issues associated with conventional support materials.

CHAPTER 1

LITERATURE REVIEW

1.1 Motivations

Three dimensional (3D) bioprinting is the sequential deposition of bioinks on a printbed in a layer-by-layer manner according to a digital model(Karvinen & Kellomäki, 2023 ; Ravanbakhsh, Bao, Luo, Mongeau, & Zhang, 2021). Depending on the bioink properties and the intended application, the process of deposition can be done through various techniques(Dey & Ozbolat, 2020 ; Unagolla & Jayasuriya, 2020). Figure 1.1a shows a schematic overview of the main 3D bioprinting techniques that can be categorized into nozzle-based and laser/light-based techniques(Hospodiuk, Dey, Sosnoski, & Ozbolat, 2017). Among the various modalities of 3D bioprinting, extrusion-based bioprinting (EBB) provides an affordable and versatile approach to fabricate complex structures with a wide range of bioinks(Y. S. Zhang et al., 2021). Depending on the characteristics of the bioink, gelation can be achieved through various methods, such as thermal, ionic, and photo crosslinking(Ashammakhi et al., 2019). Thermally crosslinking polymers (e.g., gelatin) undergo the gelation process when they reach the sol-gel transition temperature thus negating the need for additional reagents or equipment(Tanga, Aucamp, & Ramburrun, 2023). However, disadvantages such as poor mechanical properties and deficient degradation limit their applications(Han, Meng, Wu, Wu, & Qi, 2018 ; Tanga et al., 2023). Photo crosslinking hydrogels gel under a UV or visible light source and offer mild gelation conditions(Ouyang, Highley, Sun, & Burdick, 2017 ; Rui et al., 2023). However, the biocompatibility of photo crosslinking hydrogels is a concern due to the cytotoxicity of UV light exposure and the generation of free radicals through the photopolymerization reaction(Bryant, Nuttelman, & Anseth, 2012 ; Kushibiki et al., 2021). Ionically crosslinking hydrogels, such as sodium alginate, gel when ionically bonded to ions such as Ca^{2+} and Ba^{2+} (Hu, Lu, Mata, Nishinari, & Fang, 2021). Ionically crosslinking hydrogels offer biocompatibility and a convenient gelation mechanism, which is typically achieved using a liquid crosslinker (Figure 1.1b-c). However, the use of liquid crosslinker creates challenges in precise bioink deposition and can result in poor layer(Raddatz et al., 2018). The limitations of

using liquid crosslinker have been addressed by mist-based bioprinting(Badr et al., 2022 ; MacCallum et al., 2020).

Although many improvements have been made to EBB systems, there are many remaining challenges to overcome. This thesis aims to explore and address the limitations of extrusion-based bioprinting for advancing the tissue engineering field. In particular, the challenges with fabricating porous structures and addressing issues with bioprinting of low-viscosity bioinks.

Porous structures: An important characteristic of 3D bioprinted constructs is to have a controlled and high degree of porosity. Having a porous material is necessary for increasing water retention, nutrient transportation, and cell migration(Bao et al., 2020). Methods of producing porous materials have been developed such as freeze drying(X. Wu, Black, Santacana-Laffitte, & Patrick, 2007) and gas foaming(Kar, Kaur, & Thirugnanam, 2016); however, they are not applicable for 3D bioprinting. Moreover, the intrinsic porosity of bioinks is usually not suitable for cell growth as small pore size can limit the cellular activities(Bao et al., 2020). Therefore, there is a need to develop 3D printable bioinks to fabricate porous scaffolds with tunable average pore size within 10 μm to 100 μm range.

Bioprinting of low-viscosity bioinks: 3D bioprinting systems are limited by the scarcity of printable bioinks(Ravanbakhsh, Bao, et al., 2021) as many biocompatible hydrogels lack sufficient mechanical properties for 3D bioprinting(Askari et al., 2021). To address this limitation, a support bath can be used for bioprinting low-viscosity/slow-crosslinking bioinks to maintain high shape fidelity(Hinton et al., 2015 ; Zhou, Sun, Yang, Mao, & Gu, 2022) (Figure 1.1d), generally referred to as embedded bioprinting. However, the limitations of using support materials include the lack of proper oxygenation and nutrient diffusion to the bioprinted constructs(Carmeliet & Jain, 2000). Moreover, mechanisms to remove the support material can be detrimental to the cells' viability and structural fidelity, especially when lowered temperatures or mechanical agitation is mandatory to remove the support material(Q. Li et al., 2022). Therefore, there is a necessity to develop a support material for bioprinting

low-viscosity/slow-crosslinking bioinks that provides the cells with nutrients and oxygen during the bioprinting and crosslinking periods.

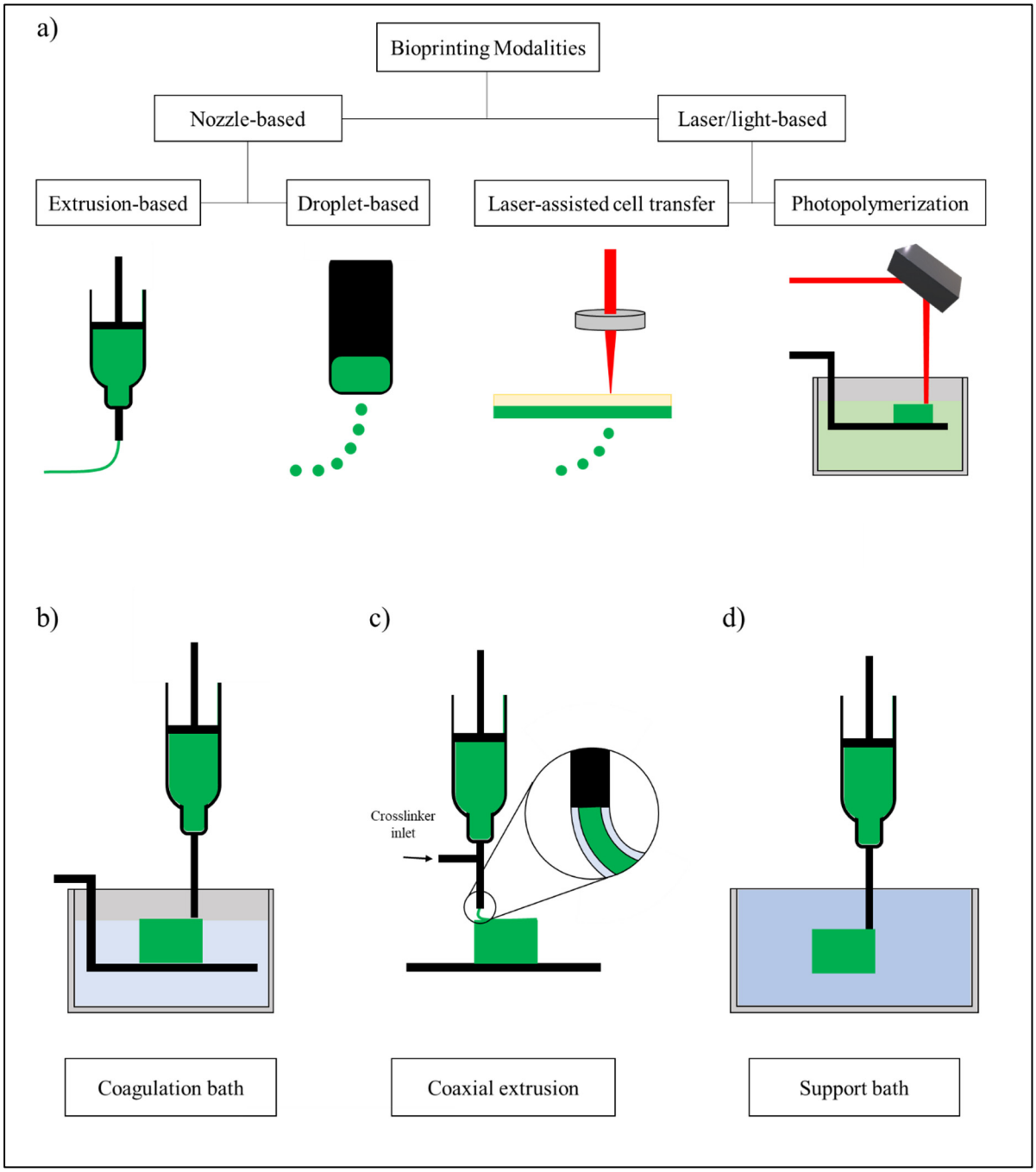

Figure 1.1 a) schematic overview of the main 3D bioprinting modalities and b) different approaches of extrusion based bioprinting systems

1.2 Research objectives

The aim of this thesis is to develop a method to 3D print highly structures as well as a method to 3D bioprint low-viscosity/slow-crosslinking bioinks with high resolution. The specific objectives of this thesis are defined as follows:

Objective 1: Develop a method to fabricate stable supermacroporous structures using highly porous and 3D-printable bioink.

Objective 2: Develop a foam-based method for 3D coaxial bioprinting of ionically crosslinking bioinks to fabricate hollow fibers.

Objective 3: Develop an embedded 3D bioprinting method using foam as support material to bioprint slow-crosslinking and low-viscosity bioinks.

1.3 Objective 1 literature review

3D printing of porous structures has many applications in biomedical engineering, such as tissue engineering(Serafin, Culebras, & Collins, 2023), drug delivery(Gulfam et al., 2023), and wound dressings(Weng et al., 2023). As for tissue engineering, porous scaffolds facilitate cell attachment and cell migration(Bao et al., 2020). Stable and porous biomimetic constructs offer enhanced nutrient transportation and facilitate specific cellular activities, such as cell growth(Oh, Park, Kim, & Lee, 2007). Porous materials are also perfect candidates for controlled drug delivery applications due to an increased surface area and tuneable pore size(Qu et al., 2006). Furthermore, the porosity of 3D printed structures is an important characteristic in wound dressing applications as it offers enhanced permeability for the diffusion of oxygen to the wound area(Cam, Zhu, Truong, Scumpia, & Segura, 2015). Additionally, porous materials keep the wound area moist due to the increased water retention

properties(Z. Lan, Kar, Chwatko, Shoga, & Cosgriff-Hernandez, 2023 ; Y. Li et al., 2019). Depending on the application and desired pore size, there are various methods to fabricate porous materials that can be selected.

One method to prepare porous scaffolds is by freeze drying(X. Wu et al., 2007). In this approach, a porous structure is obtained through the sublimation and elimination of frozen water in the sample at low pressures. The pore size can be controlled by varying factors such as the polymer concentration(Chartier, Buwalda, Van Den Berghe, Nottelet, & Budtova, 2022). The freeze drying approach can also be combined with a high temperature preparation of the polymer solution to achieve thermally induced phase separation(Rusakov, Menner, Spieckermann, Wilhelm, & Bismarck, 2022). Alternatively, solvent casting/particle leaching can be used in which a polymer and salt solution are subjected to air or freeze drying and immersed in water to initiate the diffusion of salt particles, leaving a porous material(Durán-Rey et al., 2022). A gas foaming method can also be used in which the addition of a foaming agent, such as sodium bicarbonate, to a polymer solution results in the polymerization of hydrogel around the generated a gas bubbles inside the solution, producing a porous structure(Serro et al., 2023). Using these methods porous structures can be fabricated using various types of polymers.

One polymer of interest is sodium alginate as it is naturally occurring and can be derived from multiple sources, such as marine algae, and some bacteria(Draget & Taylor, 2011). Alginate is a biocompatible, biodegradable, and widely accessible biomaterial, making it one of the most commonly used ionically crosslinking polymers in the biofabrication field(Chaturvedi et al., 2019 ; Sachan, Pushkar, Jha, & Bhattcharya, 2015). Moreover, alginate is a water-soluble biopolymer that can rapidly crosslink when exposed to various crosslinking agents, such as Ca^{2+}, Ba^{2+}, and Cu^{2+} (Hu et al., 2021), making it an ideal candidate for biomedical applications. Several methods have been used to fabricate porous structures using alginate, such as gas foaming (Barbetta, Barigelli, & Dentini, 2009), solvent casting(Thomas et al., 2020), and freeze drying(Haghbin, Sadeghi-Avalshahr, Hassanzadeh, Moloodi, & Harati, 2023).

However, they are not compatible with 3D printing. Hence, an alternative method of 3D printing of porous alginate scaffolds is required.

Albumin has been widely studied as a foaming agent in the food industry(Hardy & Jideani, 2017) and is a biocompatible, biodegradable, and water-soluble protein(Kratz, 2014). However, the application of albumin foam in biomedical applications is limited as foamed albumin is not stable over time. The addition of sodium alginate to albumin foam can enhance the stability of the foam, while further crosslinking of alginate can improve the mechanical properties of the biomaterial. We hypothesize that 3D printing sodium alginate/albumin foam crosslinked with $CaCl_2$ mist can produce highly porous structures without the need of further post processing (such as freeze drying) to maintain the porosity of the scaffolds.

1.4 Objective 2 literature review

The development of hollow fibers can be applied in various fields, including drug delivery(C. Liu, Wang, Wei, Chen, & Luo, 2021 ; Wang, Liu, Chen, & Luo, 2021), and tissue engineering(Luo, Chen, Zhang, Huang, & Wa, 2022 ; Schöneberg et al., 2018) as they can mimic blood vessels and vascular networks(Devillard & Marquette, 2021 ; G. Gao et al., 2017 ; Q. Gao et al., 2017). Various natural and synthetic hydrogels such as alginate(Q. Gao, He, Fu, Liu, & Ma, 2015), collagen(Shen, Zhang, Wang, & Meng, 2015), agarose(Norotte, Marga, Niklason, & Forgacs, 2009), and Pluronic F-127(Müller, Becher, Schnabelrauch, & Zenobi-Wong, 2015), or a combination of biomaterials, such as Alginate/PVA(Luo, Lode, & Gelinsky, 2013) and alginate/GelMA(Luo et al., 2022), have been employed to fabricate hollow fibers. There are many methods to fabricate hollow fibers, including the embedded bioprinting(Bhattacharjee et al., 2015 ; Hinton et al., 2015 ; Jin, Chai, & Huang, 2017), coaxial extrusion(Cornock, Beirne, Thompson, & Wallace, 2014 ; W. Liu et al., 2018 ; Yeo, Lee, Chun, & Kim, 2016), coaxial electrospinning(Di et al., 2008 ; G. Duan & Greiner, 2019), microfluidic chips(Iijima et al., 2019 ; Nguyen, Tran, & Lee, 2018), and electro spinning(Su et al., 2019 ; Wahyudiono, Machmudah, Kanda, Okubayashi, & Goto, 2014). Moreover, novel

methods have been used to fabricate complex tubular structures, such as extrusion of partially crosslinked bioink on a rotated rod template(Q. Gao et al., 2017). Among all methods of fabricating hollow fibers, coaxial extrusion with three-dimensional bioprinting is most commonly used, as it provides a higher resolution for fabricating complex structures(Kjar, McFarland, Mecham, Harward, & Huang, 2021).

3D bioprinting methods for fabricating hollow fibers typically require a crosslinking mechanism to maintain suitable rheological properties during printing and high shape fidelity of constructs after printing(Q. Gao et al., 2017, 2015 ; Tabriz, Hermida, Leslie, & Shu, 2015). Ionically crosslinking hydrogels are commonly used in 3D bioprinting of hollow fibers as they offer rapid gelation(Fazal et al., 2018 ; Kjar et al., 2021). To create such structures, liquid crosslinkers are introduced to the bioink via a coflow, or as a bath on the printing stage(G. Gao et al., 2019 ; Q. Gao et al., 2015). However, the use of liquid crosslinkers can result in poor layer adhesion and low shape fidelity of printed constructs, due to over-pooling of liquid on the printbed and consequently the over-gelation of the fiber(Ahn, Lee, Bonassar, & Kim, 2012 ; Badr et al., 2022 ; MacCallum et al., 2020 ; Sun & Tan, 2013). Additionally, bioactive compounds incorporated within the bioink may diffuse into the excess liquid crosslinker on the printbed(Boi et al., 2020 ; Huang, Cao, Parakhonskiy, & Skirtach, 2022). Therefore, existing methods of 3D bioprinting hollow fibers require an additional step to remove the liquid crosslinker from both the hollow fiber and the printbed(G. Gao et al., 2017 ; Q. Gao et al., 2017).

In order to overcome the limitations associated with liquid crosslinkers, sacrificial materials are employed as a core flow to provide temporary support for tubular structure of the fibers(G. Gao et al., 2017). The sacrificial materials used in bioprinting of hollow fibers are normally in solid state, resulting in the creation of fibers with internal diameters that match the diameter of the printing nozzles(Q. Gao et al., 2017 ; Miller et al., 2012). The removal mechanism for sacrificial materials is a challenging process, which depending on the material used, can be performed by reaching a specific temperature or by employing a suitable solvent.(Norotte et

al., 2009 ; Shao et al., 2020). We hypothesize that a core flow of crosslinker in foam shape can address the limitations of solid sacrificial methods and liquid crosslinkers, by providing the required support to fabricate hollow fibers, as well as the delivery of the crosslinking agents.

1.5 Objective 3 literature review

Three-dimensional bioprinting is a method for the layer-by-layer fabrication of cell-laden constructs according to a computer model.(Karvinen & Kellomäki, 2023 ; Murphy & Atala, 2014) Among the various modalities of 3D bioprinting, extrusion bioprinting has gained popularity due to its simplicity and versatility.(Ravanbakhsh, Karamzadeh, et al., 2021 ; Y. S. Zhang et al., 2021) However, the use of extrusion-based bioprinting is restricted due to the difficulty of creating cell-laden constructs with good resolution, due to the scarcity of biocompatible and printable bioinks.(Ravanbakhsh, Bao, et al., 2021) Specifically, many hydrogels with desirable biocompatible properties lack the required mechanical and rheological properties for 3D bioprinting.(Askari et al., 2021) Embedded bioprinting is a method to address the abovementioned limitations, which employs a support bath to maintain the integrity of the printed structure during the gelation of thebioink(Bhattacharjee et al., 2015 ; Highley, Rodell, & Burdick, 2015 ; Hinton et al., 2015 ; Zhou et al., 2022).

Embedded 3D bioprinting has outperformed conventional extrusion-based methods in terms of printing resolution, free-form printing, and compatibility with various bioinks.(Bao et al., 2020) The materials used for the support bath in embedded bioprinting are commonly granular hydrogels with optimized size and rheological properties that exhibit shear thinning behavior.(Bhattacharjee et al., 2015 ; Highley et al., 2015). So far, various materials, such as Pluronic F127,(Rocca, Fragasso, Liu, Heinrich, & Zhang, 2018) gelatin,(Lee et al., 2019) and xanthan gum(Noor et al., 2019) have been used as support bath materials. However, there are several limitations associated with the use of gel-based support baths. Primarily, the insufficient oxygenation and lack of nutrient diffusion to the bioprinted constructs before the bath removal can lead to necrosis or hypoxia-induced apoptosis, posing the risk of decreased

cell viability during long gelation processes, e.g., thermal gelation.(Rahimnejad, Adoungotchodo, Demarquette, & Lerouge, 2022) Moreover, some bath removal mechanisms can negatively affect cell viability and structural fidelity, especially when lowered temperatures or mechanical agitation is mandatory to remove the support material.(Q. Li et al., 2022) Additionally, removing the support material from cavities and confined parts of the printed structure is challenging. Nonetheless, there has been limited work to date aimed at addressing the deficiencies associated with embedded 3D bioprinting. The use of albumin-based foam baths enriched with nutrients and oxygen is a potentially viable approach to overcome these issues.

Albumin, a well-known foaming agent,(Abeyrathne, Lee, & Ahn, 2013 ; Elias Madadian, Naseri, Legault, & Ahmadi, 2023) has been widely studied as a biocompatible and biodegradable material.(Bajpai & Saini, 2006 ; Delkash et al., 2021) It is a natural water-soluble protein present in various sources such as bovine serum and chicken egg white.(Karimi et al., 2016) Mechanical agitation of an albumin solution denatures the protein structure and forms long protein chains that are exposed to the surrounding environment. This phenomenon enables hydrophilic and hydrophobic groups to trap the surrounding air within the solution as bubbles and subsequently lead to the creation of foam.(X. Duan et al., 2018 ; Gharbi & Labbafi, 2019) We hypothesize that by employing albumin foam as the support bath in embedded bioprinting, the gradual coalescence of bubbles would facilitate the removal of the support bath. Other advantages of using a support bath in foam phase include the improved access to the immediate atmospheric oxygen, compared to the limited dissolved oxygen in conventional baths.(Carmeliet & Jain, 2000) Furthermore, the enrichment of the foam solution with cell culture media would provide cells with supplementary nutrients during bioprinting to preserve cell viability.

CHAPTER 2

DEVELOPMENT OF 3D-PRINTABLE ALBUMIN-ALGINATE FOAM FOR WOUND DRESSING APPLICATIONS

E. Madadian [a,b,c], E. Naseri [a], R. Legault [a], and A. Ahmadi [a,b,c,d]

[a] Faculty of Sustainable Design Engineering, University of Prince Edward Island, PE, Canada
[b] Department of Biomedical Science, Atlantic Veterinary College, University of Prince Edward Island, PE, Canada
[c] University of Montreal Hospital Research Centre (CRCHUM), Montreal, Canada.
[d] Department of Mechanical Engineering, École de technologie supérieure, QC, Canada

Paper published in *3D Printing and Additive Manufacturing*, online ahead of print: March 2023

2.1 Abstract

In this paper, a method to develop 3D printable hybrid sodium alginate and albumin foam, crosslinked with calcium chloride mist is introduced. Using this method, highly porous structures are produced without the need of further post-processing (such as freeze-drying). The proposed method is particularly beneficial in development of wound dressing as the printed foams show excellent lift-off and water absorption properties. Compared to methods that use liquid crosslinker, the use of mist prevents the leaching of bio-compounds into the liquid crosslinker. 3D printing technique was chosen to provide more versatility over the wound dressing geometry. Calcium chloride and rhodamine B were used as the crosslinking material and the model drug, respectively. Various biomaterial inks were prepared by different concentrations of sodium alginate and albumin, and the fabricated scaffolds were crosslinked in mist, liquid, or kept without crosslinking. The effects of biomaterial composition and the crosslinking density on the wound dressing properties were assessed through printability studies. The mist-crosslinked biomaterial ink composed of 1% (w/v) sodium alginate and 12% (w/v) albumin showed the superior printability. The fabricated scaffolds were also characterized through porosity, mechanical, degradation, and drug release tests. The mist-

crosslinked scaffolds showed superior mechanical properties and provided relatively prolonged drug release.
Keywords: 3D printing, wound dressing, alginate, albumin, biomaterial

2.2 Introduction

Skin is the largest organ of the body that protects internal organs from the external environment, which makes it vulnerable to external injuries(H. Liu et al., 2018). Pathogenic bacteria such as *S.aureus* and *E.coli* are widely found in wounds(Ahmed et al., 2021). Self-healing process of wounds consists of several overlapping stages: hemostasis, inflammation, migration, proliferation, and remodeling(Johnson et al., 2019 ; Yang, Liang, Chen, Duan, & Guo, 2022). Self-healing stages may not be followed perfectly and may not be enough for proper tissue recovery. The self-healing process can be hindered by a compromised immune system or may be insufficient due to the severity of the wound(Powers, Higham, Broussard, & Phillips, 2016). Wound dressings can promote the healing process by providing a moist environment while releasing active agents such as anti-microbial, anti-inflammatory, and anti-proliferative agents to the wound(Adamu, Gao, Jhatial, & Kumelachew, 2021). Biomaterials and fabrication processes of wound dressings have direct effects on the properties of wound dressings, determining how they would interact with the wound and how they would deliver the active ingredients to the body(Adeli, Khorasani, & Parvazinia, 2019 ; Naseri, Cartmell, Saab, Kerr, & Ahmadi, 2021 ; Ying et al., 2019). Wound dressing biomaterials should provide the least contact with wound and exhibit oxygen permeability(Kumar, Wang, Nune, & Misra, 2017 ; Schreml et al., 2010).

Various synthetic and natural biomaterials have been used in wound dressings to accelerate wound healing. Synthetic biomaterials such as polycaprolactone (PCL)(Mouro, Gomes, Ahonen, Fangueiro, & Gouveia, 2021) , and Polylactic-co-glycolic acid (PLGA)(Peng et al., 2021) have been widely used in wound dressings; however, special attention should be paid to assuring their biocompatibility(Jurak, Wiącek, Ładniak, Przykaza, & Szafran, 2021). Alginate,

collagen, and chitosan are a few examples of the natural biomaterials, which are widely used in wound dressings, showing enhanced biocompatibility compared to the synthetic biomaterials(Reddy, Ponnamma, Choudhary, & Sadasivuni, 2021).

Sodium alginate is a biocompatible, biodegradable, and widely accessible biomaterial that is used in developing controlled release applications and drug delivery systems(Ilhan et al., 2020 ; Y. Tang et al., 2019). In addition, alginate is a water-soluble biopolymer that can be crosslinked with various crosslinking agents such as calcium chloride(Ahmad, Mushtaq, Butt, Rasheed, & Ahmad, 2021), making it an ideal candidate for wound dressing applications. Sodium alginate have been mixed with other biomaterials to improve its mechanical and wound healing properties. For instance, sodium alginate was composited with PCL to achieve a higher mechanical property(S. F. Lan et al., 2013). In another work, sodium alginate was mixed with chitosan to enhance the physiochemical properties of the biomaterial and accelerate coagulation of the blood(Mndlovu et al., 2019). A major issue with many contemporary wound dressings is that they often fully cover the wound, causing the dressing material to adhere to the wound area. This can in turn result in severe trauma to the wound and surrounding tissue when removing or changing the dressing(Kumar et al., 2017 ; Vowden & Vowden, 2017). Fabricating the wound dressing with foamed biomaterial can provide low contact covering of the wound(Probst, Saini, & Skinner, 2019).

To fabricate foamed alginate, several methods have been developed including 1) adding sodium bicarbonate to isosmotic saline alginate solution following stirring to incorporate air bubbles(Caroline et al., 2017), 2) crosslinking alginate micro-bubbles(Karimpoor et al., 2018), and 3) mixing alginate and crosslinker solutions(Andersen, Melvik, Gåserød, Alsberg, & Christensen, 2014). These foaming procedures are frequently followed by freeze drying or by incubating in a desiccator, and the foam is crosslinked throughout the process to maintain its porous structure. The crosslinked foam cannot be formed into other constructs; hence, developing another foaming method for fabricating foamed alginate scaffolds is required.

Albumin has been widely used as a foaming agent in the food industry(Hardy & Jideani, 2017), which can also be used for wound dressing applications(Jirkovec, Samkova, Kalous,

Chaloupek, & Chvojka, 2021). Albumin, a biocompatible and biodegradable material, is a natural water-soluble protein, which is the most available protein in blood plasma(Kratz, 2014). However, the application of albumin foam in wound dressing is limited as the foam is not stable over time. Adding sodium alginate to albumin foam can enhance the stability of the foam, while further crosslinking of alginate will improve the mechanical properties of the biomaterial. The addition of alginate to albumin mixed with tannic acid as crosslinker (without foam) has been previously reported (Janarthanan, Lee, & Noh, 2021). However, the use of tannic acid has limited applications due to its potential side effects.

Various fabrication techniques such as electrospinning(Y. Liu, Li, Han, Li, & Liu, 2021), and 3D printing(Long et al., 2019) have been used for fabricating wound dressings. For example, electrospinning technique has used to fabricate polyvinyl alcohol/alginate/albumin nanofibers for wound dressing applications(Jirkovec et al., 2021). Among all fabrication techniques, 3D printing as a method to deposit various biomaterial inks with desired structures on the printing bed, layer-by-layer, stands out, allowing scientists to fabricate patient-tailored drug-eluting constructs(Naseri, Cartmell, Saab, Kerr, & Ahmadi, 2020). To the best of our knowledge, 3D printing of sodium alginate and albumin foam for wound dressing applications has not been investigated. 3D printed sodium alginate/albumin foam can provide a non-adhesive wound dressing with patient-tailored drug-eluting characteristics.

In this paper, the potential application of sodium alginate and albumin foam as biomaterial ink to be used for wound dressings will be investigated. Sodium alginate and albumin hybrid foam with various concentrations and ratios were prepared and 3D printed followed by a crosslinking step, which was either in calcium chloride mist, or no crosslinking at all. The mist crosslinking method will eliminate the main liquid crosslinking disadvantage in drug delivery applications, where the incorporated active ingredients will be washed off from the scaffolds in liquid baths. The printability of the biomaterial ink hybrids was quantified through an established printability study. In addition, the 3D printed scaffolds were characterized via scanning electron microscopy (SEM), and the mechanical properties were studied by strain tests. Finally,

rhodamine B was used as a model drug, and the drug release rate of the wound dressing scaffolds crosslinked by calcium chloride liquid, mist, or not crosslinked, was characterized by *in-vitro* drug release studies, where the amount of the released rhodamine B in the dissolution medium was measured by a UV-Vis spectrophotometer. It is hypothesized that the 3D printed sodium alginate and albumin hybrid foam creates a porous structure with tunable morphology. The morphology and the respective drug release of the sodium alginate and albumin scaffolds could be controlled by the concentration of sodium alginate, the concentration of albumin, and the availability of the crosslinking agents.

2.3 Materials and methods

2.3.1 Biomaterial ink and crosslinker preparation

Table 2.1 shows different ratios of the compositions used in this study to investigate the effects of various biomaterial ink compositions on printability. These ratios were selected based on preliminary experiments. Sodium alginate solution was made by adding sodium alginate powder (W201502, Sigma-Aldrich, USA) to deionized (DI) water and then stirred at 500 rpm for 5 hours. Subsequently, egg albumin (9761, McCall's, CA) was added to the solution and was stirred at 400 rpm for 2 hours. The solution was frothed at high speed (TM-300HMCN, Toastmaster Hand Mixer) for 3 minutes to obtain a homogenous and firm foam. The 10% *w/v* crosslinker solution was prepared by stirring calcium chloride powder (1023782500, Sigma-Aldrich, USA) in DI water for 1 hour at 300 rpm.

Table 2.1 The composition of the biomaterial inks

Biomaterial ink	Sodium alginate (% *w/v*)	Albumin (% *w/v*)
SA01AL04	1	4
SA01AL08	1	8
SA01AL12	1	12
SA02AL04	2	4
SA02AL08	2	8
SA02AL12	2	12

SA03AL04	3	4
SA03AL08	3	8
SA03AL12	3	12

2.3.2 3D printing

All structures were fabricated by a commercial 3D bioprinter (BioX, Cellink, Sweden). SA01AL12 biomaterial ink was 3D printed at 11 mm/s speed and at 15 kPa pressure with a syringe nozzle with 1.524 mm inner diameter (75165A674, McMaster-Carr, USA). In our previous study, sodium alginate (5% w/w) was printed with pneumatic pressure in the range of 13-372 kPa for nozzle sizes of 0.203-0.483 mm, where larger nozzle diameters required less dispensing pressure(MacCallum et al., 2020). In this study, a nozzle size of 1.524 mm is chosen to prevent any potential cloggage, which significantly reduces the required printing pressure. The biomaterial ink was crosslinked by either crosslinker liquid (bath) or crosslinker mist. To crosslink the filaments in the crosslinker bath, two-layer scaffolds were printed in a petri-dish filled with calcium chloride. To deliver calcium chloride mist to the printing stage, a customized mist-delivery printhead was attached to the 3D bioprinter, as described in our previous study(Badr et al., 2022 ; MacCallum et al., 2020). Briefly, an ultrasonic atomizer was submerged in a container filled with calcium chloride solution. The container was connected to an air pump, delivering the mist-air mixture to the printing bed, providing crosslinking ions to the biomaterial ink while printing. Figure 2.1a shows the schematic of biomaterial ink preparation and crosslinking, Figure 2.1b shows the printing setup with the misting system and Figure 2.1c shows the schematic of the printing setup and mist exposure.

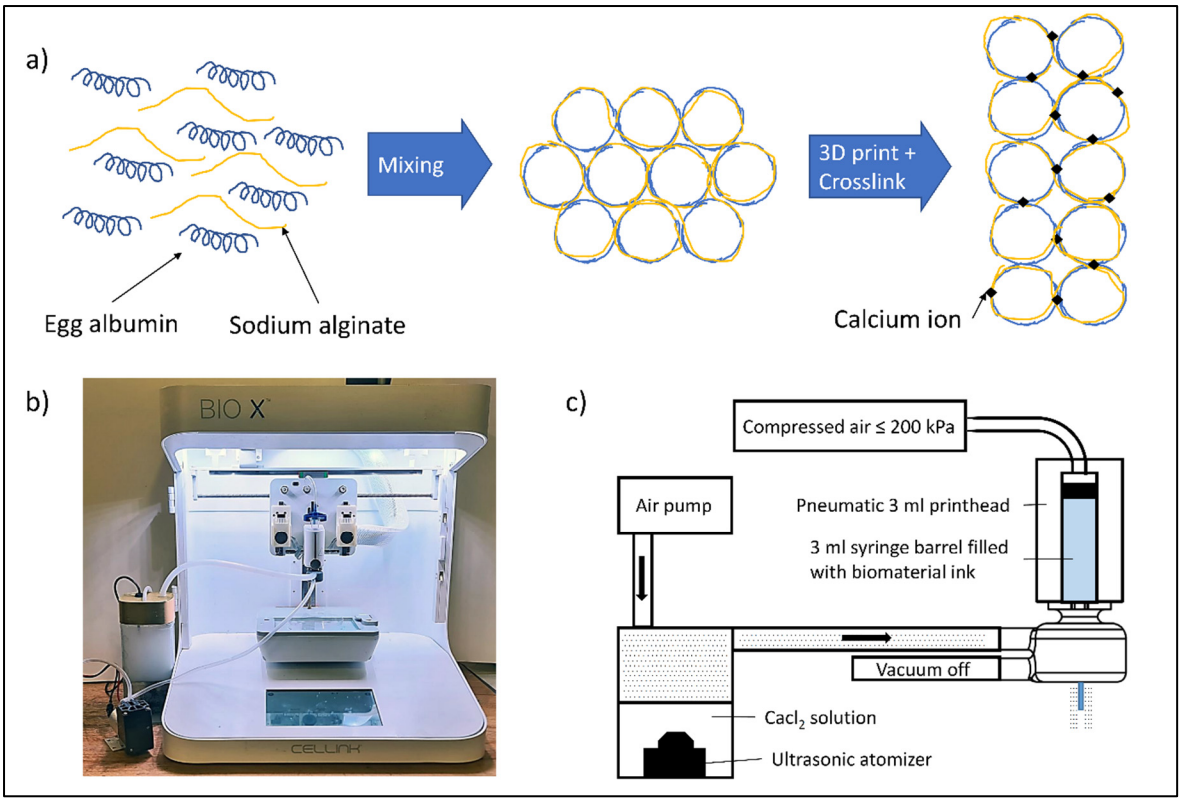

Figure 2.1 a) Schematic of biomaterial ink preparation and crosslinking, b) printing setup, c) schematic of printing setup and mist exposure

2.3.3 Printability study

Printability number (*Pr*) was used as an indicator to study the printability of the biomaterials:

$$Pr = \frac{L^2}{16\,A}, \tag{2.1}$$

where L is the perimeter of the pore between printing filaments and A is the area of the mentioned space(Ouyang, Yao, Zhao, & Sun, 2016). Printability number between 0.9 to 1.1 indicates printable biomaterial ink with the ideal printability number at 1(Ouyang et al., 2016). To validate printability(Paxton et al., 2017) and calculate the printability number, 4×4 cm two-layer square scaffolds with 1×1 cm grid were fabricated. After 24 hours, pictures were taken

and the printability number for each scaffold was calculated using an image analysis software (Fiji, ImageJ 1.53n, GNU General Public License, USA). Figures 2.2a and 2.2b show a CAD model and a 3D printed 2×2×1 cm cube with SA01AL12 biomaterial ink using calcium chloride mist (Supplementary Video), which validates the printing parameters(Bonatti, Chiesa, Vozzi, & de Maria, 2021 ; Ribeiro et al., 2017), and Figure 2.2c shows the geometrical parameters of a fabricated structure for the printability studies.

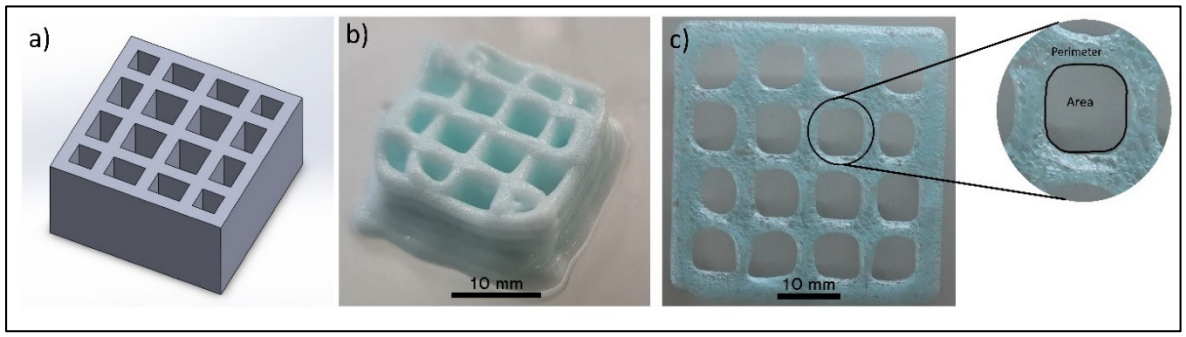

Figure 2.2 a) a CAD model and b) 3D printed structure of a multi-layer wound dressing with SA01AL12 biomaterial ink using calcium chloride mist, c) geometrical parameters for printability studies

2.3.4 Scanning electron microscopy

SEM (TM3000, Hitachi, Japan) was used to characterize surface and cross-section features of the 3D printed scaffolds. 10 mm filaments were fabricated with SA01AL12, under various crosslinking conditions: crosslinked in calcium chloride mist (SA01AL12-mist), crosslinked in calcium chloride bath (SA01AL12-bath), or not crosslinked at all (SA01AL12-nc). The filaments were freeze dried after one day of room-temperature air drying. The freeze-dried filaments were gold sputtered (thickness = 300 Å), and the SEM was run at 15 kV at analysis mode.

2.3.5 Surface morphology

To quantify the surface features of the filaments various parameters were measured based on the surface SEM images(Haeri & Haeri, 2015): 1- number of pores per unit area, 2- average area of pores, 3- distance between the pores, and 4- surface porosity. The surface porosity was calculated by dividing the total area of the pores by the total area of the surface.

2.3.6 Mechanical properties

Breaking strains of the filaments were used as an indication for characterizing the mechanical properties of the printed structures. 30 mm filaments (SA01AL12-bath, -mist, and -nc) were fabricated as described previously, and a customized device was used to elongate filaments for the strain measurements. The initial and breaking lengths of the filaments were measured using ImageJ processing software, and the breaking strain was calculated according to the following equation:

$$E = \frac{L_1 - L_0}{L_0}, \tag{2.2}$$

where L_0 and L_1 are the initial and breaking lengths of the filaments, respectively(Ferdinand P. Beer, John T. DeWolf, E. Russell Johnston, Jr., 2012).

2.3.7 Water absorption

To calculate the water absorption capacity of the filaments, 3×3 cm two-layer square scaffolds with 80% infill in a grid pattern were fabricated. The scaffolds were submerged in DI water and incubated at 37 °C for 30, 60, and 90 minutes. The dry weight of samples was measured after oven drying for one day at 37 °C. The following equation was used to calculate the absorption percentage(K. Zhang, Feng, & Jin, 2020):

$$\text{water absorption } = \frac{W_2 - W_1}{W_1} \times 100, \quad (2.3)$$

where W_2 is the weight of the wet scaffold and W_1 is the weight of the dried scaffold.

2.3.8 Degradation

The degradation percentage was calculated by the dry mass loss divided by the initial dry mass of the scaffolds. Scaffolds were fabricated as described in the water absorption section and were oven dried for one day at 37 °C. Dried samples were submerged in DI water and incubated at 37 °C for 30, 60, and 90 minutes and then oven dried again for a day at 37 °C. The following equation was used to calculate the degradation percentage:

$$\text{degradation } = \frac{W_i - W_d}{W_i} \times 100, \quad (2.4)$$

where W_i is the initial dry weight of the scaffold and W_d is the dried weight of the degraded scaffold.

2.3.9 Drug release characterization

To characterize the drug release rate of the 3D printed scaffolds, rhodamine B, a model drug(R. Zhang, Hummelgrd, Lv, & Olin, 2011), was incorporated into the scaffolds. SA01AL12 was selected as the biomaterial ink for the drug release tests based on the results for the printability study. Rhodamine B was added to SA01AL12 (0.2% *w/v*) and stirred for 1 hour. A 2×2 cm hollow square was fabricated by the same 3D printing parameters described earlier.

The scaffolds were crosslinked in calcium chloride mist (SA01AL12-mist), in calcium chloride bath (SA01AL12-bath), or not crosslinked at all (SA01AL12-nc). The exposure time to the

calcium chloride mist and bath was equal, and the scaffolds were then immediately placed in 30 mL phosphate buffer saline (PBS) with pH 7.4 (VWRL0119, VWR, USA), used as the dissolution medium, while stirring at 150 rpm at 37 °C(Fan et al., 2021). 1 mL of the dissolution medium was taken at 10, 20, 30, 60, 120, 180, 720, 1440, and 2160 minutes, and it was replaced by the same amount of fresh PBS at each time point. The release of rhodamine B was assessed by a UV-Vis spectrophotometer (Cary 100, Agilent, USA) at the rhodamine B's lambda max (554 nm), and cumulative release (%) was calculated accordingly.

2.3.10 Statistical analysis

Statistical analysis of all data was implemented using Microsoft Excel data analyzer with single factor one-way analysis of variance (ANOVA). The experiments were implemented in triplicates, and the results were reported as mean values ± standard errors. Tukey post hoc analysis was used to compare each two groups of data, and *p*-values smaller than 0.05 were considered statistically significant, in all steps.

2.4 Results and discussions

2.4.1 Printability analysis

A set of printed 4×4 cm square scaffolds, a computer model of the printed structures for qualitative assessment of shape fidelity(Ribeiro et al., 2017), and the printability numbers of different biomaterial inks crosslinked with calcium chloride mist (-mist) or without any crosslinker (-nc) are shown in Figure 2.3a, 2.3b, and 2.3c, respectively. The printability number of all scaffolds was increased after being exposed to mist crosslinker due to gelation of the alginate texture inside the biomaterial composition(Łabowska et al., 2021 ; Sarker, Izadifar, Schreyer, & Chen, 2018). The printability numbers of SA01AL08 and SA01AL12 increased after being crosslinked by mist from 0.832 ± 0.002 (-nc) and 0.834 ± 0.002 (-nc) to 0.892 ± 0.012 (-mist) and 0.929 ± 0.007 (-mist), respectively. Although the printability number of

SA01AL04 increased after being mist crosslinked, the increase was not significant. As a result, SA##AL08 and SA##AL12 biomaterial inks were chosen for further printability studies.

Increasing alginate concentration decreased the printability number. For the mist-crosslinked scaffolds, all scaffolds are exposed to the same number of crosslinking ions; consequently, with increasing the alginate concentration, a higher number of un-crosslinked polymers will remain in the scaffolds(Jia et al., 2014 ; MacCallum et al., 2020). For SA01AL08-mist and SA02AL08-mist, the printability numbers were calculated at 0.892 ± 0.012 and 0.844 ± 0.004, respectively, showing a significant decrease in the printability due to an increase in the alginate concentration.

Increasing albumin concentration led to an increase in the printability number of the mist-crosslinked scaffolds(Poole, 1989). The printability numbers of SA01AL04-mist, SA01AL08-mist, and SA01AL12-mist were calculated as 0.838 ± 0.004, 0.892 ± 0.012, 0.929 ± 0.007, respectively, indicating the direct effect of albumin concentration on the printability number. The presence of more albumin protein in the biomaterial ink resulted in a more stable and stiffer foam, visually. Albumin concentration had no significant effect on the printability numbers of the un-crosslinked scaffolds. Having more un-crosslinked alginate polymers overruled the effect of albumin on foam stiffness, and consequently, printability numbers did not change, significantly. Increasing alginate and albumin concentrations influenced printability numbers in opposite directions. These opposing effects are noticeable in comparing SA02AL08-mist to SA03AL12-mist with the printability numbers at 0.844 ± 0.004 and 0.854 ± 0.001, respectively, which are not significantly different.

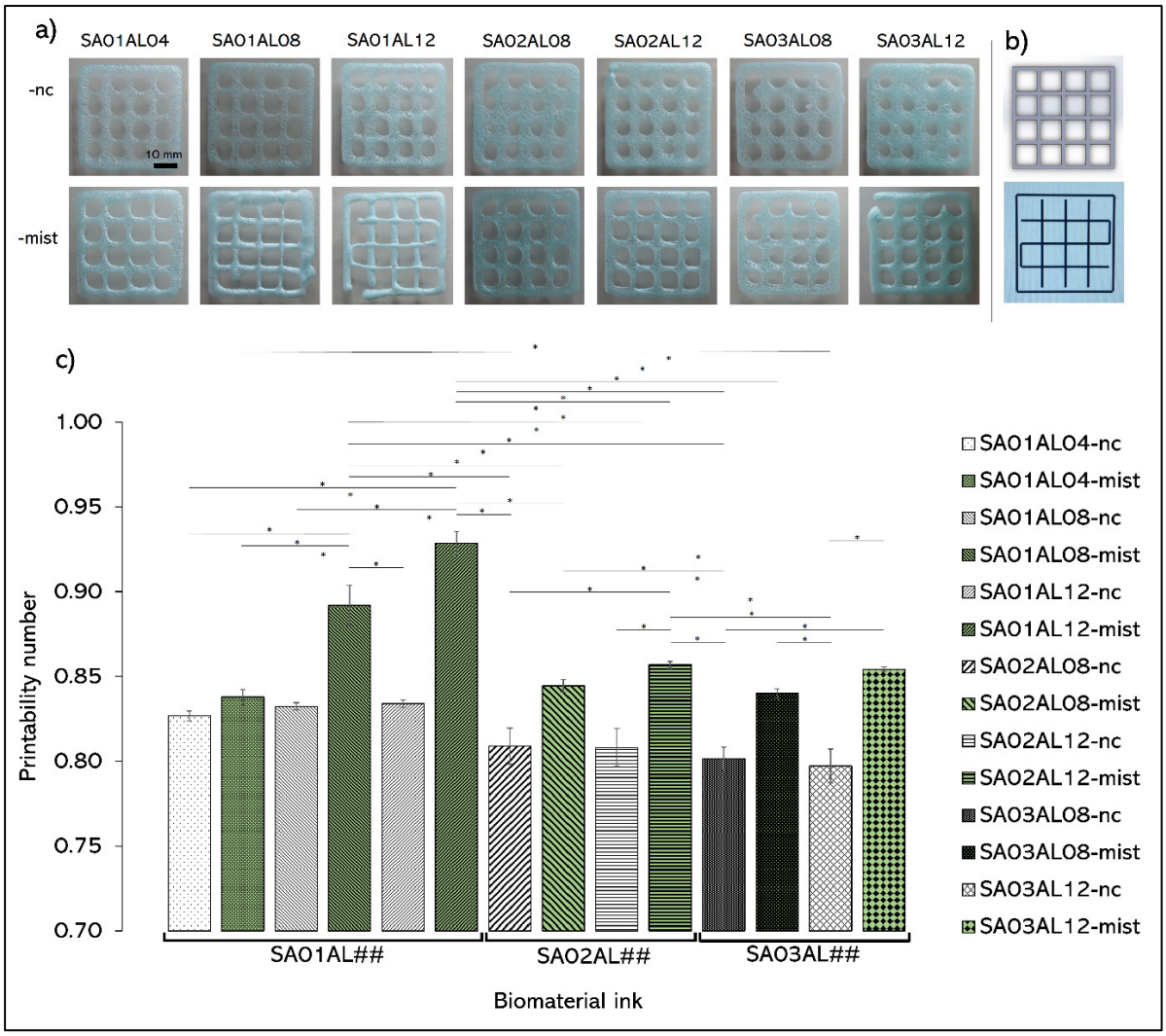

Figure 2.3 a) Printed 4×4 cm square scaffolds, b) The computer model and the printing pattern, c) printability number of various biomaterial inks. Asterisks show significant differences ($p < 0.05$)

2.4.2 Porosity assessment

SEM images of SA01AL12-bath, -mist, and -nc scaffolds are shown in Figures 2.4a-c (surface) and Figures 2.4d-f (cross section). As shown in Figures 2.4a-c, the crosslinking process has a direct effect on the surface morphology of the filaments. SA01AL12-bath showed the lowest surface porosity compared to the -mist and -nc scaffolds due to the crosslinking density as the

crosslinking occurs faster for sodium alginate soaked in the crosslinker bath compared to the misted sodium alginate(Jang et al., 2014). This phenomenon is also confirmed through the cross-section SEM images shown in Figures 2.4d-f, where the SA01AL12-nc scaffold is the most porous scaffold compared to the -mist and -bath samples.

The quantified parameters respective to the surface features of the SA01AL12-bath, -mist, and -nc scaffolds are shown in Figures 2.4g-j. The number of pores per unit area was counted at 419, 129, and 44 mm^{-2} for SA01AL12-bath, -mist, and -nc, respectively, as shown in Figure 2.4g. Sodium alginate crosslinking density is attributed to the concentration of the crosslinking ions that results in faster gelation of sodium alginate in more concentrated crosslinker environments(Jang et al., 2014): SA01AL12-bath > SA01AL12-mist > SA01AL12-nc. The rapid gelation of alginate will prevent Ostwald ripening phenomenon, exhibiting different pore counts in different crosslinking methods(Mleko, Kristinsson, Liang, & Gustaw, 2007). Ostwald ripening in foams is the process of growing the bubbles through movement of gas molecules from smaller to larger bubbles over time. As a result, the number of pores per unit area decreased by decreasing the exposure of the filaments to the crosslinker ions. In less concentrated crosslinking environments, pores have more time to merge and create larger pores, which is explained by Ostwald ripening phenomenon(Attia, Kholi, & Pilon, 2013). Consequently, the average area of pores was measured at 2.18×10^{-4}, 1.24×10^{-3}, and 6.77×10^{-3} mm^2 for SA01AL12-bath, -mist, and -nc, respectively, as shown in Figure 2.4h.

The crosslinking speed dependency on the crosslinking method influences the distance of pores from each other. In less condensed crosslinking environments, the pores will expand and merge with each other, leading more distance between pores. This effect was observed in the experiments as shown in Figure 2.4i, with the following order in the distance of the pores for the studied scaffolds: SA01AL12-bath < SA01AL12-mist < SA01AL12-nc. The surface porosity of the scaffolds is a parameter that is dependent on the previously discussed parameters. The surface porosity of the SA01AL12-bath, -mist, and -nc scaffold were

calculated at 9.18%, 16.05%, and 29.9% (Figure 2.4j). The calculated porosity was in agreement with the observed porosity in the SEM images discussed earlier.

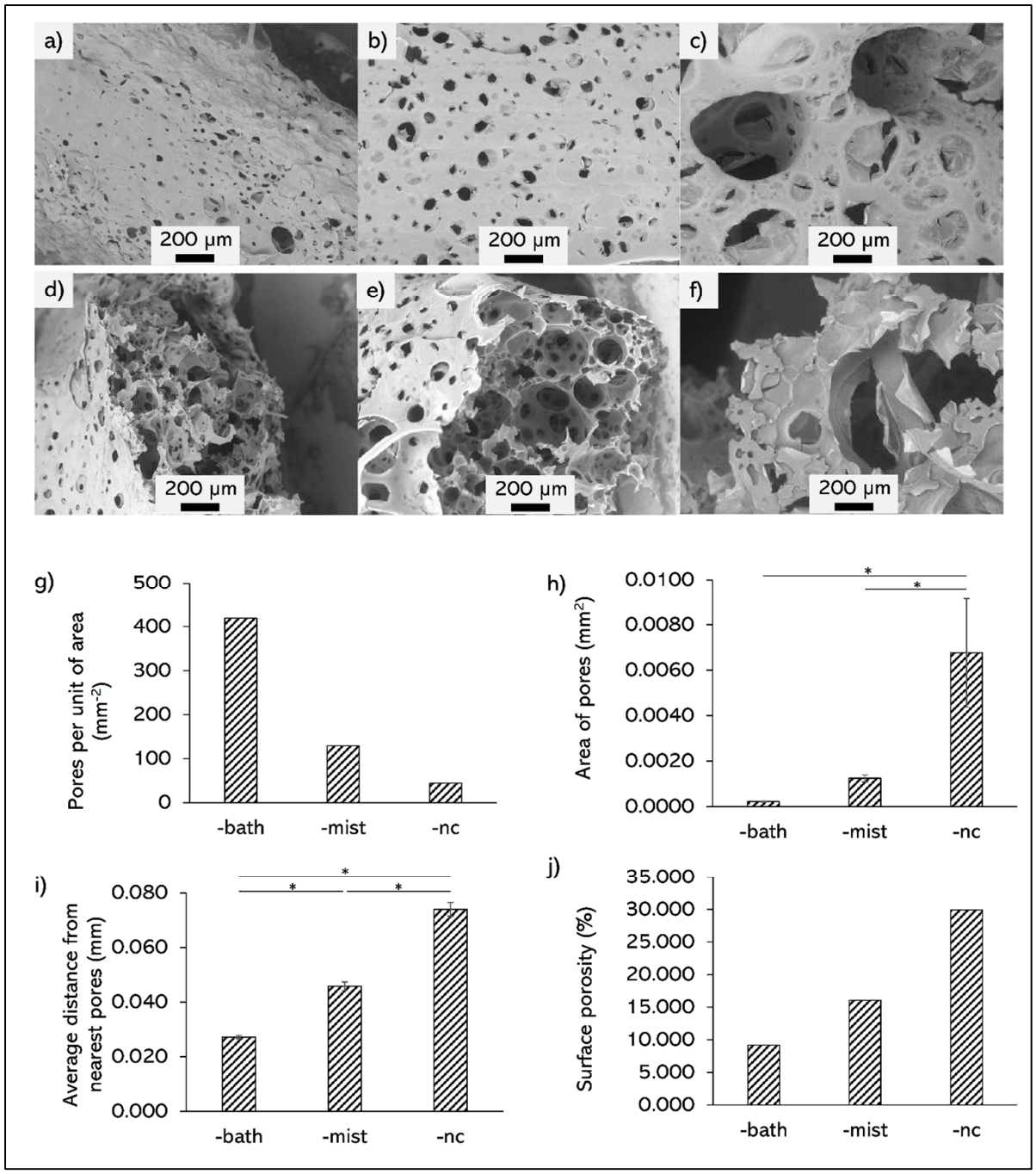

Figure 2.4 a-c) Surface SEM of SA01AL12 filaments crosslinked in -bath, -mist, and -nc, d-f) cross-section SEM of SA01AL12 filaments crosslinked in -bath, -mist, and -nc, g) number of pores per unit of area, h) average area of the pores, i) average distance from the nearest pores, j) surface porosity. Asterisks show significant differences ($p < 0.05$)

2.4.3 Mechanical properties

The breaking strains of the SA01AL12-bath, -mist, and -nc filaments are shown in Figure 2.5. The SA01AL12-mist filaments had the highest breaking strain (49.70 ± 0.77%) compared to the -bath and -nc filaments (30.83 ± 1.49% and 41.03 ± 2.54%), respectively. Filaments made of foamed alginate/albumin showed higher breaking strains compared to non-foamed alginate filaments in the literature which mostly have a breaking strain under 30%. The lower number of entangled and crosslinked polymer chains in foam due to the presence of air bubbles results in a lower toughness which leads to a higher breaking strain. SA01AL12-bath filaments behaved brittle due to a higher crosslinking density, resulting in a lower breaking strain, while SA01AL12-mist filaments were able to be stretched more, which can be a result of being partially crosslinked. In SA01AL12-nc filaments, sodium alginate chains were not crosslinked, resulting in a lower breaking strain compared to SA01AL12-mist filaments.

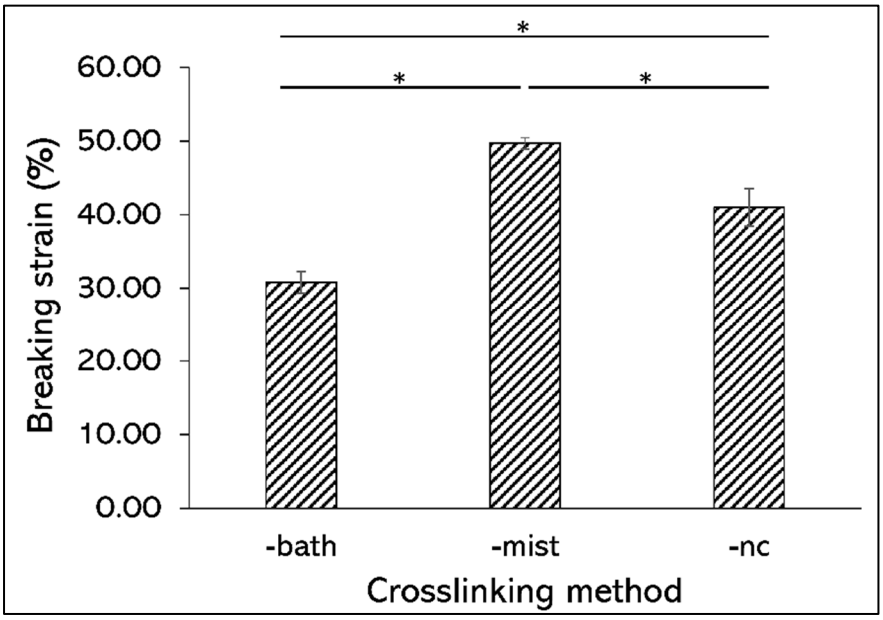

Figure 2.5 Breaking strains of SA01AL12-bath, -mist, and -nc filaments. Asterisks show significant differences ($p < 0.05$)

2.4.4 Water absorption

The water absorption of SA01AL12-mist and -bath for different time points are shown in Figure 2.6a. The water absorption of bath crosslinked scaffolds were less than -mist crosslinked scaffolds. Higher amounts of crosslinking agent in bath crosslinked scaffolds decelerated the water absorption within the scaffolds. These results agree with the porosity test results, where the higher porosity of SA01AL12-mist scaffolds is leading to higher water intake within the scaffolds, particularly in the 30 min samples. The water absorption also increased over time, which is in accordance with literature(Avossa et al., 2021).

There are studies to investigate the water absorption capacity of foams made of alginate composited with other materials. For instance, water absorption of gelatin/alginate sponge at various time points is also reported to range from 1000% to more than 2000% in 10 up to 1440 minutes.(Wen, Yu, Zhu, Yang, & Shao, 2020) The water absorption capacity can be affected by the concentration of hydrogels, concentration of crosslinker, exposure time to the crosslinker, and the porosity of the structure.

2.4.5 Degradation

The degradation percentages of SA01AL12-mist and -bath for different time points are shown in Figure 2.6b. The initial decrease in the dry weight of bath crosslinked samples is 43.3% less than the initial mass decrease in mist crosslinked samples. The high crosslinking density of alginate in the bath crosslinked samples traps the water-soluble albumin chains in the polymer network while mist crosslinking leads to partially crosslinked samples which degrade at a faster pace. As the incubation time increases, the weight loss of bath crosslinked samples increases at a higher rate compared to the mist crosslinked samples. The observed degradation trends are in accordance with the water absorption results signifying the increase in water absorption leads to a higher leach of albumin from the hydrogel. The degradation percentage of mist/bath crosslinked samples at 30, 60, and 90 minutes were calculated as 65.5 ± 1.2/37.1 ± 3.9, 69.3 ±

2.0/45.7 ± 3.7, and 70.6 ± 1.1/53.3 ± 1.4%, respectively. The degradation trend observed in this study is in agreement with the degradation trend of hybrid gels in literature(Barceló, Eichholz, Garcia, & Kelly, 2022).

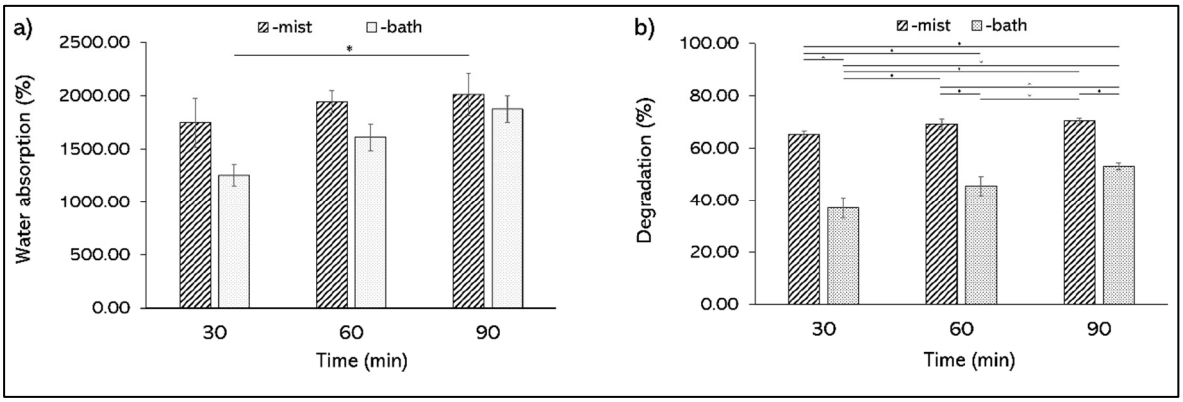

Figure 2.6 a)Water absorption of SA01AL12-mist and -bath crosslinked scaffolds over time. b) degradation of SA01AL12-mist and -bath crosslinked scaffolds over time. Asterisks shows significant difference ($p < 0.05$)

2.4.6 Drug release characterization

The rhodamine B release from the SA01AL12 (-mist, -bath, and -nc) scaffolds are shown in Figure 2.7a, with an enlarged section for the first three hours shown in Figure 2.7b. For the first 1 hour, the drug release amount of SA01AL12-mist and -bath samples overlap, and the values are not significantly different. SA01AL12-nc scaffolds showed an accelerated drug release with approximately 75% of the release amount occurring during the first hour. After 10 minutes, the drug release of SA01AL12-nc scaffold is measured at 44.90 ± 4.54 that is approximately two times larger than the release amount of SA01AL12-mist and SA01AL12-bath. The drug release of all the samples plateaus after 12 hours with the cumulative drug release measured at 91.01 ± 9.64, 76.99 ± 10.79, and 54.15 ± 3.62% for SA01AL12-mist, -bath, and -nc scaffolds, respectively. The scaffolds did not release a significant amount of drug after 12 hours, and the release amounts were measured at 91.88 ± 7.41, 82.96 ± 13.52, 55.67 ± 3.78% for SA01AL12-mist, -bath, and -nc scaffolds, respectively.

Higher amount of crosslinking agents led to a decelerating drug release, and it can be used as a controlling factor for the drug release of the scaffolds. More exposure to the crosslinking agents decelerates the drug release with the limit of deceleration to the liquid bath samples, and less exposure to the crosslinking agents will accelerate the drug release with the limit of the drug release for no-crosslinker samples(Kulkarni, Sreedhar, Mutalik, Setty, & Sa, 2010). Albumin and alginate hybrid wound dressings can provide various degradation and drug release rates, immediate or prolonged, in wound dressing applications, by changing the crosslinking time and concentration, from bath crosslinking to no crosslinking.

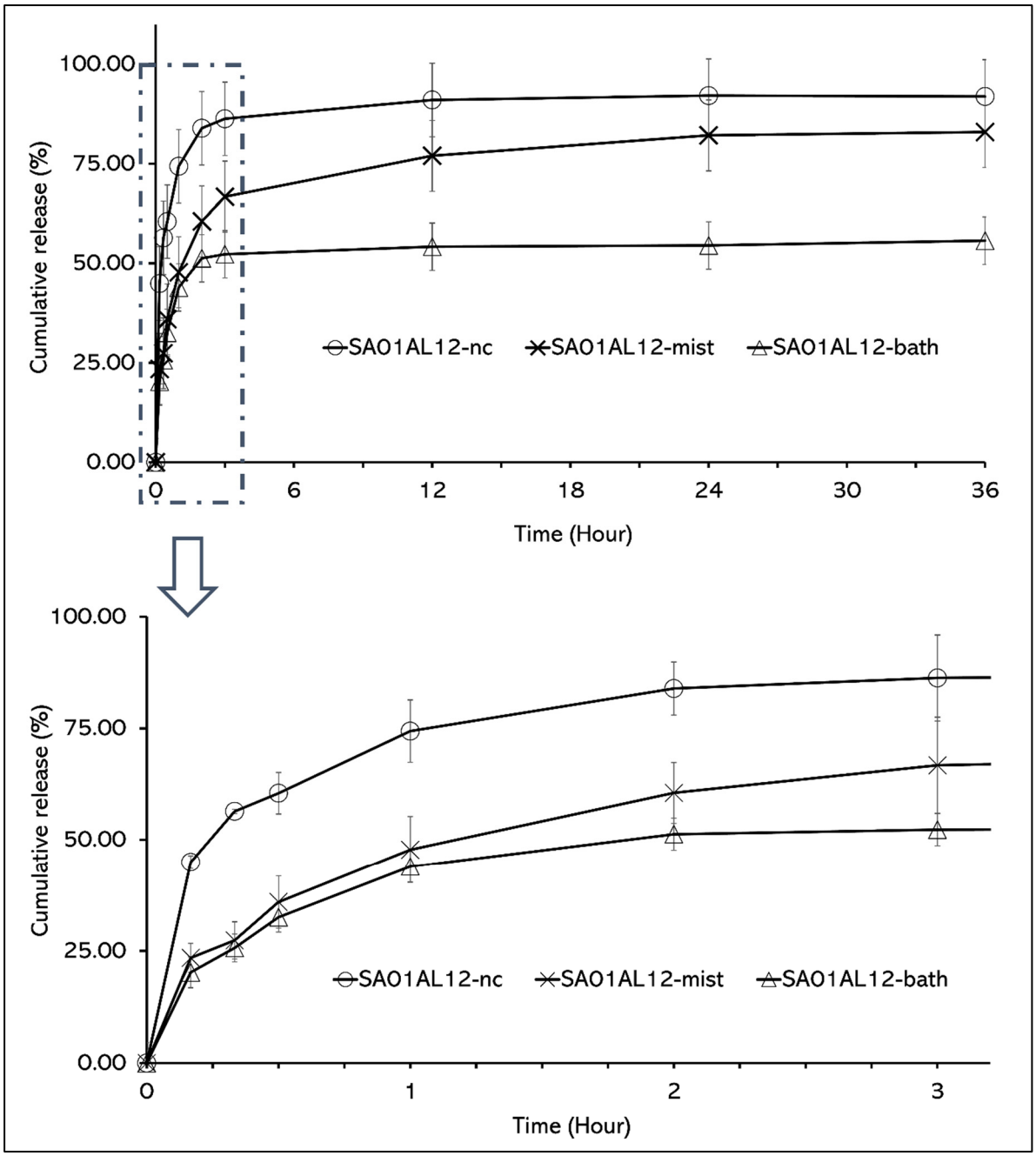

Figure 2.7 a) The cumulative release of rhodamine B in PBS, b) enlarged section of the first three hours of the release period

2.5 Conclusion

In this paper, 3D printed sodium alginate albumin foam biomaterial inks were developed, and their application as wound dressings was assessed. In this study, all the biomaterial ink ingredients were water-soluble that eliminated the need for toxic solvent removal. Using water-soluble solvents will help for moving toward green chemistry, where this method can be used in the fabrication of patient-tailored wound dressings by demand in pharmacies.

The printability of various compositions of the biomaterial inks with three different crosslinking methods (bath, mist, or no crosslinking) were assessed through the printability number studies, and SA01AL12-mist provided the most printable biomaterial ink composition. Mist-crosslinked scaffolds showed a higher porosity compared to the liquid-crosslinked scaffolds. In addition, mist-crosslinked scaffolds showed a higher breaking strain compared to the bath- and non-crosslinked scaffolds. The drug release tests showed a prolonged release for mist- and bath-crosslinked scaffolds. Non-crosslinked scaffolds provided an accelerated drug release, releasing approximately 75% of the drug within the first 3 hours. In further studies, the effect of mist-crosslinking duration on the porosity and subsequently drug release can be investigated.

The duration of mist crosslinking and the concentration of the crosslinking agent provide additional controlling parameters for controlling the wound dressing features such as porosity, mechanical stability, and drug release rate. Using the mist-crosslinking method will address the problems associated with conventional liquid bath crosslinking methods for crosslinking sodium alginate in drug release applications, where the undesired elution of the incorporated drugs will take place into the liquid crosslinker. The results of this study will provide a solid ground for further developments in wound dressing studies, particularly for non-adhesive drug-eluting wound dressings. In addition, the control over the porosity can be used for tissue engineering applications where a specific porosity is expected from the scaffolds for cell proliferation.

2.6 Acknowledgment

The authors of the paper would like to acknowledge Dr. Christian R. Lacroix, Department of Biology, University of Prince Edward Island, for their help with taking the SEM images.

2.7 Author Disclosure Statement

No competing financial interests exist.

2.8 Funding Information

This work was supported by the National Sciences and Research Council of Canada (Discovery Grant RGPIN-2017-05272) and Canada Foundation for Innovation (John R. Evans Leader Fund 37696).

2.9 Authors' Contributions

E.M.: conceptualization, methodology, software, validation, formal analysis, investigation, writing-original draft, writing-review and editing, and visualization. E.N.: methodology, validation, formal analysis, investigation, writing- original draft, and writing-review and editing. R.L.: validation, investigation, and resources. A.A.: conceptualization, methodology, software, validation, formal analysis, investigation, resources, writing-original draft, writing-review and editing, visualization, supervision, project administration, and funding acquisition.

2.10 Supplementary Material

Supplementary data associated with this article can be found, in the online version, at http://doi.org/10.1089/3dp.2022.0241

CHAPTER 3

DEVELOPMENT OF FOAM-BASED SUPPORT MATERIAL FOR COAXIAL BIOPRINTING OF IONICALLY CROSSLINKING BIOINKS

E. Madadian [a,b], S. Badr [a,b], D.S. MacDonald [c], R.A. Tasker [c], and A. Ahmadi [a,b,c]

[a] Department of Mechanical Engineering, École de technologie supérieure, Montréal, QC, Canada
[b] Faculty of Sustainable Design Engineering, University of Prince Edward Island, Charlottetown, Canada
[c] Department of Biomedical Sciences, Atlantic Veterinary College, University of Prince Edward Island, Charlottetown, Canada

Paper published in *Bioprinting*, May 2023

3.1 Abstract

In this study, a foam-based method is developed for three-dimensional coaxial bioprinting of ionically crosslinking bioinks. This method introduces the crosslinker to the bioink in calcium chloride-albumin foam which eliminates the need for multiple crosslinking steps and offers an excellent control over the crosslinking rate and the diameter of the hollow fibers. The effects of the foam and alginate flow rates were investigated on the outer diameter and the wall thickness of the hollow fibers. Various structures were 3D printed and characterized by printability number and the method showed an excellent layer adhesion among printed layers. The effects of foam composition and the alginate concentration on the mechanical properties were assessed through breaking strain and filament collapse tests to determine the optimum composition for hollow fiber fabrication. The hollow fiber composed of 2% (w/v) sodium alginate that is crosslinked with a foam made of 1.07% (w/v) albumin and 1.07% (w/v) calcium chloride showed superior mechanical properties. Furthermore, the viability of co-incubation with Neuro-2a cells over seven days was investigated and no significant negative effect of the used concentrations of albumin and calcium chloride was observed on the viability of the cells.

Keywords: Hollow fiber, Foam, Alginate, Albumin, Ionic crosslinking

3.2 Introduction

Development of hollow fibers has numerous applications in various fields, including drug delivery(C. Liu et al., 2021 ; Wang et al., 2021), and tissue engineering(Luo et al., 2022 ; Schöneberg et al., 2018) as they can mimic blood vessels and vascular networks(Devillard & Marquette, 2021 ; G. Gao et al., 2017 ; Q. Gao et al., 2017). There are many methods to fabricate hollow fibers, including the fresh method(Hinton et al., 2015), coaxial extrusion(Q. Gao et al., 2015), and microfluidic chips(Nguyen et al., 2018). Among all methods of fabricating hollow fibers, coaxial extrusion with three-dimensional (3D) bioprinting method is commonly used to produce hollow fibers as it provides a higher resolution for fabricating complex structures(Kjar et al., 2021). 3D bioprinting methods of fabricating hollow fibers normally require a crosslinking mechanism to maintain suitable rheological properties during printing and high shape fidelity of constructs after printing(Q. Gao et al., 2017, 2015 ; Tabriz et al., 2015).

Ionically crosslinking hydrogels are commonly used in 3D bioprinting of hollow fibers(Kjar et al., 2021). The required crosslinker is normally provided in liquid form and is introduced to the bioink with a coflow, or as a crosslinker bath on the printing stage(G. Gao et al., 2019 ; Q. Gao et al., 2015). Using liquid crosslinker however, has the disadvantages of poor layer adhesion and low shape fidelity of printed constructs due to over pooling of liquid on the printbed and consequently the over-gelation of the fiber(Badr et al., 2022 ; MacCallum et al., 2020 ; Sun & Tan, 2013). Additionally, the active bio-compounds embedded into the bioink may leach into the excess liquid crosslinker on the printbed(Boi et al., 2020 ; Huang et al., 2022). Therefore, current methods of 3D bioprinting of hollow fibers require an additional step of removal of the liquid crosslinker from the hollow fiber and the printbed(G. Gao et al., 2017 ; Q. Gao et al., 2017).

To address the limitations of liquid crosslinker, sacrificial material is used as core flow to provide short term support to the tubular fibers(G. Gao et al., 2017). The sacrificial materials used in bioprinting of hollow fibers are normally in solid state and lead to the production of fibers with internal diameters equal to the diameter of the nozzles used(Q. Gao et al., 2017 ; Miller et al., 2012). Depending on the material used as the core flow, this method requires the removal of sacrificial material post printing at a desirable temperature or in a suitable solvent; the removal of the sacrificial core is challenging(Norotte et al., 2009 ; Shao et al., 2020). While a core flow of air does not have the integrity to support the tubular shape of the fiber, a core flow of crosslinker in foam shape can provide the required support and crosslinker to the fiber. Additionally, the compressibility of the foam can allow for fabricating fibers with dimensions different from the nozzle. Therefore, fabrication of hollow fibers using foam as a sacrificial core can address the limitations of solid sacrificial methods and liquid crosslinkers.

In this study, a foam-based crosslinking method is developed to allow direct coaxial bioprinting of hollow fibers. Sodium alginate, an ionically crosslinking polymer, is used in sheath flow as it offers excellent properties such as water solubility and biocompatibility, and it can crosslink with a wide range of crosslinkers at a desirable pace(Ahmad Raus, Wan Nawawi, & Nasaruddin, 2021 ; Jadach, Świetlik, & Froelich, 2022). Albumin, a well-known biocompatible and biodegradable foaming agent (Abeyrathne et al., 2013 ; Çalışkan Koç et al., 2022 ; Karimi et al., 2016), is used to deliver crosslinker ions to the bioink. The porous nature of the albumin foam provides adequate crosslinker to the inner core of the fiber for controlled gelation while the majority of its volume is air. The presence of the air minimizes the leaching of bio-compounds embedded into the bioink to crosslinker foam. While the gelation occurs from the inside of the fiber, it creates an excellent layer adhesion for the fiber while printing. The foam eliminates the over-pooling of liquid crosslinker on the printbed, and additionally, by controlling the inlet flow of foam and bioink, it is possible to fabricate a fiber with varying diameter and wall thickness during the printing step.

3.3 Materials and methods

3.3.1 Materials preparation

Sodium alginate solution with 1, 2, and 3% w/v concentrations were prepared by adding sodium alginate powder (Sigma-Aldrich, USA) to deionized (DI) water and then stirring at 600 rpm for 5 hours. Crosslinker foams with various concentrations and ratios of calcium chloride ($CaCl_2$) and albumin were prepared and used to crosslink sodium alginate. Calcium chloride solution was prepared by stirring $CaCl_2$ powder (Sigma-Aldrich, USA) in DI water at 500 rpm for 1 hour. Subsequently, egg albumin (Sigma-Aldrich, USA) was added to the solution and stirred at 600 rpm for 2 hours. The solution was mechanically foamed at high speed (TM-300HMCN, Toastmaster Hand Mixer) for 90 seconds to obtain a homogenous foam. The process of mechanical foaming increased the crosslinker volume by 750%, hence the final concentration of albumin and $CaCl_2$ in the foam dropped from the initial concentrations in solution (4% or 8% w/v) to 0.53% or 1.07% w/v in foam, respectively. Table 3.1 presents all the final concentrations used to fabricate the hollow fibers.

Table 3.1 Final compositions of crosslinker foam and sodium alginate used for hollow fiber fabrication

Compositions	Albumin (% *w/v*)	$CaCl_2$ (% *w/v*)	Sodium Alginate (% *w/v*)
AL4CC4SA1	0.53	0.53	1
AL4CC4SA2	0.53	0.53	2
AL4CC4SA3	0.53	0.53	3
AL4CC8SA1	0.53	1.07	1
AL4CC8SA2	0.53	1.07	2
AL4CC8SA3	0.53	1.07	3
AL8CC4SA1	1.07	0.53	1
AL8CC4SA2	1.07	0.53	2
AL8CC4SA3	1.07	0.53	3
AL8CC8SA1	1.07	1.07	1
AL8CC8SA2	1.07	1.07	2
AL8CC8SA3	1.07	1.07	3

3.3.2 Fabrication setup

Hollow fibers were fabricated with a co-flow of crosslinker foam (as the inner flow) and alginate solution (as the outer flow) through a coaxial needle with a 20G inner needle (584 µm inner diameter and 889 µm outer diameter) and a 16G outer needle (1190 µm inner diameter and 1650 µm outer diameter). Syringe pumps were used to control the flow rates of both foam and alginate solution. Alternatively, for the foam flow, the built-in pressure system of the 3D bioprinter (BioX, Cellink) was also used to extrude crosslinker foam through the coaxial needle. The printing setup and a schematic of the inlet flows for printing are shown in Fig 3.1.

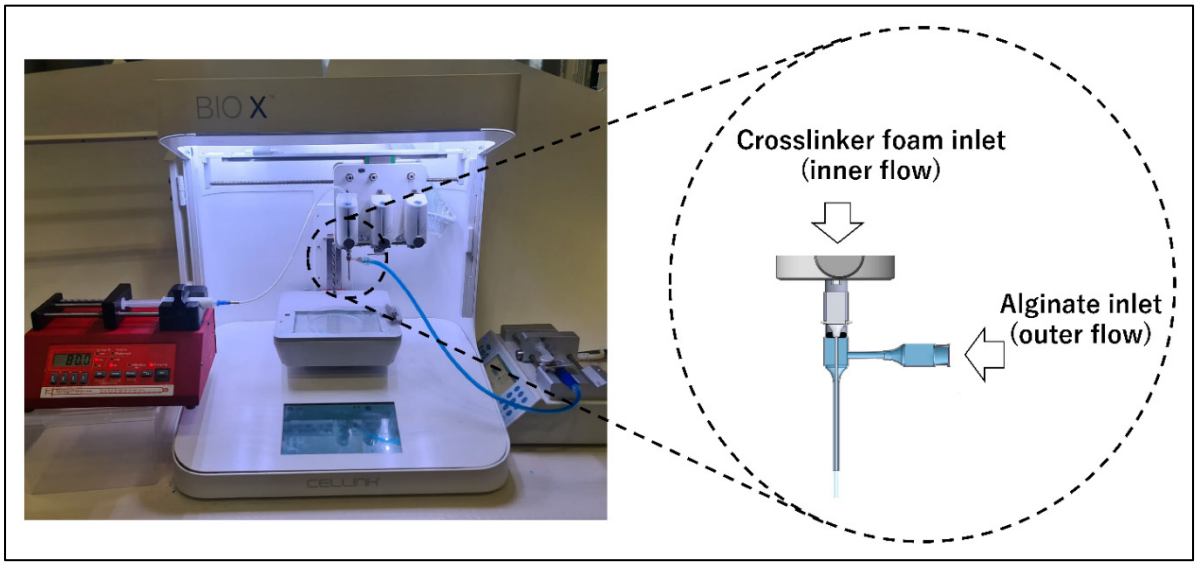

Figure 3.1 The printing setup and a schematic of the inlet flows

3.3.3 Mechanical properties

The mechanical properties of the hollow fibers were characterized by the breaking strain and filament collapse tests. Using an in-house built system(Choo et al., 2010), tensile testing was conducted on the 1.2 mm diameter filaments immediately after the fabrication. The individual filaments were softly gripped(Mohammadpour, Kharaziha, & Zarrabi, 2023) to prevent the filament from breaking at the grip point at an initial distance of 50 mm. The filaments were

elongated at a rate of approximately 1 cm/s and the distance between the grip points was also measured at the time of breaking the filament. Various sodium alginate and crosslinker compositions listed in Table 3.1 were used with flow rates of 40 and 140 ml/h, respectively. the breaking strain was calculated as:

$$E = \frac{L_1 - L_0}{L_0}, \tag{3.1}$$

where L_0 and L_1 are the initial and breaking lengths of the fibers, respectively.

Filament collapse tests were performed on AL4CC8SA1 and AL8CC8SA2 filaments which exhibited the lowest and highest breaking strains to identify the time dependent deflection of the filament(Ribeiro et al., 2017 ; Therriault, White, & Lewis, 2007). To briefly explain the procedure, a platform with 2 mm width pillars was designed and 3D printed by a commercial 3D printer (Ender-3 V2, Creality). The gap between the pillars (L) was set to be 2, 4, 8, and 16 mm and the hollow fiber was printed directly on the platform. The displacements of the filaments were filmed with a compact camera (Canon PowerShot, SX740 HS) at 25 fps and the maximum deflection of filament for each gap was measured using an image processing software (Fiji, ImageJ) up to 10 seconds when no apparent movement was observed afterwards.

3.3.4 Diameter and wall thickness control

Based on the results of the breaking strain study, AL8CC8SA2 composition was selected to investigate the effect of alginate and crosslinker foam flow rates on the diameter and the wall thickness of the fibers. Various AL8CC8SA2 fibers with the flow rates listed in Table 3.2 were fabricated and observed under the microscope. Images were taken using a high-resolution microscope camera (MU1803-HS, AmScope) and an image processing software was used to analyze the images and measurements.

Table 3.2 Flow rates used for the diameter and wall thickness control of the hollow fibers

Flow rates	Alginate (ml/h)	Crosslinker foam (ml/h)
FR-20-80	20	80
FR-20-140	20	140
FR-20-200	20	200
FR-40-80	40	80
FR-40-140	40	140
FR-40-200	40	200
FR-60-80	60	80
FR-60-140	60	140
FR-60-200	60	200

3.3.5 Printability

To examine the printability with the proposed method, a hollow cylinder with a 15 mm diameter and 10 mm height and a cuboid with 15 mm width and length and 10 mm height was printed using the 3D bioprinter. Additionally, 2-layer grid scaffolds were printed to measure the printability number of AL8CL8SA1, AL8CL8SA2, and AL8CL8SA3 fibers. The printability number was calculated as:

$$Pr = \frac{L^2}{16\,A}, \tag{3.2}$$

where L and A are the perimeter and area of the pores in the printed scaffolds, respectively(Butler, Naseri, MacDonald, Andrew Tasker, & Ahmadi, 2020 ; Ouyang et al., 2016). The samples were printed with 32 kPa pressure from the built-in pressure system of the bioprinter for the foam extrusion. The flow of alginate was provided by a syringe pump at a flow rate of 20 ml/h, and the printing speed was set to 14 mm/s.

3.3.6 Cell viability

To investigate the impact of $CaCl_2$ release from the fibers on cell viability, the viability of Neuro-2a cells seeded on scaffolds printed using different concentrations of sodium alginate and crosslinker compositions (AL4CC4SA3, AL4CC8SA1, AL4CC8SA3, AL8CC8SA3) was investigated over 7 days. It must be mentioned that due to the intrinsic limitations of the alginate, the seeded cells detach from the fiber surface and attach to the bottom of the culture plate. The scaffolds were printed on tissue-culture-treated dishes, sterilized under ultraviolet (UV) light for 10 min, and subsequently seeded with approximately 300,000 Neuro-2a cells. The dishes were then incubated at 37 ºC with 5% CO_2, and the culture media was changed every 3 days.

On days 3 and 7, cells were stained with 4'6-diamidino-2-phenylindole dihydrochloride (DAPI) and propidium iodide (PI) (5 µg/ml) and incubated for a total of 15 and 30 min, respectively, then imaged using a fluorescence microscope (Revolve 3, Echo). For a standardized area, blue (all cells) and red (damaged cells) channels were separated and the color intensities were normalized using a grayscale filter, consequently, images were analyzed using image processing software (Fiji, ImageJ). The cell viability percentage was calculated as(Badr et al., 2022):

$$\text{Cell viability } \% = \left(1 - \frac{\text{damaged cells}}{\text{all cells}}\right) \times 100, \tag{3.3}$$

3.3.7 Permeability

To characterize the permeability of the hollow fibers and investigate the impact of albumin on the permeability, rhodamine B, a model drug(Elias Madadian et al., 2023), was incorporated into the crosslinker foam (0.1% w/v). Based on the results of the mechanical properties study, the release of Rhodamine B in DI water was investigated on AL8CC8SA2 and AL4CC8SA2

compositions. Filaments with 7 cm lengths were made with the same fabrication parameters used for breaking strain tests. Both ends of the filaments were clipped to prevent the direct release of rhodamine B and immediately placed in 30 ml DI water while stirring at 100 rpm. After 30 minutes, 1 ml of the medium was taken and the release of rhodamine B was assessed using a UV-Vis spectrometer (UV-3100PC, VWR) at $\lambda = 554$ nm.

3.3.8 Statistical analysis

Design Expert software and Microsoft Excel data analyzer with analysis of variance (ANOVA) were used to implement the statistical analysis of data. In all steps, p-values smaller than 0.05 were considered statistically significant. Tukey post hoc analysis was used to compare each two groups of the data. Each experiment was implemented in triplicates, and the results are reported as mean values ± standard deviations.

3.4 Results and discussions

3.4.1 Mechanical properties

A schematic of the initial length and the breaking length of the filament is shown in Fig 3.2a and breaking strains for various compositions of bioinks and crosslinker foam are shown in Fig 3.2b. The breaking strain of hollow fibers plays a crucial role in fabrication of hollow fibers as it determines the strength and reliability of the printed structure. Exhibiting a low breaking strain may lead to the failure of fibers under stress, which compromises the integrity and function of the structure for the intended application. Maximum and minimum breaking strains observed belong to AL8CC8SA2 and AL4CC8SA1 with values of 0.63 ± 0.05 and 0.30 ± 0.04, respectively. Increasing the alginate concentrations from 1% to 2% leads to an overall increase in the breaking strain, particularly for higher concentrations of calcium chloride. However, the same trend was not observed when the alginate concentration was increased from 2% to 3% due to an increase in the number of uncrosslinked alginate chains. The breaking strains of fibers

fabricated with the same concentrations of $CaCl_2$ and alginate indicate that changing the concentration of albumin has no significant effect on the breaking strain: albumin does not crosslink with alginate. Increasing the concentration of $CaCl_2$ increased the breaking strain in samples with 2% and 3% w/v alginate due to an increased crosslinking density of alginate. The increase in crosslinker concentration had no significant impact on samples with 1% w/v alginate as all the alginate chains crosslinked rapidly with the crosslinker.

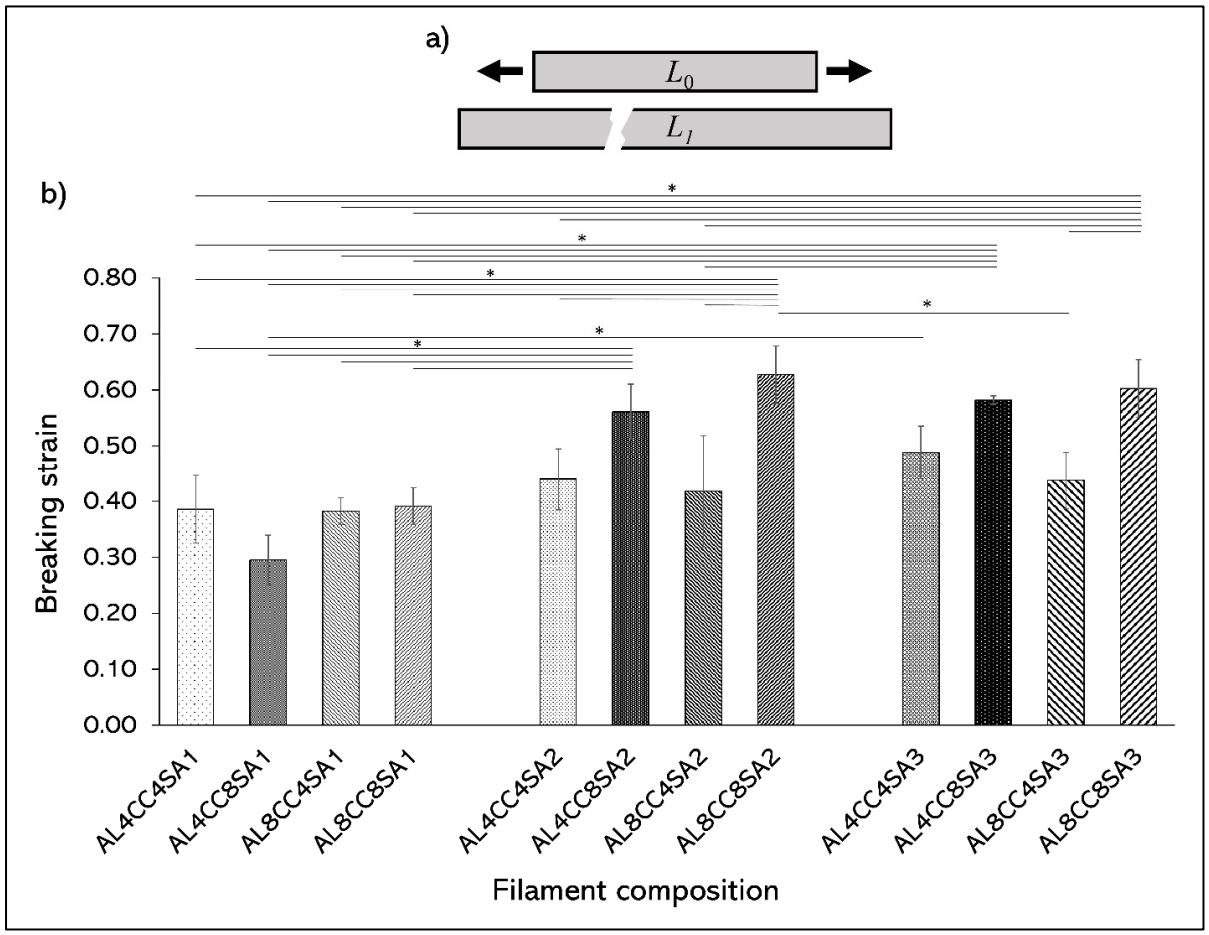

Figure 3.2 a) Schematic demonstration of the initial length and the breaking length of the filament. b) Breaking strain for fibers with various compositions. Asterisks show significant differences ($p < 0.05$)

The results of the filament collapse tests are shown in Fig 3.3. As expected, both AL4CC8SA1 and AL8CC8SA2 filaments showed an increase in sagging as *L/d* increased. The maximum deflection for AL4CC8SA1/AL8CC8SA2 filaments was measured at 146/131 µm and 23/15 µm for *L/d* = 12.9 and 1.6, respectively. The deflection of the filament is affected by two main factors: the crosslinking level of the hydrogel and the weight of the filament between the two pillars. The maximum deflection for *L/d* ≤ 6.5 mm is not considerable as the deflection is lower than 5% of the filament diameter confirming that the filament can hold the integrity of the structures under the stress caused by its weight. While AL4CC8SA1 filaments are slightly lighter than AL8CC8SA2 filaments due to the albumin and alginate concentrations, they didn't show a significantly different deflection for the tested gaps. The overall low weight of the hollow fibers caused by the foam support makes the deflections considerably lower than the solid (non-hollow) fibers reported in the literature(Cai, Heid, Boccaccini, Aldo Boccaccini, & Y W O R D S Ada-, 2021 ; Gonzalez-Fernandez, Tenorio, Campbell, Silva, & Leach, 2020).

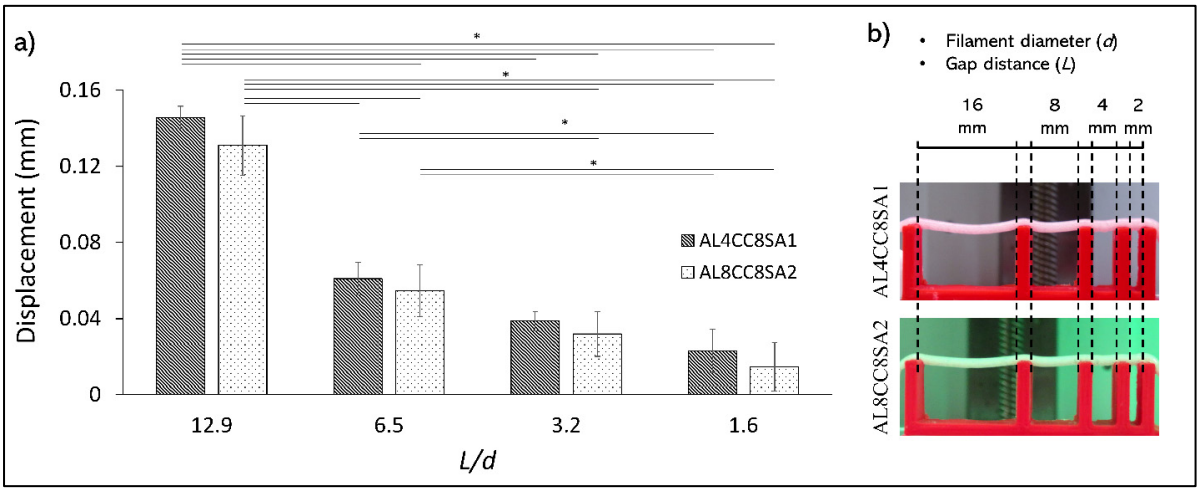

Figure 3.3 a) Time dependent deflection of AL4CC8SA1 and AL8CC8SA2 filaments for various *L/d*, 10 seconds after printing. Asterisks show significant differences ($p < 0.05$). b) Snapshots of the filament collapse test 10 seconds after the filament fabrication on the pillars

3.4.2 Diameter and wall thickness control

Wall thickness and outer diameter of AL8CC8SA2 fibers fabricated with different bioink and crosslinker flow rates are shown in Fig 3.4. The maximum/minimum wall thickness and outer diameter measured were 81.2/3.4 and 1564.0/829.5 µm, respectively. Increasing the alginate flow rate increased the wall thickness and decreased the diameter of the fibers, while increasing the foam flow had the opposite effect. The increase in foam flow rate leads to a higher radial force from inside the fiber and consequently increases the final outer diameter and decreases the wall thickness. The increase in alginate flow rate leads to an increase in the wall thickness and consequently, increased resistance against the radial force from the inside foam. The use of crosslinker in the foam form provides a wider range of filament diameter compared to the use of liquid crosslinker reported in the literature(Q. Gao et al., 2015).

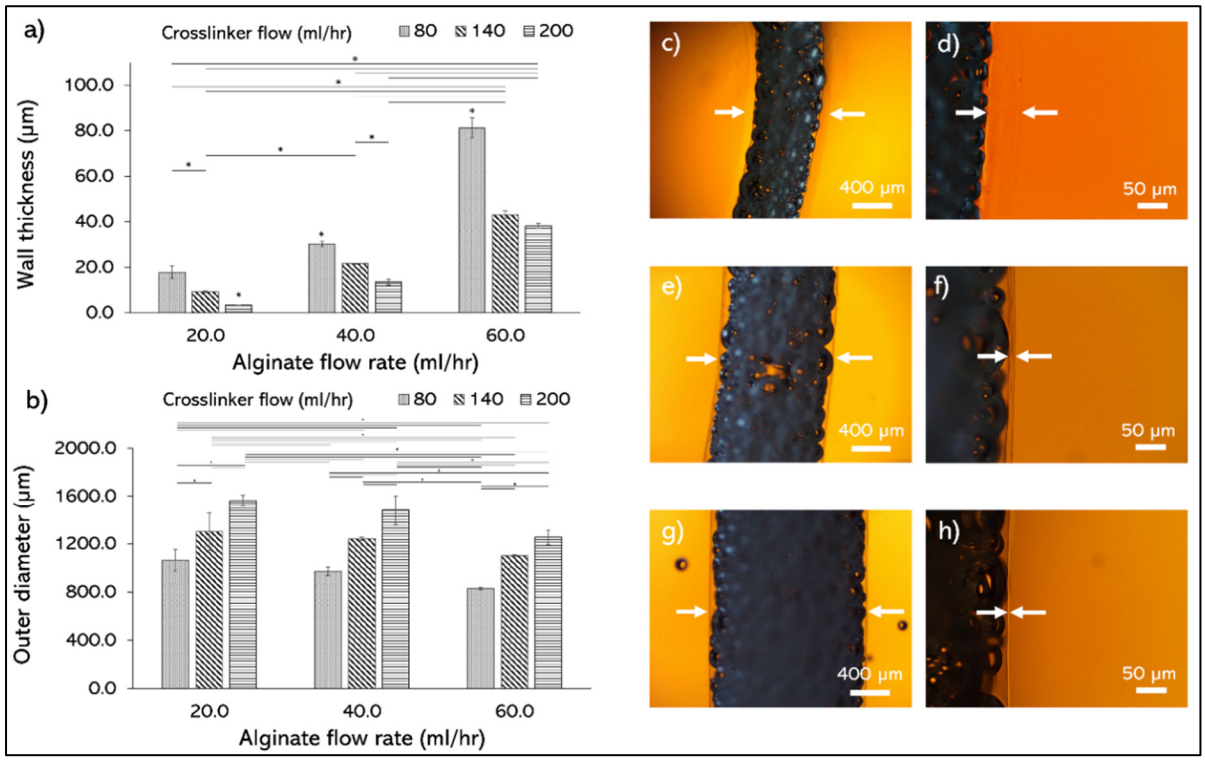

Figure 3.4 a) Wall thickness and b) outer diameter of AL8CC8SA2 fibers with fabricated various flow rates of alginate and crosslinker foam. Asterisks show significant differences (*p*

< 0.05). c-d, e-f, and g-h demonstration of outer diameter and wall thickness of fibers fabricated with FR-60-80, FR-40-140, and FR-20-200, respectively

3.4.3 Printability

Structures printed with AL8CC8SA2 composition are shown in Fig 3.5a-c. A 15×15×10 mm cuboid is shown in Fig 3.5a and to show the layer adhesion, the petri dish is kept vertically in Fig 3.5b. Since the diffusion of crosslinker ions is from the inner surface of the fiber, outer layers will adhere to each other before the present alginate polymers are fully crosslinked. Fig 3.5c shows a hollow cylinder with a diameter of 15 mm and a height of 10 mm. Fig 3.5d-f are the 3×3 cm square scaffolds printed with AL8CC8SA1, AL8CC8SA2, and AL8CC8SA3 bioinks, respectively (Supplementary video S1). While the printability number of all printed scaffolds are in the acceptable range of 0.9 to 1.1 (for an ideal condition of $Pr = 1$) (Butler et al., 2020 ; Ouyang et al., 2016), the increase of the alginate concentration increased the printability number as a result of a higher crosslinking density. Compared to other reported hollow fiber fabrication techniques, the use of foam as support material offers a removal mechanism that does not affect the integrity and fidelity of the printed construct as no external force is necessary for the removal of inner support. The printability number for the middle squares of the samples was calculated at 0.911, 0.920, and 0.936, respectively.

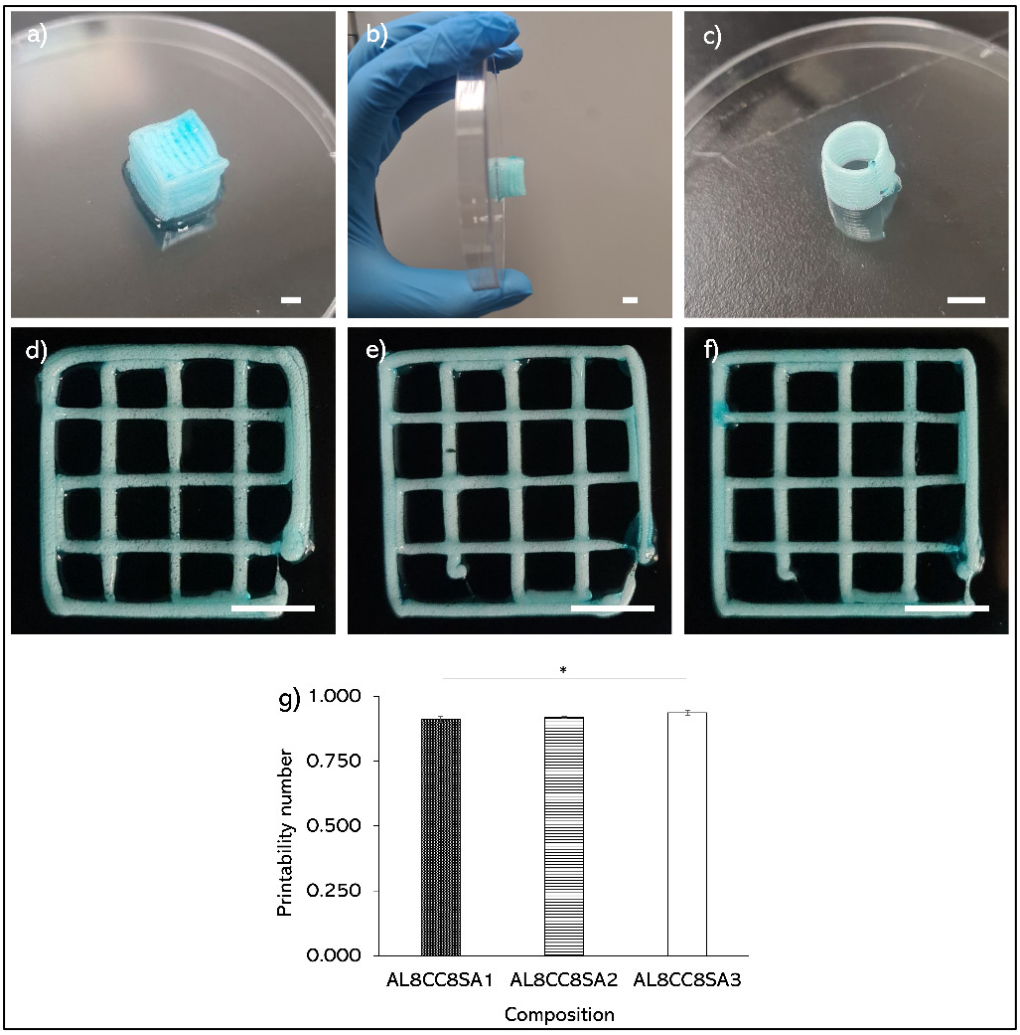

Figure 3.5 a-b) 15×15×10 mm cuboid on a petri dish and held vertically to demonstrate the layer adhesion. printed with AL8CC8SA2 composition. c) A hollow cylinder printed with AL8CC8SA2 composition, d-f) 30×30 mm grid scaffolds printed to calculate printability number with AL8CC8SA1, AL8CC8SA2, and AL8CC8SA3 compositions, respectively. g) Printability number calculated for grid scaffolds. Asterisks show significant differences ($p < 0.05$). Scale bars are 5 mm

3.4.4 Changing the foam phase over time

Fig 3.6a-f show the change of foam within a printed AL8CC8SA2 fiber submerged (after printing) in DI water inside a petri dish for various time points. The bubbles in the foam start to merge and while the fiber is submerged in liquid, the surrounding liquid penetrates the fiber.

Eventually, the surrounding liquid substitutes the air within the fiber. Fig 3.6g-h show the change of foam in a 15×15×10 mm cuboid 3D printed with AL8CC8SA2 fiber without being submerged in the liquid immediately after printing and after 24 hours, respectively. When the printed structure is not submerged in liquid, the coalescence of the bubbles results in changing the foam phase back to the liquid phase leaving the crosslinked structure with hollow fibers. Fig 3.6i shows the cross section of the cube illustrating the hollow fibers within the 3D printed structure. Fig 3.6j shows a fiber perfused with DI water and red dye with microscopic images of various sections of the fiber. After the perfusion, no visual trace of foam remains within the structure. Furthermore, the effect of the bubbles on the interior surface of the hollow fibers was investigated through microscopic videos before and after perfusing a fiber. Supplementary video S2 shows the fiber wall with the bubbles within the fiber under the microscope before the perfusion. Supplementary video S3 shows the same fiber wall after the perfusion. As observed in Fig 3.6j and supplementary videos S2 and S3, the bubbles do not result in significant variation of the inner diameter.

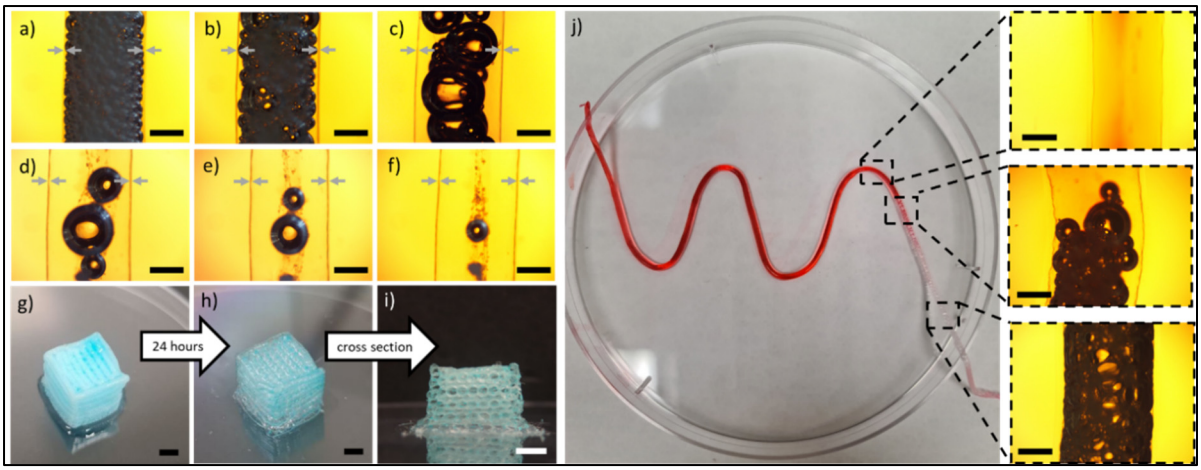

Figure 3.6 a-f) The change of bubbles at AL8CC8SA2 fiber fabricated with FR-40-140 flow rates right after printing, 2 hours, 8 hours, 48 hours, 72 hours, and 96 hours after printing, respectively. Arrows show the wall thickness and scale bars are 500 µm. g-i) Change of foam in 24 hours for a 15×15×10 mm cuboid printed with AL8CC8SA2 composition and a cross section of the cube showing the hollow fiber. Scale bars are 5 mm. j) Perfusion of an AL8CC8SA2 fiber and enlarged sections of various sections of the fiber. Scale bars are 500 µm

3.4.5 Cell viability

Cells were imaged on days 3 and 7, and the overlay of fluorescence images and quantitative viability results are shown in Fig 3.7. The viability percentage for AL4CC4SA3, AL4CC8SA1, AL4CC8SA3, AL8CC8SA3, and control on days 3/7 are 99/95%, 98/93%, 97/92%, 99/93%, 99/95%, respectively. The different concentrations and ratios of sodium alginate (1,3% w/v), albumin (0.53, 1.07% w/v), and $CaCl_2$ (0.53, 1.07% w/v) used in this study did not affect the cell viability, as no significant differences among the various groups and controls were observed. Additionally, there was no significant difference between the viability % of cells seeded on the scaffolds and the control group. It was observed that clusters of cells grow near the printed fibers indicating that the release of $CaCl_2$ from the fibers does not prohibit the cell growth. Thus, the presence of albumin and $CaCl_2$ does not compromise cell viability, suggesting that scaffolds crosslinked using the proposed method are biocompatible with Neuro-2a cells. Furthermore, it has been previously reported that cells used with albumin/alginate scaffolds exhibited high viability (Delkash et al., 2021 ; S. Liu et al., 2020).

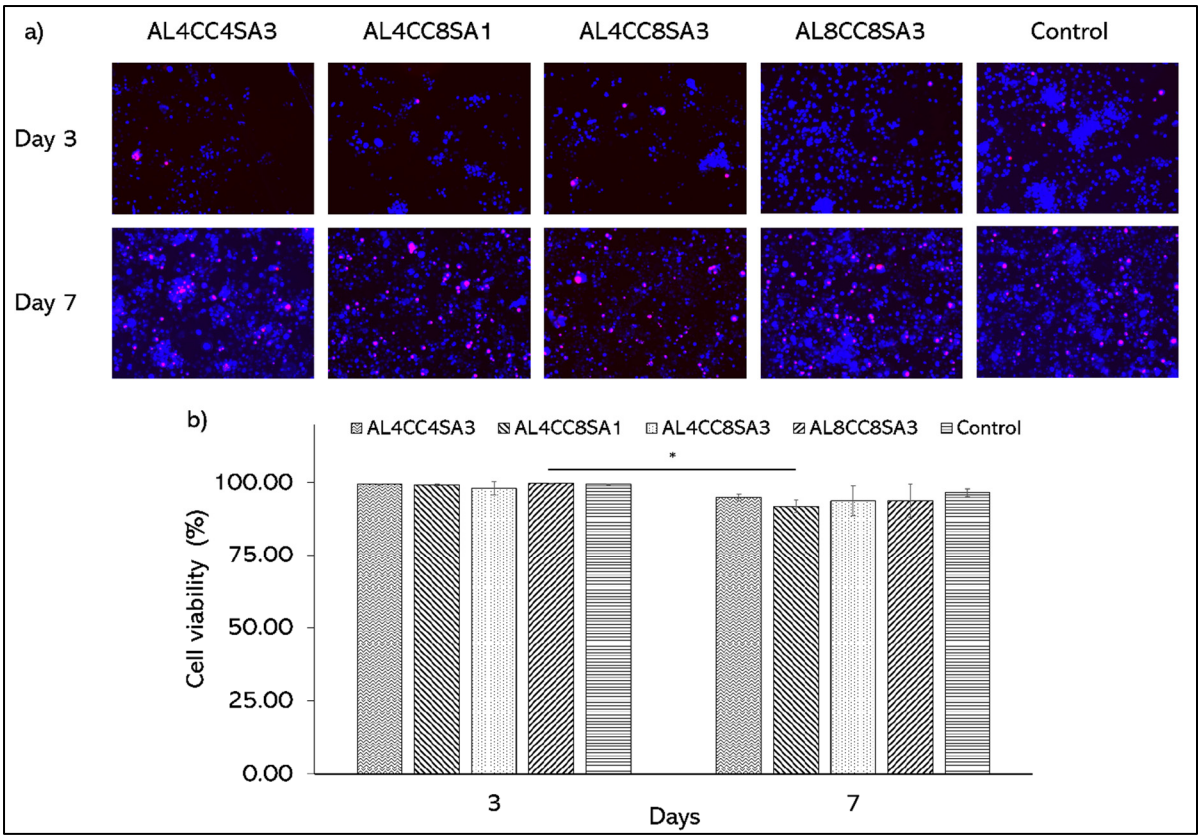

Figure 3.7 a) fluorescence images of cells stained with DAPI (blue) and PI (red), and b) quantitative cell viability results for AL4CC4SA3, AL4CC8SA1, AL4CC8SA3, AL8CC8SA3, and control group on days 3 and 7. Asterisk shows significant difference ($p < 0.05$)

3.4.6 Permeability

Fig 3.8a shows the release of rhodamine B in DI water from AL4CC8SA2 and AL8CC8SA2 compositions after 30 minutes. Fig 3.8b and 8c show the average diameter of the bubbles and the bubble size distribution for 600 bubbles in AL4CC8 and AL8CC8 foams, respectively. Fig 3.8d and 3.8e show microscopic images of AL4CC8 and AL8CC8 right after mechanical foaming, respectively. The release of 65.56 ± 8.37% was measured for AL8CC8SA2 filaments which is 24.8% less compared to the release from AL4CC8SA2 filaments. The size of bubbles was measured at 122.61 ± 5.64 µm and 117.51 ± 11.50 µm for AL4CC8 and AL8CC8 foams,

respectively. The average size and distribution of the bubbles in the crosslinker foams are not significantly different and the concentrations of alginate (2%) and $CaCl_2$ (1.07%) are the same in both compositions. Subsequently, the reduction in the release of rhodamine B is attributed to the increase of albumin concentration rather than the crosslinking density of the alginate wall. The results of the breaking strain tests shown in Fig 3.2b support this conclusion as no pair of the filaments made with different concentrations of albumin and the same concentrations of alginate and $CaCl_2$ had a significantly different breaking strain.

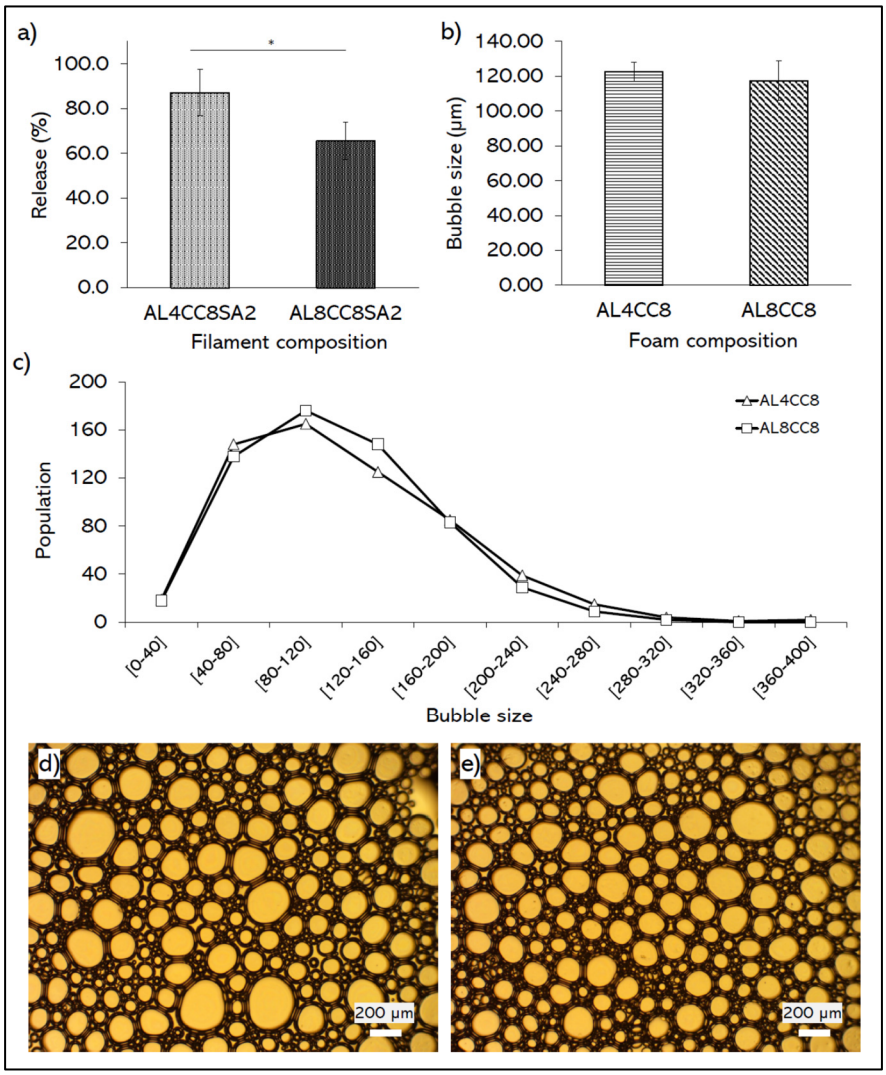

Figure 3.8 a) The release of rhodamine B in DI water from AL4CC8SA2 and AL8CC8SA2 compositions after 30 minutes. b) the average diameter of the bubbles in AL4CC8 and AL8CC8 foams

right after mechanical foaming. c) Bubble size distribution for 600 bubbles in AL4CC8 and AL8CC8 foams. d and e) Microscopic images of a single layer of AL4CC8 and AL8CC8 foams, respectively

3.5 Conclusion

In this work, a method to expose the bioink to the crosslinker is introduced and successfully utilized to fabricate crosslinked and perfusable alginate hollow fibers. Foam functioned as an excellent substitute for sacrificial material used in coaxial extrusion systems which offers promising control on the diameter and the wall thickness of the filament. The proposed method addresses the issues associated with the use of liquid crosslinker in the printing process which includes over-crosslinking of the hydrogel and the necessity of performing extra steps to remove the excess liquid from within the filament and the printbed. Increasing the alginate concentration from 1% to 2% led to an increase in the breaking strain while the concentration of albumin had no significant effect on the breaking strain. Several structures were successfully printed using this method showing a perfect layer adhesion and for printed grid scaffolds an acceptable printability number (0.9 – 1.1) was calculated. Additionally, the proposed method showed excellent cell viability for Neuro-2a cells over a seven day period. The results of this study can be used in drug release and tissue engineering applications for fabrication of complex structures as the fabricated hollow fibers can mimic blood vessels and vascular networks.

3.6 Funding

This work was supported by the National Sciences and Research Council of Canada (Discovery Grant RGPIN-2017-05272) and Canada Foundation for Innovation (John R. Evans Leader Fund 37696).

CHAPTER 4

IN-FOAM BIOPRINTING: AN EMBEDDED BIOPRINTING TECHNIQUE WITH SELF-REMOVABLE SUPPORT BATH

E. Madadian [a,b,#], H. Ravanbakhsh [a,b,#], F. Touani Kameni [b,c], M. Rahimnejad [b,c], S. Lerouge [a,b,c*], and A. Ahmadi [a,b*]

[a] Department of Mechanical Engineering, École de technologie supérieure, Montreal, QC, Canada
[b] Biomaterials and Biofabrication Lab (BBF), Centre de Recherche du Centre Hospitalier de l'Université de Montréal (CRCHUM), Montreal, QC, Canada
[c] Department of Pharmacology and Physiology, University of Montreal, Montreal, QC, Canada

[#] Elias Madadian and Hossein Ravanbakhsh should be considered joint first author.
[*] Correspondence: ali.ahmadi@etsmtl.ca; sophie.lerouge@etsmtl.ca

Paper submitted for publication in *Advanced Functional Materials*, July 2023

4.1 Abstract

The emergence of embedded three-dimensional (3D) bioprinting has revolutionized the biofabrication of free-form constructs out of low-viscosity and slow-crosslinking hydrogels. Using gel-based support baths has limitations including lack of proper oxygenation and nutrition and complications with bath removal. Here, a novel embedded 3D bioprinting technique is developed with an albumin foam support bath as a promising substitute. The proposed technique, in-foam bioprinting, offers excellent printability and convenience in bath removal while providing cells with easy access to oxygen and nutrients. The foam-based support bath is characterized through foam stability and rheological tests. The bubble size in the foam is measured to study the change in the structure of the bath due to the coalescence of the bubbles over time. Free-form structures are successfully 3D printed with thermo-responsive chitosan-based bioinks to demonstrate the capability of the in-foam bioprinting technique. The viability of bioprinted fibroblast L929 cells is studied over a seven-day period, showing high cell viability of over 97%, which is attributed to the abundance of oxygen and

nutrition in the foam support bath. Importantly, in-foam bioprinting is beneficial for biofabricating large samples with a long printing time without jeopardizing cell viability.
Keywords: Biofabrication, Embedded bioprinting, Albumin foam, Chitosan hydrogel, Tissue engineering

4.2 Introduction

Three-dimensional (3D) bioprinting is the method of fabricating cell-laden biological constructs in a layerwise manner.(Murphy & Atala, 2014) Owing to its simplicity, extrusion bioprinting, which works based on the programmed deposition of cell-laden bioinks on a build plate, is the most prevalent and inexpensive technique among various modalities of bioprinting.(Ravanbakhsh, Karamzadeh, et al., 2021 ; Y. S. Zhang et al., 2021) One of the critical bottlenecks for the development of extrusion bioprinting is the paucity of biocompatible, yet printable bioinks.(Ravanbakhsh, Bao, et al., 2021) Specifically, many biocompatible hydrogels do not possess sufficient mechanical and rheological properties to be 3D bioprinted.(Askari et al., 2021) A strategy to address the above-mentioned limitation of extrusion bioprinting is using a support bath for bioprinting low-viscosity materials to maintain high shape fidelity.(Zhou et al., 2022) The method, generally known as embedded 3D bioprinting, was introduced in 2011(W. Wu, Deconinck, & Lewis, 2011) and later expanded through different terminologies: self-healing hydrogels,(Highley et al., 2015) granular hydrogels,(Bhattacharjee et al., 2015) and freeform reversible embedding of suspended hydrogels (FRESH).(Hinton et al., 2015)

Embedded 3D bioprinting has outperformed conventional extrusion methods in terms of printing resolution, free-form printing, and the versatility of compatible bioinks.(Bao et al., 2020) An important aspect of this technique is the choice of material for the support bath. Various materials, such as Pluronic F127,(Rocca et al., 2018) gelatin,(Lee et al., 2019) Carbopol,(Abdollahi, Davis, Miller, & Feinberg, 2018 ; Hinton, Hudson, Pusch, Lee, & Feinberg, 2016) hyaluronic acid,(Song, Highley, Rouff, & Burdick, 2018) agarose,(Cidonio et

al., 2019) gellan gum,(Compaan, Song, & Huang, 2019) xanthan gum,(Noor et al., 2019) Laponite nanoclays,(Jin et al., 2017) and poly(ethylene oxide)(G. Tang et al., 2023) have been utilized as support baths so far. Although embedded 3D bioprinting in its current format is conducive to biofabricating superlative constructs out of low-viscosity bioinks, there are several considerations and limitations when gel-based support baths are utilized. Primarily, the lack of proper oxygenation and nutrient diffusion to the bioprinted cell-laden constructs before the bath removal may cause necrosis or hypoxia-induced apoptosis, which is a major obstacle to keeping the cells viable during long gelation processes, e.g., thermal gelation.(Rahimnejad et al., 2022 ; Tomasina, Bodet, Mota, Moroni, & Camarero-Espinosa, 2019) Furthermore, some bath removal mechanisms can be detrimental to cell viability and structural fidelity, especially when lowering the temperature or mechanical agitation is the only way to remove the bath.(Q. Li et al., 2022) Moreover, removing gel support from cavities and confined parts of the printed structure can be cumbersome. Scant attention has been devoted to rectifying such deficiencies associated with embedded 3D bioprinting. Therefore, there is a need for developing nutrient- and oxygen-enriched support baths that can be conveniently removed to overcome the above-mentioned issues.

Albumin, a well-known foaming agent,(Abeyrathne et al., 2013 ; E. Madadian, Badr, MacDonald, Tasker, & Ahmadi, 2023 ; Elias Madadian et al., 2023) has been previously used as a biocompatible and biodegradable material.(Bajpai & Saini, 2006) It is a natural water-soluble protein present in human blood, bovine serum, and chicken egg white.(Karimi et al., 2016) Mechanical mixing of albumin solution denatures the protein structure and creates long protein chains exposed to the surrounding environment. This phenomenon allows hydrophilic and hydrophobic groups to trap the adjacent gas phase (i.e., surrounding air) within the solution and subsequently, create foam when mechanically mixed.(X. Duan et al., 2018 ; Gharbi & Labbafi, 2019) After foaming, the liquid phase of the foam flows downward due to its higher density.(Gharbi & Labbafi, 2019) We hypothesize that by employing amphipathic molecules, such as egg white albumin as the support bath in bioprinting, the gradual coalescence of bubbles would be advantageous to further simplify the removal of the support bath thus

extracting the printed structures after the bioprinting process. Other possible advantages of albumin foam as the support bath can include the ease of access to the surrounding oxygen in the gas phase rather than the limited dissolved oxygen in conventional baths(Carmeliet & Jain, 2000) and the possibility of providing cells with nutrients during bioprinting via enriching the foam solution with cell culture media.

In this work, we introduced in-foam bioprinting (Figure 4.1), a method of biofabrication based on using albumin foam as the support bath for bioprinting free-form structures out of low-viscosity slow-crosslinking hydrogels in a biocompatible setting. We tested different concentrations of albumin with various foaming times to determine the optimum experimental conditions for creating the foam. Rheological and physical characterization of the foam revealed that the bubbles in the foam play an important role in making a self-removable substrate for bioprinting. We have shown that a unique advantage of using foam-based support baths in embedded bioprinting is the capability of bubbles to merge after bioprinting, resulting in a sacrificial support bath. As proof of concept, the in-foam bioprinting technique was used for bioprinting various structures with chitosan-based thermosensitive hydrogels, that are not printable using conventional bioprinting modalities due to their low viscosity and long gelation time. The cell compatibility of the process was demonstrated using L929 fibroblasts as a model cell. The results support the fact that in-foam bioprinting can be readily employed for fabricating complex cell-laden structures with applications in tissue engineering and therapeutic technologies.

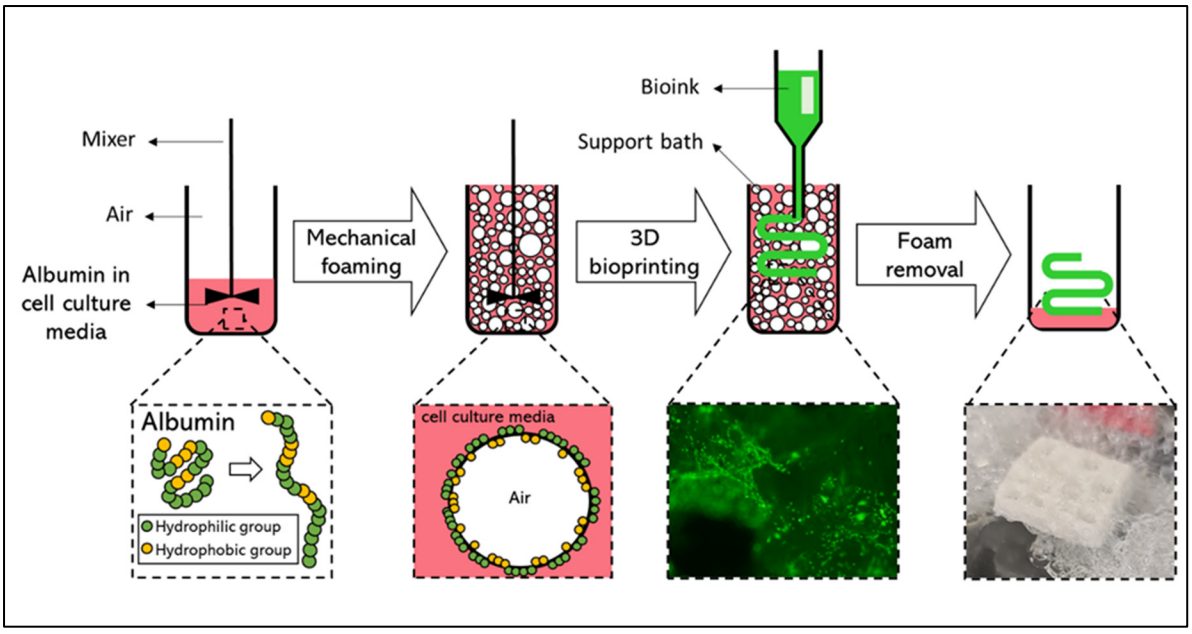

Figure 4.1 Schematic illustration of the in-foam bioprinting process. The chicken egg white albumin foam was prepared by mechanical mixing of albumin powder in cell culture media. The produced foam was then employed as the support bath for bioprinting cell-laden constructs

4.3 Results and discussions

4.3.1 Rheology

An ideal support bath must be stable over the period of bioprinting. It must be able to recover its original state and rheological properties, such as storage modulus, after the bioprinter nozzle moves inside it. Albumin support bath groups (i.e., foams with different concentrations of albumin) were first characterized to assess their stability at the bioprinting temperature, i.e., 37 °C, via time sweep tests. Their shear thinning and recovery behaviors at 37 °C were also studied. The main results of rheological tests are presented in Figure 4.2, for a foaming time of 2 min (left) or 4 min (right), and described in detail in the following sections.

4.3.1.1 Time sweep

Figure 4.2A shows the storage modulus over time for various baths mechanically foamed for 2 minutes. The storage modulus slowly decreased over time for all the foam compositions. However, it was more stable for concentrations of 12% and 8% w/v albumin compared to 4% w/v albumin. Within 30 min, *G'* decreased from ~280 Pa to 220 Pa, i.e., 21% decrease for albumin 12%, from ~250 Pa to 180 Pa, i.e., 28% decrease for albumin 8%, and from ~270 Pa to 140 Pa, i.e., 48% decrease for albumin 4%. Such decrease in storage moduli can be explained by bubbles merging and coalescence over time. When the foaming time increased to 4 min, higher *G*' was observed for all formulations, as shown in Figure 4.2B. Longer foaming time resulted in unfolding more albumin proteins in the liquid phase of the foam. This phenomenon resulted in stiffer bubbles and increased *G*' for samples foamed for 4 min. The collapse of stiffer foam over time resulted in a sharper decrease of storage modulus in the 4-min foamed albumin. A decrease of ~65% in the storage modulus for these samples indicates that although increasing the foaming time boosts the storage modulus, the stability of the storage modulus is negatively affected, which is not preferable in embedded bioprinting. It was concluded that 2 min of mechanical foaming is sufficient for making stable foam.

4.3.1.2 Shear-thinning viscosity

The support bath must maintain a shear-thinning behavior in order not to hinder the movement of the bioprinting needle(Rahimnejad et al., 2022). The viscosity of the support bath was studied as a function of applied shear rate. All albumin foam groups showed a general shear-thinning behavior, as demonstrated in Figure 4.2C and 4.2D. Such shear-thinning trend is similar to that of the previously developed gel-based support baths.(Kim, Banerjee, Celik, & Ozbolat, 2022 ; Ning et al., 2020) An increase in viscosity (i.e., shear-thickening) was observed when the applied shear stress was larger than 10 s^{-1}, which is attributed to the instability of the rheometer in high frequencies. Changing the foaming time did not have any noticeable effect on the general shear thinning behavior of the foam, while a lower concentration of albumin

resulted in a lower viscosity. Such observation is in accordance with the fact that low concentrations of albumin yield more dispersed molecules and thus less intermolecular interaction between solute, i.e., albumin, and solvent, i.e., cell culture media, molecules, which led to lower viscosity.(Yadav, Shire, & Kalonia, 2011) However, the foaming time, which does not change the content of the albumin solution, has minimal effect on the viscosity.

4.3.1.3 Recovery

An important property of support bath materials is their capability to recover the initial state when the needle passes through and deposits the filaments. Figure 4.2E and 4.2F shows the ability of the albumin support baths mechanically foamed for 2 and 4 minutes, to recover throughout cyclic deformation. Among the foam groups, albumin 8% mechanically foamed for 2 min showed the best cyclic recovery with only 31.0% ± 5.5% drop of storage modulus after several cycles, while other formulations showed more than 40% decrease in the storage modulus (Figure 4.2E). This observation is justified by the fact that using lower concentrations of albumin, results in higher liquid drainage of the foam.(Razi, Motamedzadegan, Shahidi, & Rashidinejad, 2019) The liquid drainage results in a drier foam which exhibits poor recovery. On the other hand, the abundance of entangled albumin chains in 12% albumin concentration resulted in a stiffer foam (as discussed in section 3.1.1), which is not capable of recovering its shape. As a result, there is an optimum albumin concentration that yields a support bath with acceptable recovery. Such rapid recovery to an initial state ensures that the extruded bioink is soundly embedded.(Lee et al., 2019) Similar to other support baths, a recovery of ~80% of the initial moduli is considered acceptable for embedded bioprinting.(Cooke & Rosenzweig, 2021)

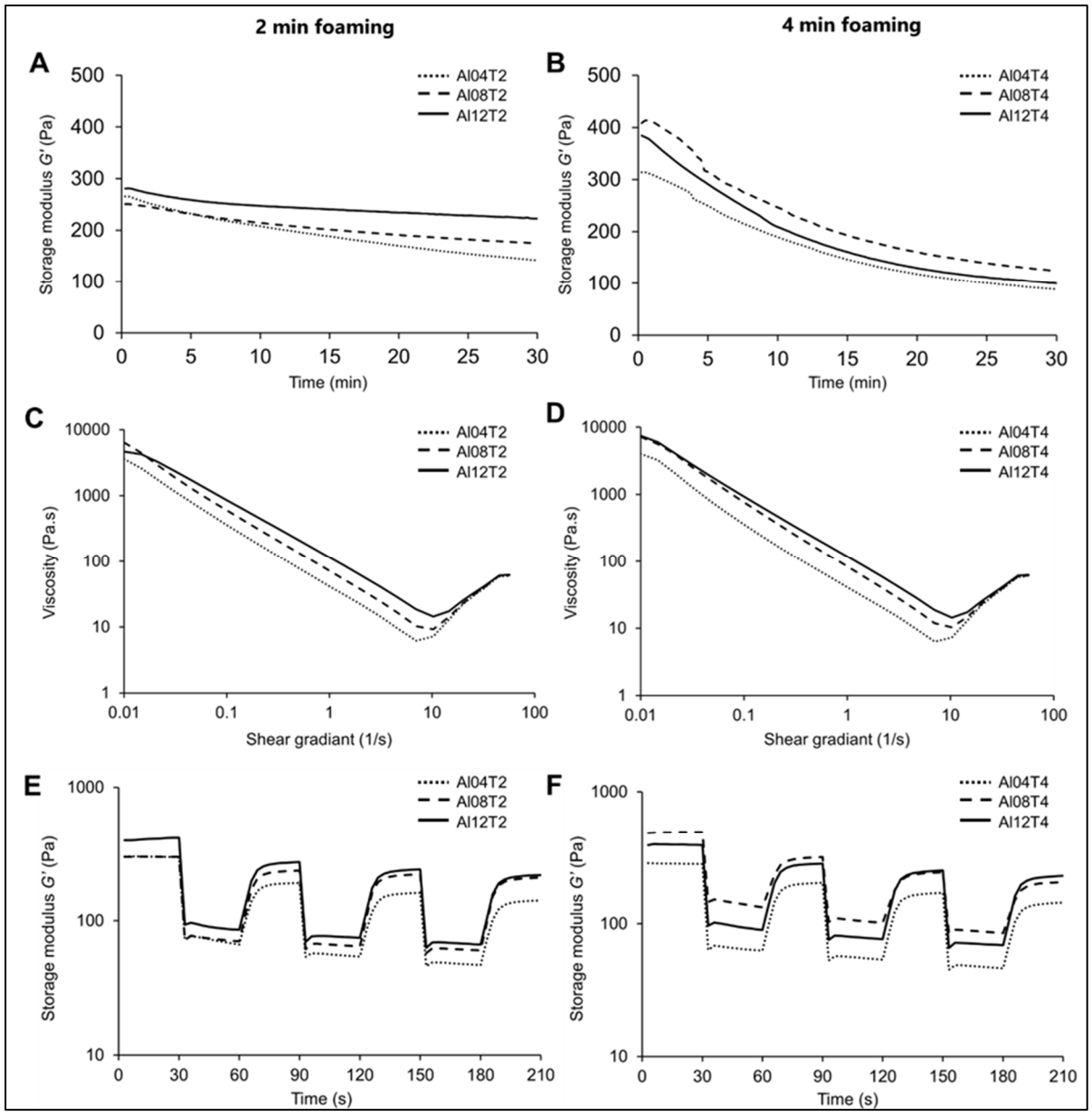

Figure 4.2 Rheological properties of albumin support baths (AlαTβ: α% w/v albumin foamed for β minutes): **A-B)** Evolution of the storage modulus (*G*') as a function of time at 37 °C; **C-D)** Shear-thinning behavior: viscosity as a function of shear rate; **E-F)** Recovery test: storage modulus of albumin support baths during various cycles of strain at 37 °C (30 seconds rest at 1% strain, 30 seconds under shear at 100% strain) (mean values of triplicates are plotted)

4.3.2 Bubbles size

As shown in supplementary video S1, the bubbles in the foam merge over time and gradually disappear as the phase separation between liquid and gas occurs. Figure 4.3A shows microscopic images of bubbles captured from various foams, and Figure 4.3B shows a histogram of the diameter of bubbles. The size distribution is similar for all foam compositions and foaming times where the majority of bubbles have a diameter of 50 to 150 μm. As shown in Figure 4.3C and 4.3D, the average bubble size increases over time until the large bubbles start bursting. Such behavior of the albumin foam addresses a persistent issue with bath removal in conventional embedded bioprinting methods. This feature gives the user the capability to bioprint delicate structures without jeopardizing the fidelity of the structure during crosslinking and bath removal.

4.3.3 Foam stability

The coalescence of bubbles after mechanical foaming results in the gradual phase separation within the foam. Albumin concentration and foaming time are the two main factors investigated in this study as they can influence the rate of phase separation. As shown in Figure 4.3E and 4.3F and supplementary video S2, the liquid phase of all the study groups gradually flowed downward over time. Although the groups with a lower concentration of albumin tend to be less stable, as mentioned in section 3.1.3, the difference is not statistically significant. It has been shown that the stability of the albumin foam is significantly related to the pH of the solution and additives such as polysaccharides can be used as stabilizers to enhance the albumin foam stability.(Miquelim, Lannes, & Mezzenga, 2010 ; X. Zhang et al., 2023) In the case of bioprinting large structures with several hours of printing time, stabilizers might be recommended to be added to the albumin solution to ensure the stability of the bath during the whole bioprinting procedure.

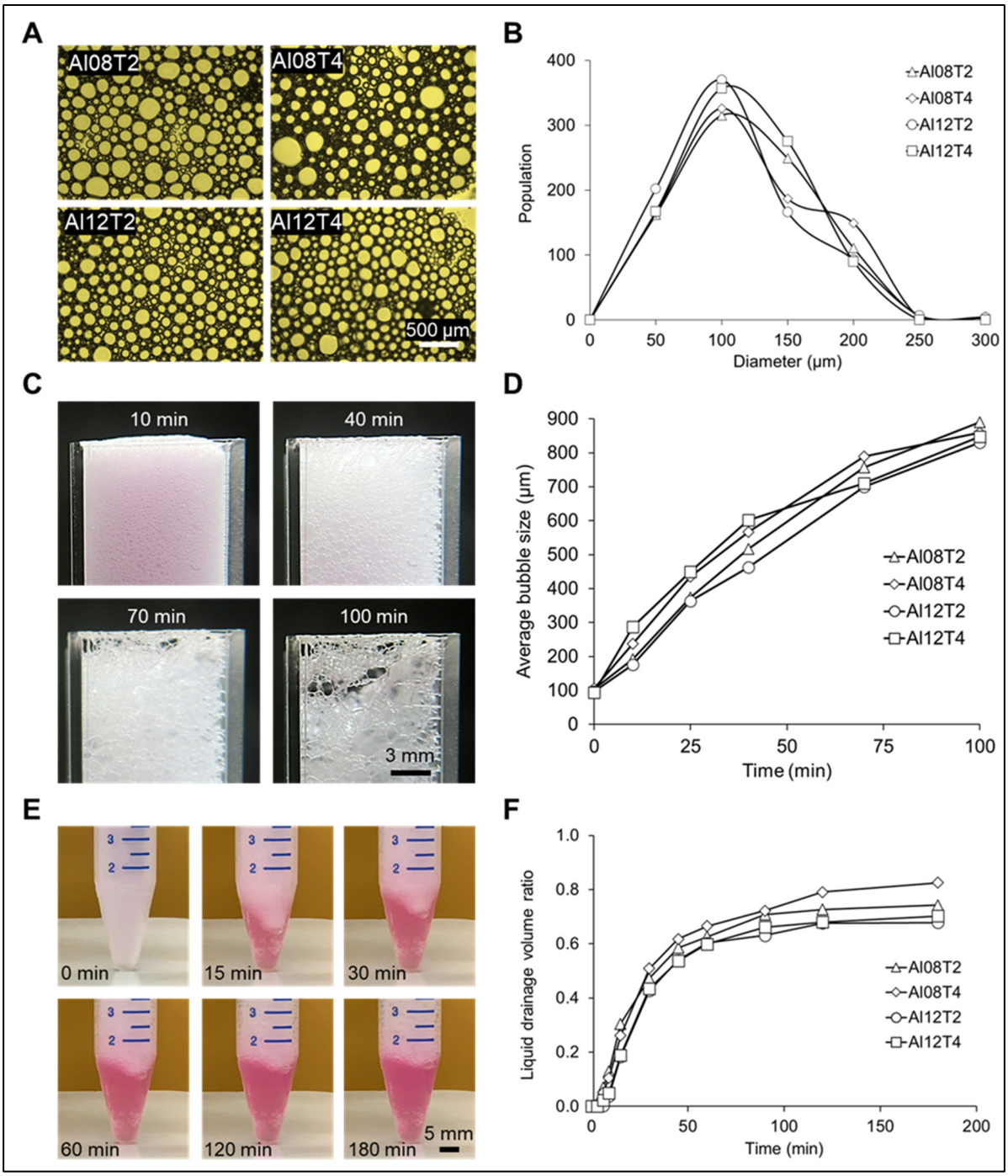

Figure 4.3 Physical characterization of albumin foam in cell culture media. **A)** Optical microscope images of bubbles immediately after preparing the foams. **B)** Size distribution of the bubbles. **C)** Images of bubbles merging over time in 8% albumin foam. **D)** Average bubble size for various albumin foams over time. **E)** Images of 8% albumin foam in a 15-ml

conical centrifuge tube while the phase separation between liquid and gas develops. **F)** Quantification of foam stability based on the liquid drainage volume ratio over time

4.3.4 Printability

The feasibility of the in-foam embedded printing process was examined by 3D printing several constructs made of slow-crosslinking chitosan or chitosan-collagen hydrogels. As shown in Figure 4.4A, the in-foam printing method was successfully used to fabricate various constructs from grid patterns to free-form conical structures (supplementary videos S3: 3D printing with RegenHU bioprinter and S4: 3D printing using BioX bioprinter). To highlight the importance of using foam as the support bath, we tried to print a grid structure without the foam (Figure 4.4B). This failed printing job indicated the essential role of support baths in printing chitosan and chitosan-collagen.

After bioprinting, the two phases of the foam separated over time, while the samples slowly gelled at 37 °C (Figure 4.4C). The coalescence of bubbles in the foam led to the gradual disappearance of the foam without jeopardizing the viability of embedded cells (supplementary video S5). Since the foam was intrinsically made of air bubbles, most of the remaining foam (if any) was readily removed using negative pressure (supplementary video S6). This convenient support bath removal is a paramount advantage of the in-foam printing method. Due to its negative electrical charge, traces of albumin could however be observed on the printed structures, making a rough surface on the positively charged chitosan samples. Such a rough surface could be beneficial to cell adhesion and growth on the samples.(Majhy, Priyadarshini, & Sen, 2021) However, albumin protein residues could also influence the biocompatibility of the printed structures, and will require, in the future, the use of human albumin instead of chicken egg white albumin. The presence of these albumin residues on the samples hindered the ability to accurately characterize the printability of the in-foam bioprinting samples with methods such as printability number.(Elias Madadian et al., 2023) However, the overall resolution of the printed samples, either with chitosan bioink or chitosan-

collagen bioink, was visually acceptable and comparable to the other embedded bioprinting methods.(Rahimnejad et al., 2022)

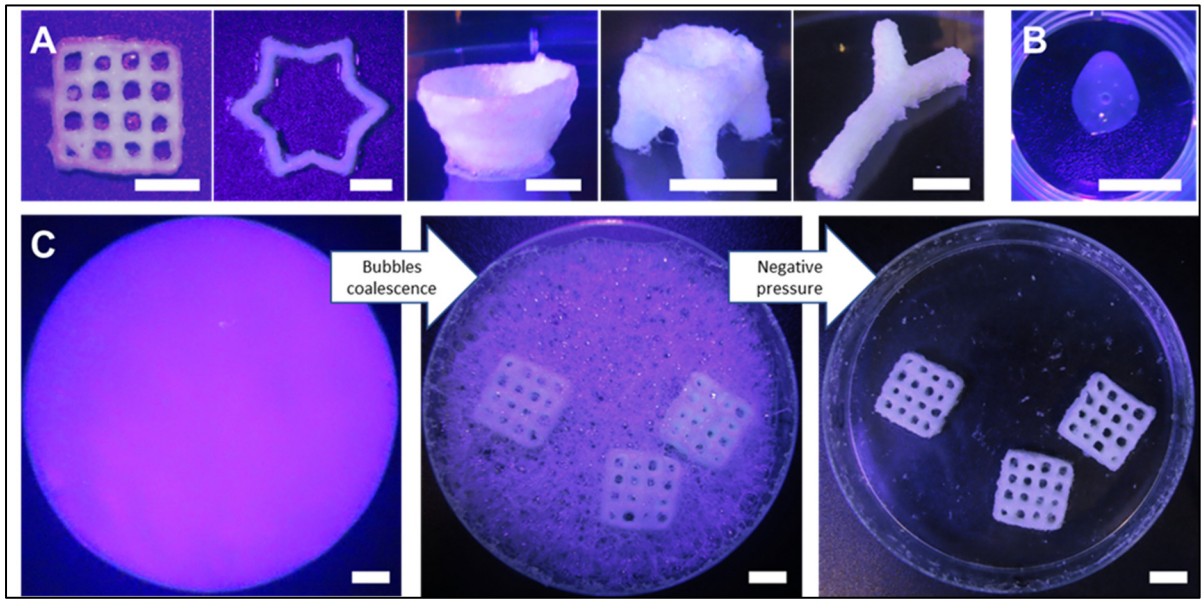

Figure 4.4 In-foam printability **A)** various chitosan structures fabricated in 8% albumin foam. **B)** A chitosan grid structure printed without foam. The print has failed due to poor shape fidelity. **C)** Pictures of samples in the foam right after printing, phase change of foam over time, and after removing the foam with the use of negative pressure. Scale bars are 1 cm

4.3.5 Cell Viability

Cell viability studies were first performed to understand how long the cells can stay viable in chitosan-collagen constructs when bioprinted in the nutrient-enriched foam bath. A delay between bioprinting and foam removal is needed to ensure the samples are well crosslinked before adding cell culture media, otherwise, the bioprinted constructs would collapse. Cell-laden grid constructs were bioprinted inside and outside of the 8% albumin foam, and the cell culture media was added at 30 min, 240 min, or 24 hours, after removing the excessive bath. For control groups, bioprinted out of the foam, PBS 1× was immediately added before adding media to avoid drying off. Figure 4.5A shows the live/dead fluorescent images of samples on day 1. As shown in Figure 4.5B, cell viability was significantly decreased for control samples when incubated for 240 min without media. As expected, the majority of cells died after 24

hours of starvation. It was observed that the cells in the control samples were more concentrated in the peripheral area of the hydrogel. The percentage of viable cells in the in-foam bioprinted samples was not significantly influenced by this delay, even when incubated for 24 hours in the foam without adding additional cell culture media. However, at the 24h timepoint, a significant percentage of the cells have left the structure and the size of the live cells significantly decreased, which can be a sign of initiation of apoptosis.(Friis et al., 2005) The observations of this study support our hypothesis on the advantages of a nutrient-enriched foam bath in keeping the cells viable during and after bioprinting for 24 hours. Also, when a foam support bath is used, the bioprinted cells have access to proper oxygenation throughout the structure, preventing hypoxia. The capability of keeping the cells viable for an extended time alludes to another advantage of the in-foam method when the bioprinting procedure takes several hours, especially when slow-crosslinking bioinks or large constructs such as full organs are bioprinted.(Mirdamadi, Tashman, Shiwarski, Palchesko, & Feinberg, 2020)

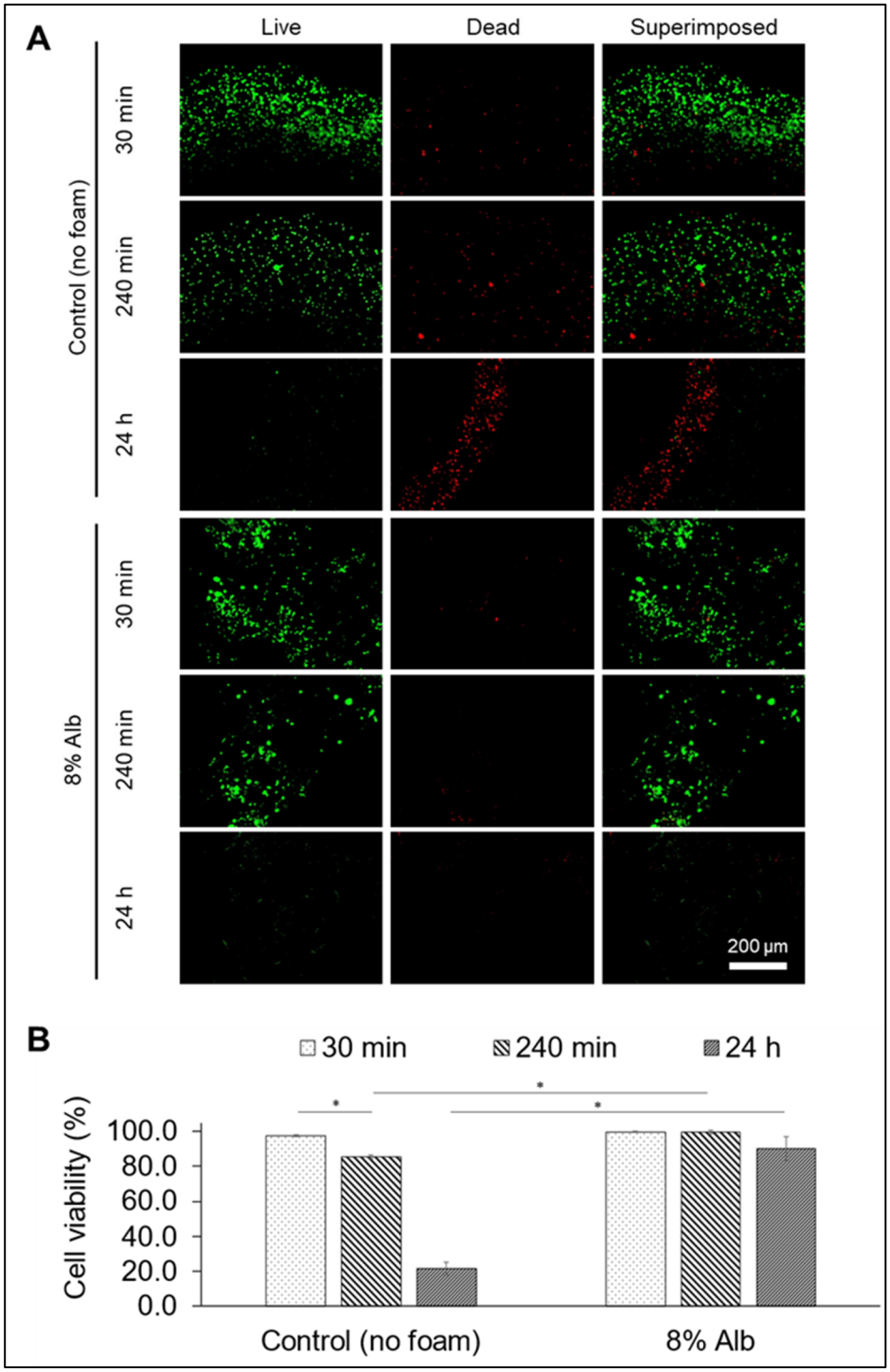

Figure 4.5 Effect of time before adding cell culture media (and removing the support foam) on the cell viability in bioprinted chitosan-collagen grid constructs, compared to control (without support

bath). **A)** Live/dead fluorescence images; **B)** Quantified cell viability values. (Alb: albumin, mean ± SD, n=3, *p < 0.05)

In the second step, 7-day period cell viability study was performed to evaluate the effect of albumin concentration (8% and 12% in completed DMEM) on the viability of cells embedded in chitosan-collagen structures. The foam was removed, and cell culture media was added 30 min after bioprinting. Two control groups bioprinted without foam were tested, where the cell culture media was added either immediately (positive control) or 30 min after bioprinting (negative control). Analyzing the live/dead fluorescent microscopy images on days 1, 4, and 7 (Figure 4.6) revealed that the in-foam bioprinted samples have significantly higher cell viability compared to the negative control group. We observed the concentration of albumin had minimal effect on cell viability. The cell viability rate for the positive control is not significantly different from that of the in-foam bioprinted group. However, adding media immediately after bioprinting, which was done for the positive control, is not always feasible for two reasons: i) many bioinks do not crosslink immediately, thus a wait time is needed before adding media, and ii) bioprinting large constructs can be time-consuming and adding media needs to be delayed until the whole construct is biofabricated. Moreover, a support bath is needed in many cases to get acceptable printing resolution, as exemplified here by the poor aspect of the control grid structure printed without foam (see Figure 4.4B). With this observation, we echo the biocompatibility of our in-foam bioprinting method and its potential in adding more flexibility and versatility to conventional bioprinting methods. The cell viability range for the in-foam bioprinting method is comparable to other embedded bioprinting methods. (Afghah, Altunbek, Dikyol, & Koc, 2020 ; Bao et al., 2020 ; Hinton et al., 2015)

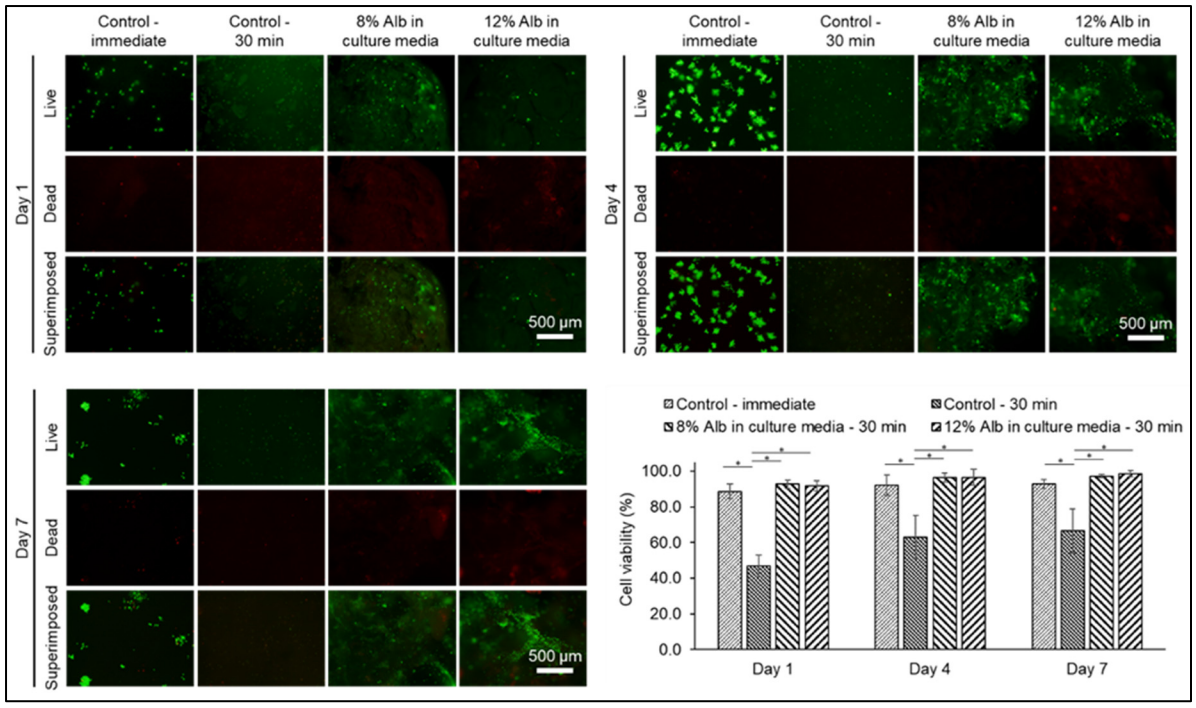

Figure 4.6 Live/dead fluorescence microscopy images and cell viability results for control and in-foam bioprinted samples for a 7-day cell culture. Using albumin foam as the support bath in bioprinting has significantly enhanced cell viability compared to the control - 30 min group. (Alb: albumin, mean ± SD, n=3, *p < 0.05)

4.4 Conclusion

In this study, In-foam bioprinting, a novel embedded bioprinting modality was propounded based on utilizing a non-liquid support bath, albumin foam. Our support bath offers a biocompatible environment with a number of distinct characteristics. Since the foam is intrinsically made of bubbles, the bioprinted cells are well-oxygenated during biofabrication and gelation time. The abundance of cell culture media and other nutrients in the foam holds promise for high cell viability. In addition, the foam bath can be gradually removed after bioprinting without the intervention of any external mechanisms that might compromise the shape fidelity of the printed structures. The in-foam bioprinting method is reliable and effective for bioprinting low-viscosity hydrogels with either a short or long gelation time without compromising cell viability. Additionally, using this method, large structures with a prolonged

printing time can be biofabricated. While our results demonstrate the feasibility and potential of the in-foam bioprinting approach, further studies are required to investigate the use of other foaming agents as the support bath or the addition of foam stabilizers to enhance the stability of the foam for embedded bioprinting. This bioprinting technique is suitable for the biofabrication of free-form constructs with applications in tissue engineering and precision medicine.

4.5 Experimental Section

4.5.1 Bioink preparation

Two bioinks were tested in this study, namely chitosan and chitosan-collagen physical hydrogels, the composition of which is presented in Table 4.1. Both bioinks form low-viscosity solutions at room temperature and crosslink when the temperature is raised to 37 °C. Chitosan bioink was prepared by mixing chitosan solution and a gelling agent following the previously-published protocol.(Assaad, Maire, & Lerouge, 2015) Briefly, shrimp shell chitosan powder (ChitoClear, HQG110, Primex, Siglufjordur, Iceland) with a molecular weight of 155 kDa and a degree of deacetylation of 83% was dissolved in hydrochloric acid (0.1 M, HCL-Fisher Scientific) using a mechanical mixer for 4 hours to achieve a homogenous chitosan solution. The solution was then autoclaved to ensure aseptic conditions for cell studies. The gelling agent used in this study was a mixture of β-glycerol phosphate (Sigma-Aldrich, Oakville, ON, Canada) and sodium hydrogen carbonate (MP Biomedicals, Solon, OH, USA) dissolved in Milli-Q water and sterilized by filtration. Since the chitosan gelation mechanism is affected by the basicity of the gelling agent, pH measurements were conducted immediately before mixing the components using a pH meter (LAQUAtwin, Horiba Advanced Techno, Kyoto, Japan). The pH of the gelling agent was adjusted to 8.0 via dropwise addition of HCl (0.1 M). Chitosan solution and the gelling agent were mixed using two syringes connected by a luer lock immediately before bioprinting. For preparing chitosan-collagen bioink, the gelling agent was first added to a collagen type I solution (Corning, Glendale, AZ), which was previously

dissolved in acetic acid, prior to its mixing with the chitosan solution. The final bioink was composed of 2% w/v chitosan and 1% w/v collagen as briefed in Table 4.1.

Table 4.1 Composition of chitosan and chitosan-collagen bioinks

	Chitosan (% w/v)	β-glycerol phosphate (M)	sodium hydrogen carbonate (M)	Collagen type I (% w/v)
Chitosan	2.0	0.1	0.075	-
Chitosan-collagen	2.0	0.1	0.075	1.0

4.5.2 Foam-based supporting bath preparation

Albumin solution was made by adding albumin powder from chicken egg white (A5253, Sigma-Aldrich, USA) in concentrations of 4%, 8%, and 12% w/v to either deionized (DI) water or Dulbecco's Modified Eagle Medium (DMEM) with fetal bovine serum (FBS, 10%) and then stirred at 600 rpm for 4 hours. The solution was then mechanically foamed using a hand-held mixer (TM-300HMCN, Toastmaster Hand Mixer) for 2 or 4 min to obtain a homogenous foam.

4.5.3 Rheology

Albumin solutions (4%, 8%, and 12% w/v) in DI water were mechanically foamed for 2 and 4 min. Rheological characterization of the albumin foams was carried out using an Anton Paar rheometer (Physica MCR 301, Germany) with concentric cylinder geometry (CC10/T200) and a 1 mm gap. Various tests, explained in the following sub-sections, were conducted to characterize the physical and rheological properties of the foams.

Time sweep: The storage modulus (G') and loss modulus (G'') of the foams with different concentrations (4%, 8%, and 12% w/v) and foaming time (2 and 4 min) were measured using

time sweep tests for 30 min at 37 ºC, using the oscillatory mode in the linear viscoelastic region (LVE), at a constant shear strain of 1% and constant frequency of 1 Hz to assess mechanical stability of the foam during the bioprinting process.
Recovery: Cyclic recovery tests at 37 ºC were performed to verify the self-recovery properties of the foams when the nozzle moves in the foam bath. The storage modulus of the foams was measured during various cycles mimicking the bioprinting process: (i) pre-printing (30 seconds at 1% strain), (ii) printing (sudden increase to 100% strain for 30 seconds), and (iii) post-printing (back to 1% strain).

Viscosity: The viscosity of the support bath at 37 ºC was assessed using rotational rheometry tests by altering the applied shear rate from 0.01 s^{-1} to 100 s^{-1} to verify the shear thinning behavior of the support foam. The graph was plotted in a logarithmic scale.

4.5.4 Bubble size

Albumin foams with the same concentrations and mechanically foaming times tested in the rheology section were prepared to characterize the air bubbles within the foams. However, due to the observed poor recovery of 4% albumin foam, this study group was not further characterized. A thin layer of foam samples was collected on a petri dish and observed with an optical microscope (AmScope, United Scope LLC, Irvine CA). Three images from random locations of the samples were taken using a high-resolution microscope camera (MU1803-HS, AmScope, United Scope LLC, Irvine CA). The diameter of 900 bubbles from each sample was measured using the AmScope image processing software (United Scope LLC, Irvine CA) to investigate the effect of albumin concentration and the mechanical foaming time on the initial bubble size.

The thin layer of the albumin foam used for measuring the initial bubble size could not be observed to study the coalescence of the bubbles over time since the samples dried off after some time. Therefore, bulks of foam samples were transferred to UV quartz cuvettes (Sigma-

Aldrich, Oakville, ON, Canada) using a syringe and imaged from the transparent side using the macro mode of a camera (SX740 HS, Canon, Tokyo, Japan). The samples were imaged every 10 seconds for a total time of 1.5 hours. Between 200 to 500 randomly selected bubbles were measured at certain time points using the AmScope software to investigate the trend of bubbles diameter change over time.

4.5.5 Foam stability

The stability of albumin foam groups (i.e., foams with different concentrations of albumin) was determined based on the rate of phase separation in the foam. For this purpose, the same study groups used in bubble size measurements were prepared and transferred to tubes(15-ml). The samples were placed on a hot plate at 37℃ and videoed for 3 hours. The level of precipitated liquid was measured at certain time points using the AmScope software to quantify the foam stability over time.

4.5.6 Cell culture

Mouse fibroblast L929 cells were cultured in a humidified incubator (37 ℃ and 5% CO_2) in DMEM supplemented with FBS (10% v/v) and penicillin/streptomycin (1% v/v). The cells were trypsinized (Trypsin 0.05%/ EDTA) and passed to a new flask at 80% confluency. The cell culture media was changed every 3 days to ensure sufficient and consistent nutrients are provided to the cells. For bioprinting, cell solution (100 µl) was prepared so that a final concentration of 5 million cells/ml was obtained in the bioink. The cell solution was added to the gelling agent syringe and encapsulated in the hydrogel during the two-syringe mixing procedure detailed previously.(Rahimnejad et al., 2022) The cell-laden bioink was then transferred to the bioprinter cartridge for biofabricating in-foam constructs.

4.5.7 Bioprinting setup

Bioprinting in albumin foam was performed using two different bioprinters: an extrusion-based 3Ddiscovery bioprinter (RegenHU, Villaz-St-Pierre, Switzerland) with a plunger printhead and a BioX bioprinter (Cellink, Gothenburg, Sweden) with a pneumatic printhead. Cell viability studies were conducted using the 3Ddiscovery bioprinter as it provides aseptic conditions, while printability experiments were performed using both 3Ddiscovery and BioX bioprinters to demonstrate the compatibility of the in-foam bioprinting method with different settings. For the plunger-based bioprinter, the feed rate and filament thickness were adjusted on 7 mm/s and 0.4 mm, respectively, to ensure decent printing resolution can be achieved. For the pneumatic bioprinter, the printing speed and the pressure were set at 12 mm/s and 8 kPa, respectively. The bioprinting process was conducted using a stainless steel 1-inch long 21G blunt needle (McMaster-Carr, Elmhurst, IL, USA). While the bioink cartridge was at room temperature during bioprinting, the foam was kept at 37 ℃ to accelerate chitosan gelation.(Rahimnejad, Labonté-Dupuis, Demarquette, & Lerouge, 2020) A sterilization process with ethanol and overnight ultra-violet (UV) exposure was followed to ensure the bioprinter and the experiment environment are in aseptic condition for cell studies. Immediately after printing, the in-foam bioprinted samples were transferred to a humidified incubator with 5% CO_2. After 24 hours, the samples were washed with phosphate-buffered saline (PBS) 1× and cell culture media was added. The media was changed every other day to ensure sufficient nutrient is accessible to the cells.

4.5.8 Cell viability

Live/dead assays were performed to determine the effect of two parameters on cell viability: i) incubation time before adding media, and ii) albumin concentration in the foam support bath. Firstly, the bioprinted samples (control and in-foam) were incubated for 30 min, 240 min, or 24 hours, then the cell culture media was added. It should be noted that the control samples were kept in PBS 1× before adding media to avoid drying off. At day 1 after bioprinting, the

samples were stained and imaged using a fluorescent microscope to assess the effect of delay in adding media on the cell viability. For studying the effect of albumin concentration, 1, 3, and 7 days after bioprinting, the cell culture media was washed off from the bioprinted samples using PBS 1×. Calcein, AM (Invitrogen, Life Technologies, Carlsbad, CA, USA) at a concentration of 2 μM and Ethidium Homodimer-1 (EthD-1, Invitrogen, Life Technologies, Carlsbad, CA, USA) at a concentration of 5.5 μM in DEMEM serum free were used as per the manufacturer's protocol to stain live and dead cells, respectively for 45 minutes. After staining, the samples were washed with PBS 1× and imaged using an inverted fluorescent contrast microscope (Leica DMIRB, Microscope Central, Feasterville, PA, USA). Three samples were prepared for each study group, and three images were captured at random locations of each sample. Subsequently, by normalizing green (live cells) and red (dead cells) channels using a grayscale filter, and proper thresholding of contrast and brightness levels the cell viability rate was calculated using ImageJ through measuring the projected area of red and green signals.(Badr et al., 2022) The cell viability percentage was calculated as

$$\text{Cell viability } \% = \left(\frac{\text{live cells}}{\text{live cells+dead cells}}\right) \times 100, \tag{4.1}$$

4.5.9 Statistical analysis

Analysis of variance (ANOVA) was used to implement the statistical analysis of data. In all tests, *p*-values lower than 0.05 were considered statistically significant. To compare every two groups of data, Tukey post hoc analysis was implemented. All the results were reported as mean values ± standard deviations, and all the tests were done in triplicate.

4.6 Supporting Information

Supporting Information is available from the Wiley Online Library or from the author.

4.7 Acknowledgments

E.M. and H.R. contributed equally to this work. E.M. and A.A. initiated and conceptualized the study. E.M. and H.R. performed the tests, designed the figures, and drafted the manuscript. F.T.K. contributed to performing cell viability experiments. M.R. designed the rheological experiments. S.L. and A.A. supervised the project. All the authors reviewed and commented on the manuscript. H.R. acknowledges the funding from the Fonds de Recherche du Québec Nature et technologies (FRQNT) Postdoctoral Fellowship (B3X-296447). This work was supported by the Natural Sciences and Engineering Research Council of Canada (NSERC) (I2IPJ-557094-20, and Discovery grants RGPIN-2017-05272 and RGPIN-2020-06684), Canada Foundation for innovation (John R. Evans Leader Fund 37696), and FRQNT (MR scholarship and team project 2024-PR-328371).

4.8 Conflict of Interest

The authors declare no conflict of interest.

4.9 Data Availability Statement

The data that support the findings of this study are available from the corresponding authors upon reasonable request.

CONCLUSION

The methods presented in this thesis have demonstrated the potential of using albumin in extrusion based bioprinting systems. The use of albumin/alginate foam crosslinked with $CaCl_2$ mist allowed direct 3D printing of highly porous structures. The application of the porous bioink was investigated for wound dressing applications; although, porous structures fabricated using this technique hold promise for additional applications, such as tissue engineering and controlled drug delivery. The successful implementation of albumin-based porous structures highlights the importance of biomaterial selection in achieving desired properties and functionalities for advanced biomedical applications.

Furthermore, the use of albumin as a support material in coaxial and embedded bioprinting showed significant potential. By employing albumin foam as a sacrificial material, hollow fibers were fabricated wherein the crosslinking agents were supplied to the bioink in the form of form. The proposed method showed excellent control over the wall thickness and the diameter of the fibers, while offering excellent biocompatibility. This innovative approach holds great promise for various applications, including tissue engineering and drug delivery systems.

The biocompatible and tunable properties of albumin foam make it an ideal candidate to be used as support material for embedded bioprinting. The successful implementation of a foam-based support bath containing cell culture media provided a supportive environment for the bioprinting process, providing oxygen and nutrient to the cells. As both oxygen and nutrients are essential for cell viability, this approach has eliminated the potentially detrimental effects observed with long printing times of previous techniques. The foam-based support bath also offered a convenient removing mechanism as the coalescence of the foam bubbles resulted in the disappearance of the foamed structure of the support bath.

LIST OF BIBLIOGRAPHICAL REFERENCES

Abdollahi, S., Davis, A., Miller, J. H., & Feinberg, A. W. (2018). Expert-guided optimization for 3D printing of soft and liquid materials. *PLOS ONE*, *13*(4), e0194890. https://doi.org/10.1371/JOURNAL.PONE.0194890

Abeyrathne, E. D. N. S., Lee, H. Y., & Ahn, D. U. (2013). Egg white proteins and their potential use in food processing or as nutraceutical and pharmaceutical agents—A review. *Poultry Science*, *92*(12), 3292-3299. https://doi.org/10.3382/PS.2013-03391

Adamu, B. F., Gao, J., Jhatial, A. K., & Kumelachew, D. M. (2021). A review of medicinal plant-based bioactive electrospun nano fibrous wound dressings. *Materials & Design*, *209*, 109942. https://doi.org/10.1016/J.MATDES.2021.109942

Adeli, H., Khorasani, M. T., & Parvazinia, M. (2019). Wound dressing based on electrospun PVA/chitosan/starch nanofibrous mats: Fabrication, antibacterial and cytocompatibility evaluation and in vitro healing assay. *International Journal of Biological Macromolecules*, *122*, 238-254. https://doi.org/10.1016/J.IJBIOMAC.2018.10.115

Afghah, F., Altunbek, M., Dikyol, C., & Koc, B. (2020). Preparation and characterization of nanoclay-hydrogel composite support-bath for bioprinting of complex structures. *Scientific Reports*, *10*(1), 1-13. https://doi.org/10.1038/s41598-020-61606-x

Ahmad, F., Mushtaq, B., Butt, F. A., Rasheed, A., & Ahmad, S. (2021). Preparation and characterization of wool fiber reinforced nonwoven alginate hydrogel for wound dressing. *Cellulose*, *28*(12), 7941-7951. https://doi.org/10.1007/s10570-021-04043-x

Ahmad Raus, R., Wan Nawawi, W. M. F., & Nasaruddin, R. R. (2021). Alginate and alginate composites for biomedical applications. *Asian Journal of Pharmaceutical Sciences*, *16*(3), 280-306. https://doi.org/10.1016/J.AJPS.2020.10.001

Ahmed, M. K., Moydeen, A. M., Ismail, A. M., El-Naggar, M. E., Menazea, A. A., & El-Newehy, M. H. (2021). Wound dressing properties of functionalized environmentally biopolymer loaded with selenium nanoparticles. *Journal of Molecular Structure*, *1225*, 129138. https://doi.org/10.1016/J.MOLSTRUC.2020.129138

Ahn, S., Lee, H., Bonassar, L. J., & Kim, G. (2012). Cells (MC3T3-E1)-laden alginate scaffolds fabricated by a modified solid-freeform fabrication process supplemented with an aerosol spraying. *Biomacromolecules*, *13*(9), 2997-3003. https://doi.org/10.1021/BM3011352

Andersen, T., Melvik, J. E., Gåserød, O., Alsberg, E., & Christensen, B. E. (2014). Ionically gelled alginate foams: Physical properties controlled by type, amount and source of gelling ions. *Carbohydrate Polymers*, *99*, 249-256. https://doi.org/10.1016/J.CARBPOL.2013.08.036

Ashammakhi, N., Ahadian, S., Xu, C., Montazerian, H., Ko, H., Nasiri, R., … Khademhosseini, A. (2019). Bioinks and bioprinting technologies to make heterogeneous and biomimetic tissue constructs. *Materials Today Bio*, *1*, 100008. https://doi.org/10.1016/J.MTBIO.2019.100008

Askari, M., Afzali Naniz, M., Kouhi, M., Saberi, A., Zolfagharian, A., & Bodaghi, M. (2021). Recent progress in extrusion 3D bioprinting of hydrogel biomaterials for tissue regeneration: a comprehensive review with focus on advanced fabrication techniques. *Biomaterials Science*, *9*(3), 535-573. https://doi.org/10.1039/D0BM00973C

Assaad, E., Maire, M., & Lerouge, S. (2015). Injectable thermosensitive chitosan hydrogels with controlled gelation kinetics and enhanced mechanical resistance. *Carbohydrate Polymers*, *130*, 87-96. https://doi.org/10.1016/J.CARBPOL.2015.04.063

Attia, J. A., Kholi, S., & Pilon, L. (2013). Scaling laws in steady-state aqueous foams including Ostwald ripening. *Colloids and Surfaces A: Physicochemical and Engineering Aspects*, *436*, 1000-1006. https://doi.org/10.1016/J.COLSURFA.2013.08.025

Avossa, J., Pota, G., Vitiello, G., Macagnano, A., Zanfardino, A., Di Napoli, M., … Luciani, G. (2021). Multifunctional mats by antimicrobial nanoparticles decoration for bioinspired smart wound dressing solutions. *Materials Science and Engineering: C*, *123*, 111954. https://doi.org/10.1016/J.MSEC.2021.111954

Badr, S., MacCallum, B., Madadian, E., Kerr, G., Naseri, E., MacDonald, D., … Ahmadi, A. (2022). Development of a mist-based printhead for droplet-based bioprinting of ionically crosslinking hydrogel bioinks. *Bioprinting*, *27*, e00207. https://doi.org/10.1016/J.BPRINT.2022.E00207

Bajpai, A. K., & Saini, R. (2006). Preparation and characterization of novel biocompatible cryogels of poly (vinyl alcohol) and egg-albumin and their water sorption study. *Journal of Materials Science: Materials in Medicine*, *17*(1), 49-61. https://doi.org/10.1007/S10856-006-6329-Z

Bao, G., Jiang, T., Ravanbakhsh, H., Reyes, A., Ma, Z., Strong, M., … Mongeau, L. (2020). Triggered micropore-forming bioprinting of porous viscoelastic hydrogels. *Materials Horizons*, *7*(9), 2336-2347. https://doi.org/10.1039/D0MH00813C

Barbetta, A., Barigelli, E., & Dentini, M. (2009). Porous alginate hydrogels: Synthetic methods for tailoring the porous texture. *Biomacromolecules*, *10*(8), 2328-2337. https://doi.org/10.1021/BM900517Q

Barceló, X., Eichholz, K. F., Garcia, O., & Kelly, D. J. (2022). Tuning the Degradation Rate of Alginate-Based Bioinks for Bioprinting Functional Cartilage Tissue. *Biomedicines*, *10*(7). https://doi.org/10.3390/BIOMEDICINES10071621

Bhattacharjee, T., Zehnder, S. M., Rowe, K. G., Jain, S., Nixon, R. M., Sawyer, W. G., & Angelini, T. E. (2015). Writing in the granular gel medium. *Science Advances*, *1*(8). https://doi.org/10.1126/SCIADV.1500655

Boi, S., Rouatbi, N., Dellacasa, E., di Lisa, D., Bianchini, P., Monticelli, O., & Pastorino, L. (2020). Alginate microbeads with internal microvoids for the sustained release of drugs. *International Journal of Biological Macromolecules*, *156*, 454-461. https://doi.org/10.1016/J.IJBIOMAC.2020.04.083

Bonatti, A. F., Chiesa, I., Vozzi, G., & de Maria, C. (2021). Open-source CAD-CAM simulator of the extrusion-based bioprinting process. *Bioprinting*, *24*, e00172. https://doi.org/10.1016/J.BPRINT.2021.E00172

Bryant, S. J., Nuttelman, C. R., & Anseth, K. S. (2012). Cytocompatibility of UV and visible light photoinitiating systems on cultured NIH/3T3 fibroblasts in vitro. *Journal of Biomaterials Science, Polymer Edition*, *11*(5), 439-457. https://doi.org/10.1163/156856200743805

Butler, H. M., Naseri, E., MacDonald, D. S., Andrew Tasker, R., & Ahmadi, A. (2020). Optimization of starch- and chitosan-based bio-inks for 3D bioprinting of scaffolds for neural cell growth. *Materialia*, *12*, 100737. https://doi.org/10.1016/J.MTLA.2020.100737

Cai, F.-F., Heid, S., Boccaccini, A. R., Aldo Boccaccini, C. R., & Y W O R D S Ada-, K. E. (2021). Potential of Laponite® incorporated oxidized alginate–gelatin (ADA-GEL) composite hydrogels for extrusion-based 3D printing. *Journal of Biomedical Materials Research Part B: Applied Biomaterials*, *109*(8), 1090-1104. https://doi.org/10.1002/JBM.B.34771

Çalışkan Koç, G., Tekgül, Y., Yüksel, A. N., Khanashyam, A. C., Kothakota, A., & Pandiselvam, R. (2022). Recent development in foam-mat drying process: Influence of foaming agents and foam properties on powder properties. *Journal of Surfactants and Detergents*, *25*(5), 539-557. https://doi.org/10.1002/JSDE.12608

Cam, C., Zhu, S., Truong, N. F., Scumpia, P. O., & Segura, T. (2015). Systematic evaluation of natural scaffolds in cutaneous wound healing. *Journal of Materials Chemistry B*, *3*(40), 7986-7992. https://doi.org/10.1039/C5TB00807G

Carmeliet, P., & Jain, R. K. (2000). Angiogenesis in cancer and other diseases. *Nature*, *407*(6801), 249-257. https://doi.org/10.1038/35025220

Caroline, C., Raya, B., Daniel, C., Benjamin, D., Christophe, T., Philippe, B., … Sophie, G. F. (2017). Elaboration and evaluation of alginate foam scaffolds for soft tissue engineering. *International Journal of Pharmaceutics*, *524*(1-2), 433-442. https://doi.org/10.1016/J.IJPHARM.2017.02.060

Chartier, C., Buwalda, S., Van Den Berghe, H., Nottelet, B., & Budtova, T. (2022). Tuning the properties of porous chitosan: Aerogels and cryogels. *International Journal of Biological Macromolecules*, *202*, 215-223. https://doi.org/10.1016/J.IJBIOMAC.2022.01.042

Chaturvedi, K., Ganguly, K., More, U. A., Reddy, K. R., Dugge, T., Naik, B., … Noolvi, M. N. (2019). Sodium alginate in drug delivery and biomedical areas. *Natural Polysaccharides in Drug Delivery and Biomedical Applications*, 59-100. https://doi.org/10.1016/B978-0-12-817055-7.00003-0

Choo, J. Q., Lau, D. P. C., Chui, C. K., Yang, T., Chng, C. B., & Teoh, S. H. (2010). Design of a mechanical larynx with agarose as a soft tissue substitute for vocal fold applications. *Journal of Biomechanical Engineering*, *132*(6). https://doi.org/10.1115/1.4001161

Cidonio, G., Cooke, M., Glinka, M., Dawson, J. I., Grover, L., & Oreffo, R. O. C. (2019). Printing bone in a gel: using nanocomposite bioink to print functionalised bone scaffolds. *Materials Today Bio*, *4*, 100028. https://doi.org/10.1016/J.MTBIO.2019.100028

Compaan, A. M., Song, K., & Huang, Y. (2019). Gellan Fluid Gel as a Versatile Support Bath Material for Fluid Extrusion Bioprinting. *ACS Applied Materials and Interfaces*. https://doi.org/10.1021/ACSAMI.8B13792

Cooke, M. E., & Rosenzweig, D. H. (2021). The rheology of direct and suspended extrusion bioprinting. *APL Bioengineering*, *5*(1). https://doi.org/10.1063/5.0031475

Cornock, R., Beirne, S., Thompson, B., & Wallace, G. G. (2014). Coaxial additive manufacture of biomaterial composite scaffolds for tissue engineering. *Biofabrication*, *6*(2), 025002. https://doi.org/10.1088/1758-5082/6/2/025002

Delkash, Y., Gouin, M., Rimbeault, T., Mohabatpour, F., Papagerakis, P., Maw, S., & Chen, X. (2021). Bioprinting and In Vitro Characterization of an Eggwhite-Based Cell-Laden

Patch for Endothelialized Tissue Engineering Applications. *Journal of Functional Biomaterials 2021, Vol. 12, Page 45*, *12*(3), 45. https://doi.org/10.3390/JFB12030045

Devillard, C. D., & Marquette, C. A. (2021). Vascular Tissue Engineering: Challenges and Requirements for an Ideal Large Scale Blood Vessel. *Frontiers in Bioengineering and Biotechnology*, *9*, 913. https://doi.org/10.3389/FBIOE.2021.721843

Dey, M., & Ozbolat, I. T. (2020). 3D bioprinting of cells, tissues and organs. *Scientific Reports 2020 10:1*, *10*(1), 1-3. https://doi.org/10.1038/s41598-020-70086-y

Di, J., Chen, H., Wang, X., Zhao, Y., Jiang, L., Yu, J., & Xu, R. (2008). Fabrication of zeolite hollow fibers by coaxial electrospinning. *Chemistry of Materials*, *20*(11), 3543-3545. https://doi.org/10.1021/CM8006809

Draget, K. I., & Taylor, C. (2011). Chemical, physical and biological properties of alginates and their biomedical implications. *Food Hydrocolloids*, *25*(2), 251-256. https://doi.org/10.1016/J.FOODHYD.2009.10.007

Duan, G., & Greiner, A. (2019). Air-Blowing-Assisted Coaxial Electrospinning toward High Productivity of Core/Sheath and Hollow Fibers. *Macromolecular Materials and Engineering*, *304*(5), 1800669. https://doi.org/10.1002/MAME.201800669

Duan, X., Li, M., Shao, J., Chen, H., Xu, X., Jin, Z., & Liu, X. (2018). Effect of oxidative modification on structural and foaming properties of egg white protein. *Food Hydrocolloids*, *75*, 223-228. https://doi.org/10.1016/J.FOODHYD.2017.08.008

Durán-Rey, D., Brito-Pereira, R., Ribeiro, C., Ribeiro, S., Sánchez-Margallo, J. A., Crisóstomo, V., … Sánchez-Margallo, F. M. (2022). Development of Silk Fibroin Scaffolds for Vascular Repair. *Biomacromolecules*. https://doi.org/10.1021/ACS.BIOMAC.2C01124

Fan, W., Zhang, Z., Liu, Y., Wang, J., Li, Z., & Wang, M. (2021). Shape memory polyacrylamide/gelatin hydrogel with controllable mechanical and drug release properties potential for wound dressing application. *Polymer*, *226*, 123786. https://doi.org/10.1016/J.POLYMER.2021.123786

Fazal, F., Raghav, S., Callanan, A., -, al, Pagan, E., Stefanek, E., … Barbetta, A. (2018). Co-axial wet-spinning in 3D bioprinting: state of the art and future perspective of microfluidic integration. *Biofabrication*, *11*(1), 012001. https://doi.org/10.1088/1758-5090/AAE605

Ferdinand P. Beer, John T. DeWolf, E. Russell Johnston, Jr., D. M. (2012). Mechanics of Materials. *McGraw-Hill Education*. Repéré à https://www.google.ca/books/edition/Mechanics_of_Materials/g635kQAACAAJ?hl=en

Friis, M. B., Friborg, C. R., Schneider, L., Nielsen, M. B., Lambert, I. H., Christensen, S. T., & Hoffman, E. K. (2005). Cell shrinkage as a signal to apoptosis in NIH 3T3 fibroblasts. *The Journal of Physiology*, *567*(Pt 2), 427. https://doi.org/10.1113/JPHYSIOL.2005.087130

Gao, G., Kim, H., Kim, B. S., Kong, J. S., Lee, J. Y., Park, B. W., … Cho, D. W. (2019). Tissue-engineering of vascular grafts containing endothelium and smooth-muscle using triple-coaxial cell printing. *Applied Physics Reviews*, *6*(4), 041402. https://doi.org/10.1063/1.5099306

Gao, G., Lee, J. H., Jang, J., Lee, D. H., Kong, J. S., Kim, B. S., … Cho, D. W. (2017). Tissue Engineered Bio-Blood-Vessels Constructed Using a Tissue-Specific Bioink and 3D Coaxial Cell Printing Technique: A Novel Therapy for Ischemic Disease. *Advanced Functional Materials*, *27*(33), 1700798. https://doi.org/10.1002/ADFM.201700798

Gao, Q., He, Y., Fu, J. zhong, Liu, A., & Ma, L. (2015). Coaxial nozzle-assisted 3D bioprinting with built-in microchannels for nutrients delivery. *Biomaterials*, *61*, 203-215. https://doi.org/10.1016/J.BIOMATERIALS.2015.05.031

Gao, Q., Liu, Z., Lin, Z., Qiu, J., Liu, Y., Liu, A., … He, Y. (2017). 3D Bioprinting of Vessel-like Structures with Multilevel Fluidic Channels. *ACS Biomaterials Science and Engineering*, *3*(3), 399-408. https://doi.org/10.1021/ACSBIOMATERIALS.6B00643

Gharbi, N., & Labbafi, M. (2019). Influence of treatment-induced modification of egg white proteins on foaming properties. *Food Hydrocolloids*, *90*, 72-81. https://doi.org/10.1016/J.FOODHYD.2018.11.060

Gonzalez-Fernandez, T., Tenorio, A. J., Campbell, K. T., Silva, E. A., & Leach, J. K. (2020). Evaluation of Alginate-Based Bioinks for 3D Bioprinting, Mesenchymal Stromal Cell Osteogenesis, and Application for Patient-Specific Bone Grafts. *bioRxiv*, 2020.08.09.242131. https://doi.org/10.1101/2020.08.09.242131

Gulfam, M., Jo, S. H., Vu, T. T., Ali, I., Rizwan, A., Joo, S. Bin, … Lim, K. T. (2023). NIR-degradable and biocompatible hydrogels derived from hyaluronic acid and coumarin for drug delivery and bio-imaging. *Carbohydrate Polymers*, *303*, 120457. https://doi.org/10.1016/J.CARBPOL.2022.120457

Haeri, M., & Haeri, M. (2015). ImageJ Plugin for Analysis of Porous Scaffolds used in Tissue Engineering. *Journal of Open Research Software*, *3*(1). https://doi.org/10.5334/JORS.BN

Haghbin, M., Sadeghi-Avalshahr, A., Hassanzadeh, H., Moloodi, A., & Harati, Z. (2023). Preparation of porous alginate-based smart dressings used in real-time monitoring of pH in chronic wounds by evaluating two fabrication routes: freeze-drying vs. electrospinning. *Journal of Porous Materials 2023*, 1-11. https://doi.org/10.1007/S10934-023-01477-5

Han, X., Meng, X., Wu, Z., Wu, Z., & Qi, X. (2018). Dynamic imine bond cross-linked self-healing thermosensitive hydrogels for sustained anticancer therapy via intratumoral injection. *Materials Science and Engineering: C*, *93*, 1064-1072. https://doi.org/10.1016/J.MSEC.2018.08.064

Hardy, Z., & Jideani, V. A. (2017). Foam-mat drying technology: A review. *Critical Reviews in Food Science and Nutrition*, *57*(12), 2560-2572. https://doi.org/10.1080/10408398.2015.1020359

Highley, C. B., Rodell, C. B., & Burdick, J. A. (2015). Direct 3D Printing of Shear-Thinning Hydrogels into Self-Healing Hydrogels. *Advanced Materials*, *27*(34), 5075-5079. https://doi.org/10.1002/ADMA.201501234

Hinton, T. J., Hudson, A., Pusch, K., Lee, A., & Feinberg, A. W. (2016). 3D Printing PDMS Elastomer in a Hydrophilic Support Bath via Freeform Reversible Embedding. *ACS Biomaterials Science and Engineering*, *2*(10), 1781-1786. https://doi.org/10.1021/ACSBIOMATERIALS.6B00170

Hinton, T. J., Jallerat, Q., Palchesko, R. N., Park, J. H., Grodzicki, M. S., Shue, H. J., … Feinberg, A. W. (2015). Three-dimensional printing of complex biological structures by freeform reversible embedding of suspended hydrogels. *Science Advances*, *1*(9). https://doi.org/10.1126/SCIADV.1500758

Hospodiuk, M., Dey, M., Sosnoski, D., & Ozbolat, I. T. (2017). The bioink: A comprehensive review on bioprintable materials. *Biotechnology Advances*, *35*(2), 217-239. https://doi.org/10.1016/J.BIOTECHADV.2016.12.006

Hu, C., Lu, W., Mata, A., Nishinari, K., & Fang, Y. (2021). Ions-induced gelation of alginate: Mechanisms and applications. *International Journal of Biological Macromolecules*, *177*, 578-588. https://doi.org/10.1016/J.IJBIOMAC.2021.02.086

Huang, Y., Cao, L., Parakhonskiy, B. v., & Skirtach, A. G. (2022). Hard, Soft, and Hard-and-Soft Drug Delivery Carriers Based on CaCO3 and Alginate Biomaterials: Synthesis, Properties, Pharmaceutical Applications. *Pharmaceutics 2022, Vol. 14, Page 909*, *14*(5), 909. https://doi.org/10.3390/PHARMACEUTICS14050909

Iijima, K., Ichikawa, S., Ishikawa, S., Matsukuma, D., Yataka, Y., Otsuka, H., & Hashizume, M. (2019). Preparation of Cell-Paved and -Incorporated Polysaccharide Hollow Fibers

Using a Microfluidic Device. *ACS Biomaterials Science and Engineering*, *5*(11), 5688-5697. https://doi.org/10.1021/ACSBIOMATERIALS.8B01500

Ilhan, E., Cesur, S., Guler, E., Topal, F., Albayrak, D., Guncu, M. M., … Gunduz, O. (2020). Development of Satureja cuneifolia-loaded sodium alginate/polyethylene glycol scaffolds produced by 3D-printing technology as a diabetic wound dressing material. *International Journal of Biological Macromolecules*, *161*, 1040-1054. https://doi.org/10.1016/J.IJBIOMAC.2020.06.086

Jadach, B., Świetlik, W., & Froelich, A. (2022). Sodium Alginate as a Pharmaceutical Excipient: Novel Applications of a Well-known Polymer. *Journal of Pharmaceutical Sciences*, *111*(5), 1250-1261. https://doi.org/10.1016/J.XPHS.2021.12.024

Janarthanan, G., Lee, S., & Noh, I. (2021). 3D Printing of Bioinspired Alginate-Albumin Based Instant Gel Ink with Electroconductivity and Its Expansion to Direct Four-Axis Printing of Hollow Porous Tubular Constructs without Supporting Materials. *Advanced Functional Materials*, *31*(45), 2104441. https://doi.org/10.1002/ADFM.202104441

Jang, J., Seol, Y. J., Kim, H. J., Kundu, J., Kim, S. W., & Cho, D. W. (2014). Effects of alginate hydrogel cross-linking density on mechanical and biological behaviors for tissue engineering. *Journal of the Mechanical Behavior of Biomedical Materials*, *37*, 69-77. https://doi.org/10.1016/J.JMBBM.2014.05.004

Jia, J., Richards, D. J., Pollard, S., Tan, Y., Rodriguez, J., Visconti, R. P., … Mei, Y. (2014). Engineering alginate as bioink for bioprinting. *Acta Biomaterialia*, *10*(10), 4323-4331. https://doi.org/10.1016/J.ACTBIO.2014.06.034

Jin, Y., Chai, W., & Huang, Y. (2017). Printability study of hydrogel solution extrusion in nanoclay yield-stress bath during printing-then-gelation biofabrication. *Materials Science and Engineering: C*, *80*, 313-325. https://doi.org/10.1016/J.MSEC.2017.05.144

Jirkovec, R., Samkova, A., Kalous, T., Chaloupek, J., & Chvojka, J. (2021). Preparation of a Hydrogel Nanofiber Wound Dressing. *Nanomaterials 2021, Vol. 11, Page 2178*, *11*(9), 2178. https://doi.org/10.3390/NANO11092178

Johnson, Z. I., Mahoney, C., Heo, J., Frankel, E., Julian, D. R., & Yates, C. C. (2019). The Role of Chemokines in Fibrotic Dermal Remodeling and Wound Healing, 3-24. https://doi.org/10.1007/978-3-319-98143-7_1

Jurak, M., Wiącek, A. E., Ładniak, A., Przykaza, K., & Szafran, K. (2021). What affects the biocompatibility of polymers? *Advances in Colloid and Interface Science*, *294*, 102451. https://doi.org/10.1016/J.CIS.2021.102451

Kar, S., Kaur, T., & Thirugnanam, A. (2016). Microwave-assisted synthesis of porous chitosan–modified montmorillonite–hydroxyapatite composite scaffolds. *International Journal of Biological Macromolecules*, *82*, 628-636. https://doi.org/10.1016/J.IJBIOMAC.2015.10.060

Karimi, M., Bahrami, S., Ravari, S. B., Zangabad, P. S., Mirshekari, H., Bozorgomid, M., … Hamblin, M. R. (2016). Albumin nanostructures as advanced drug delivery systems. *Expert Opinion on Drug Delivery*, *13*(11), 1609-1623. https://doi.org/10.1080/17425247.2016.1193149

Karimpoor, M., Yebra-Fernandez, E., Parhizkar, M., Orlu, M., Craig, D., Khorashad, J. S., & Edirisinghe, M. (2018). Alginate foam-based three-dimensional culture to investigate drug sensitivity in primary leukaemia cells. *Journal of The Royal Society Interface*, *15*(141). https://doi.org/10.1098/RSIF.2017.0928

Karvinen, J., & Kellomäki, M. (2023). Design aspects and characterization of hydrogel-based bioinks for extrusion-based bioprinting. *Bioprinting*, *32*, e00274. https://doi.org/10.1016/J.BPRINT.2023.E00274

Kim, M. H., Banerjee, D., Celik, N., & Ozbolat, I. T. (2022). Aspiration-assisted freeform bioprinting of mesenchymal stem cell spheroids within alginate microgels. *Biofabrication*, *14*(2), 024103. https://doi.org/10.1088/1758-5090/AC4DD8

Kjar, A., McFarland, B., Mecham, K., Harward, N., & Huang, Y. (2021). Engineering of tissue constructs using coaxial bioprinting. *Bioactive Materials*, *6*(2), 460-471. https://doi.org/10.1016/J.BIOACTMAT.2020.08.020

Kratz, F. (2014). A clinical update of using albumin as a drug vehicle — A commentary. *Journal of Controlled Release*, *190*, 331-336. https://doi.org/10.1016/J.JCONREL.2014.03.013

Kulkarni, R. V., Sreedhar, V., Mutalik, S., Setty, C. M., & Sa, B. (2010). Interpenetrating network hydrogel membranes of sodium alginate and poly(vinyl alcohol) for controlled release of prazosin hydrochloride through skin. *International Journal of Biological Macromolecules*, *47*(4), 520-527. https://doi.org/10.1016/J.IJBIOMAC.2010.07.009

Kumar, A., Wang, X., Nune, K. C., & Misra, R. D. K. (2017). Biodegradable hydrogel-based biomaterials with high absorbent properties for non-adherent wound dressing. *International Wound Journal*, *14*(6), 1076-1087. https://doi.org/10.1111/IWJ.12762

Kushibiki, T., Mayumi, Y., Nakayama, E., Azuma, R., Ojima, K., Horiguchi, A., & Ishihara, M. (2021). Photocrosslinked gelatin hydrogel improves wound healing and skin flap survival by the sustained release of basic fibroblast growth factor. *Scientific Reports 2021 11:1*, *11*(1), 1-12. https://doi.org/10.1038/s41598-021-02589-1

Łabowska, M. B., Cierluk, K., Jankowska, A. M., Kulbacka, J., Detyna, J., & Michalak, I. (2021). A Review on the Adaption of Alginate-Gelatin Hydrogels for 3D Cultures and Bioprinting. *Materials (Basel, Switzerland)*, *14*(4), 1-28. https://doi.org/10.3390/MA14040858

Lan, S. F., Kehinde, T., Zhang, X., Khajotia, S., Schmidtke, D. W., & Starly, B. (2013). Controlled release of metronidazole from composite poly-ε-caprolactone/alginate (PCL/alginate) rings for dental implants. *Dental Materials*, *29*(6), 656-665. https://doi.org/10.1016/J.DENTAL.2013.03.014

Lan, Z., Kar, R., Chwatko, M., Shoga, E., & Cosgriff-Hernandez, E. (2023). High porosity PEG-based hydrogel foams with self-tuning moisture balance as chronic wound dressings. *Journal of Biomedical Materials Research Part A*, *111*(4), 465-477. https://doi.org/10.1002/JBM.A.37498

Lee, A., Hudson, A. R., Shiwarski, D. J., Tashman, J. W., Hinton, T. J., Yerneni, S., … Feinberg, A. W. (2019). 3D bioprinting of collagen to rebuild components of the human heart. *Science*, *365*(6452), 482-487. https://doi.org/10.1126/SCIENCE.AAV9051

Li, Q., Jiang, Z., Ma, L., Yin, J., Gao, Z., Shen, L., … Zhou, H. (2022). A versatile embedding medium for freeform bioprinting with multi-crosslinking methods. *Biofabrication*, *14*(3), 035022. https://doi.org/10.1088/1758-5090/AC7909

Li, Y., Zhu, C., Fan, D., Fu, R., Ma, P., Duan, Z., … Li, Y. (2019). A Bi-Layer PVA/CMC/PEG Hydrogel with Gradually Changing Pore Sizes for Wound Dressing. *Macromolecular Bioscience*, *19*(5), 1800424. https://doi.org/10.1002/MABI.201800424

Lin, C. C., & Metters, A. T. (2006). Hydrogels in controlled release formulations: Network design and mathematical modeling. *Advanced Drug Delivery Reviews*, *58*(12-13), 1379-1408. https://doi.org/10.1016/J.ADDR.2006.09.004

Liu, C., Wang, Z., Wei, X., Chen, B., & Luo, Y. (2021). 3D printed hydrogel/PCL core/shell fiber scaffolds with NIR-triggered drug release for cancer therapy and wound healing. *Acta Biomaterialia*, *131*, 314-325. https://doi.org/10.1016/J.ACTBIO.2021.07.011

Liu, H., Wang, C., Li, C., Qin, Y., Wang, Z., Yang, F., … Wang, J. (2018, 16 février). A functional chitosan-based hydrogel as a wound dressing and drug delivery system in the

treatment of wound healing. *RSC Advances*. Royal Society of Chemistry. https://doi.org/10.1039/c7ra13510f

Liu, S., Zhang, H., Hu, Q., Shen, Z., Rana, D., & Ramalingam, M. (2020). Designing vascular supportive albumen-rich composite bioink for organ 3D printing. *Journal of the Mechanical Behavior of Biomedical Materials*, *104*, 103642. https://doi.org/10.1016/J.JMBBM.2020.103642

Liu, W., Zhong, Z., Hu, N., Zhou, Y., Maggio, L., Miri, A. K., … Zhang, Y. S. (2018). Coaxial extrusion bioprinting of 3D microfibrous constructs with cell-favorable gelatin methacryloyl microenvironments. *Biofabrication*, *10*(2), 024102. https://doi.org/10.1088/1758-5090/AA9D44

Liu, Y., Li, T., Han, Y., Li, F., & Liu, Y. (2021). Recent development of electrospun wound dressing. *Current Opinion in Biomedical Engineering*, *17*, 100247. https://doi.org/10.1016/J.COBME.2020.100247

Long, J., Etxeberria, A. E., Nand, A. V., Bunt, C. R., Ray, S., & Seyfoddin, A. (2019). A 3D printed chitosan-pectin hydrogel wound dressing for lidocaine hydrochloride delivery. *Materials Science and Engineering: C*, *104*, 109873. https://doi.org/10.1016/J.MSEC.2019.109873

Luo, Y., Chen, B., Zhang, X., Huang, S., & Wa, Q. (2022). 3D printed concentrated alginate/GelMA hollow-fibers-packed scaffolds with nano apatite coatings for bone tissue engineering. *International Journal of Biological Macromolecules*, *202*, 366-374. https://doi.org/10.1016/J.IJBIOMAC.2022.01.096

Luo, Y., Lode, A., & Gelinsky, M. (2013). Direct Plotting of Three-Dimensional Hollow Fiber Scaffolds Based on Concentrated Alginate Pastes for Tissue Engineering. *Advanced Healthcare Materials*, *2*(6), 777-783. https://doi.org/10.1002/ADHM.201200303

MacCallum, B., Naseri, E., Butler, H., MacNevin, W., Tasker, R. A., & Ahmadi, A. (2020). Development of a 3D bioprinting system using a Co-Flow of calcium chloride mist. *Bioprinting*, *20*, e00085. https://doi.org/10.1016/J.BPRINT.2020.E00085.

Madadian, E., Badr, S., MacDonald, D. S., Tasker, R. A., & Ahmadi, A. (2023). Development of foam-based support material for coaxial bioprinting of ionically crosslinking bioinks. *Bioprinting*, *32*, e00281. https://doi.org/10.1016/J.BPRINT.2023.E00281

Madadian, E, Naseri, E., Legault, R., & Ahmadi, A. (2023). Development of 3D-Printable Albumin–Alginate Foam for Wound Dressing Applications. *3D Printing and Additive Manufacturing*. https://doi.org/10.1089/3DP.2022.0241

Madduma-Bandarage, U. S. K., & Madihally, S. V. (2021). Synthetic hydrogels: Synthesis, novel trends, and applications. *Journal of Applied Polymer Science*, *138*(19), 50376. https://doi.org/10.1002/APP.50376

Majhy, B., Priyadarshini, P., & Sen, A. K. (2021). Effect of surface energy and roughness on cell adhesion and growth – facile surface modification for enhanced cell culture. *RSC Advances*, *11*(25), 15467. https://doi.org/10.1039/D1RA02402G

Miller, J. S., Stevens, K. R., Yang, M. T., Baker, B. M., Nguyen, D. H. T., Cohen, D. M., … Chen, C. S. (2012). Rapid casting of patterned vascular networks for perfusable engineered three-dimensional tissues. *Nature Materials 2012 11:9*, *11*(9), 768-774. https://doi.org/10.1038/nmat3357

Miquelim, J. N., Lannes, S. C. S., & Mezzenga, R. (2010). pH Influence on the stability of foams with protein–polysaccharide complexes at their interfaces. *Food Hydrocolloids*, *24*(4), 398-405. https://doi.org/10.1016/J.FOODHYD.2009.11.006

Mirdamadi, E., Tashman, J. W., Shiwarski, D. J., Palchesko, R. N., & Feinberg, A. W. (2020). FRESH 3D Bioprinting a Full-Size Model of the Human Heart. *ACS Biomaterials Science and Engineering*, *6*(11), 6453-6459. https://doi.org/10.1021/ACSBIOMATERIALS.0C01133

Mleko, S., Kristinsson, H. G., Liang, Y., & Gustaw, W. (2007). Rheological properties of foams generated from egg albumin after pH treatment. *LWT - Food Science and Technology*, *40*(5), 908-914. https://doi.org/10.1016/J.LWT.2006.04.007

Mndlovu, H., du Toit, L. C., Kumar, P., Marimuthu, T., Kondiah, P. P. D., Choonara, Y. E., & Pillay, V. (2019). Development of a fluid-absorptive alginate-chitosan bioplatform for potential application as a wound dressing. *Carbohydrate Polymers*, *222*, 114988. https://doi.org/10.1016/J.CARBPOL.2019.114988

Mohammadpour, Z., Kharaziha, M., & Zarrabi, A. (2023). 3D-Printing of Silk Nanofibrils Reinforced Alginate for Soft Tissue Engineering. *Pharmaceutics 2023, Vol. 15, Page 763*, *15*(3), 763. https://doi.org/10.3390/PHARMACEUTICS15030763

Mouro, C., Gomes, A. P., Ahonen, M., Fangueiro, R., & Gouveia, I. C. (2021). Chelidoniummajus L. Incorporated Emulsion Electrospun PCL/PVA_PEC Nanofibrous Meshes for Antibacterial Wound Dressing Applications. *Nanomaterials 2021, Vol. 11, Page 1785*, *11*(7), 1785. https://doi.org/10.3390/NANO11071785

Müller, M., Becher, J., Schnabelrauch, M., & Zenobi-Wong, M. (2015). Nanostructured Pluronic hydrogels as bioinks for 3D bioprinting. *Biofabrication*, *7*(3), 035006. https://doi.org/10.1088/1758-5090/7/3/035006

Murphy, S. V., & Atala, A. (2014). 3D bioprinting of tissues and organs. *Nature Biotechnology*, *32*(8), 773-785. https://doi.org/10.1038/nbt.2958

Naseri, E., Cartmell, C., Saab, M., Kerr, R. G., & Ahmadi, A. (2020). Development of 3D Printed Drug-Eluting Scaffolds for Preventing Piercing Infection. *Pharmaceutics*, *12*(9), 901. https://doi.org/10.3390/pharmaceutics12090901

Naseri, E., Cartmell, C., Saab, M., Kerr, R. G., & Ahmadi, A. (2021). Development of N,O-Carboxymethyl Chitosan-Starch Biomaterial Inks for 3D Printed Wound Dressing Applications. *Macromolecular Bioscience*, 2100368. https://doi.org/10.1002/MABI.202100368

Nguyen, T. P. T., Tran, B. M., & Lee, N. Y. (2018). Microfluidic approach for the fabrication of cell-laden hollow fibers for endothelial barrier research. *Journal of Materials Chemistry B*, *6*(38), 6057-6066. https://doi.org/10.1039/C8TB02031K

Ning, L., Mehta, R., Cao, C., Theus, A., Tomov, M., Zhu, N., … Serpooshan, V. (2020). Embedded 3D Bioprinting of Gelatin Methacryloyl-Based Constructs with Highly Tunable Structural Fidelity. *ACS Applied Materials and Interfaces*, *12*(40), 44563-44577. https://doi.org/10.1021/acsami.0c15078

Noor, N., Shapira, A., Edri, R., Gal, I., Wertheim, L., & Dvir, T. (2019). 3D Printing of Personalized Thick and Perfusable Cardiac Patches and Hearts. *Advanced Science*, *6*(11), 1900344. https://doi.org/10.1002/ADVS.201900344

Norotte, C., Marga, F. S., Niklason, L. E., & Forgacs, G. (2009). Scaffold-free vascular tissue engineering using bioprinting. *Biomaterials*, *30*(30), 5910-5917. https://doi.org/10.1016/J.BIOMATERIALS.2009.06.034

Oh, S. H., Park, I. K., Kim, J. M., & Lee, J. H. (2007). In vitro and in vivo characteristics of PCL scaffolds with pore size gradient fabricated by a centrifugation method. *Biomaterials*, *28*(9), 1664-1671. https://doi.org/10.1016/J.BIOMATERIALS.2006.11.024

Ouyang, L., Highley, C. B., Sun, W., & Burdick, J. A. (2017). A Generalizable Strategy for the 3D Bioprinting of Hydrogels from Nonviscous Photo-crosslinkable Inks. *Advanced Materials*, *29*(8), 1604983. https://doi.org/10.1002/ADMA.201604983

Ouyang, L., Yao, R., Zhao, Y., & Sun, W. (2016). Effect of bioink properties on printability and cell viability for 3D bioplotting of embryonic stem cells. *Biofabrication*, *8*(3). https://doi.org/10.1088/1758-5090/8/3/035020

Paxton, N., Smolan, W., Böck, T., Melchels, F., Groll, J., & Jungst, T. (2017). Proposal to assess printability of bioinks for extrusion-based bioprinting and evaluation of rheological properties governing bioprintability. *Biofabrication*, *9*(4), 044107. https://doi.org/10.1088/1758-5090/AA8DD8

Peng, Y., Ma, Y., Bao, Y., Liu, Z., Chen, L., Dai, F., & Li, Z. (2021). Electrospun PLGA/SF/artemisinin composite nanofibrous membranes for wound dressing. *International Journal of Biological Macromolecules*, *183*, 68-78. https://doi.org/10.1016/J.IJBIOMAC.2021.04.021

Poole, S. (1989). The foam-enhancing properties of basic biopolymers. *International Journal of Food Science & Technology*, *24*(2), 121-137. https://doi.org/10.1111/J.1365-2621.1989.TB00626.X

Powers, J. G., Higham, C., Broussard, K., & Phillips, T. J. (2016). Wound healing and treating wounds: Chronic wound care and management. *Journal of the American Academy of Dermatology*, *74*(4), 607-625. https://doi.org/10.1016/J.JAAD.2015.08.070

Probst, S., Saini, C., & Skinner, M. B. (2019). Comparison of sterile polyacrylate wound dressing with activated carbon cloth and a standard non-adhesive hydrocellular foam dressing with silver: a randomised controlled trial protocol. *Journal of Wound Care*, *28*(11), 722-728. https://doi.org/10.12968/JOWC.2019.28.11.722

Qu, F., Zhu, G., Huang, S., Li, S., Sun, J., Zhang, D., & Qiu, S. (2006). Controlled release of Captopril by regulating the pore size and morphology of ordered mesoporous silica. *Microporous and Mesoporous Materials*, *92*(1-3), 1-9. https://doi.org/10.1016/J.MICROMESO.2005.12.004

Raddatz, L., Lavrentieva, A., Pepelanova, I., Bahnemann, J., Geier, D., Becker, T., … Beutel, S. (2018). Development and Application of an Additively Manufactured Calcium Chloride Nebulizer for Alginate 3D-Bioprinting Purposes. *Journal of Functional Biomaterials 2018, Vol. 9, Page 63*, *9*(4), 63. https://doi.org/10.3390/JFB9040063

Rahimnejad, M., Adoungotchodo, A., Demarquette, N. R., & Lerouge, S. (2022). FRESH bioprinting of biodegradable chitosan thermosensitive hydrogels. *Bioprinting*, *27*, e00209. https://doi.org/10.1016/J.BPRINT.2022.E00209

Rahimnejad, M., Labonté-Dupuis, T., Demarquette, N. R., & Lerouge, S. (2020). A rheological approach to assess the printability of thermosensitive chitosan-based biomaterial inks. *Biomedical Materials*, *16*(1), 015003. https://doi.org/10.1088/1748-605X/ABB2D8

Ravanbakhsh, H., Bao, G., Luo, Z., Mongeau, L. G., & Zhang, Y. S. (2021). Composite Inks for Extrusion Printing of Biological and Biomedical Constructs. *ACS Biomaterials Science and Engineering*, *7*(9), 4009-4026. https://doi.org/10.1021/ACSBIOMATERIALS.0C01158

Ravanbakhsh, H., Karamzadeh, V., Bao, G., Mongeau, L., Juncker, D., & Zhang, Y. S. (2021). Emerging Technologies in Multi-Material Bioprinting. *Advanced Materials*, *33*(49), 2104730. https://doi.org/10.1002/ADMA.202104730

Razi, S. M., Motamedzadegan, A., Shahidi, S. A., & Rashidinejad, A. (2019). Physical and Rheological Properties of Egg Albumin Foams Are Affected by Ionic Strength and Basil Seed Gum Supplementation. *International Journal of Chemical Engineering*, *2019*. https://doi.org/10.1155/2019/2502908

Reddy, M. S. B., Ponnamma, D., Choudhary, R., & Sadasivuni, K. K. (2021). A comparative review of natural and synthetic biopolymer composite scaffolds. *Polymers*, *13*(7). https://doi.org/10.3390/POLYM13071105

Ribeiro, A., Blokzijl, M. M., Levato, R., Visser, C. W., Castilho, M., Hennink, W. E., … Malda, J. (2017). Assessing bioink shape fidelity to aid material development in 3D bioprinting. *Biofabrication*, *10*(1). https://doi.org/10.1088/1758-5090/AA90E2

Rocca, M., Fragasso, A., Liu, W., Heinrich, M. A., & Zhang, Y. S. (2018). Embedded Multimaterial Extrusion Bioprinting. *SLAS Technology*, *23*(2), 154-163. https://doi.org/10.1177/2472630317742071

Rui, K., Tang, X., Shen, Z., Jiang, C., Zhu, Q., Liu, S., … Yang, Y. (2023). Exosome inspired photo-triggered gelation hydrogel composite on modulating immune pathogenesis for treating rheumatoid arthritis. *Journal of nanobiotechnology*, *21*(1), 111. https://doi.org/10.1186/S12951-023-01865-8

Rusakov, D., Menner, A., Spieckermann, F., Wilhelm, H., & Bismarck, A. (2022). Morphology and properties of foamed high crystallinity PEEK prepared by high temperature thermally induced phase separation. *Journal of Applied Polymer Science*, *139*(1), 51423. https://doi.org/10.1002/APP.51423

Sachan, N., Pushkar, S., Jha, A., & Bhattcharya, A. (2015). Sodium alginate: the wonder polymer for controlled drug delivery. *Journal of Pharmacy Research*. 1191-1199.

Sarker, M., Izadifar, M., Schreyer, D., & Chen, X. (2018). Influence of ionic crosslinkers (Ca 2+ /Ba 2+ /Zn 2+) on the mechanical and biological properties of 3D Bioplotted Hydrogel Scaffolds. *Journal of Biomaterials science*, *29*(10), 1126-1154. https://doi.org/10.1080/09205063.2018.1433420

Schöneberg, J., de Lorenzi, F., Theek, B., Blaeser, A., Rommel, D., Kuehne, A. J. C., … Fischer, H. (2018). Engineering biofunctional in vitro vessel models using a multilayer bioprinting technique. *Scientific Reports 2018 8:1*, *8*(1), 1-13. https://doi.org/10.1038/s41598-018-28715-0

Schreml, S., Szeimies, R. M., Prantl, L., Karrer, S., Landthaler, M., & Babilas, P. (2010). Oxygen in acute and chronic wound healing. *British Journal of Dermatology*, *163*(2), 257-268. https://doi.org/10.1111/J.1365-2133.2010.09804.X

Serafin, A., Culebras, M., & Collins, M. N. (2023). Synthesis and evaluation of alginate, gelatin, and hyaluronic acid hybrid hydrogels for tissue engineering applications. *International Journal of Biological Macromolecules*, *233*, 123438. https://doi.org/10.1016/J.IJBIOMAC.2023.123438

Serro, A. P., Fernandes, A. I., Silva, D., Pinthong, T., Yooyod, M., Daengmankhong, J., … Ross, G. M. (2023). Development of Natural Active Agent-Containing Porous Hydrogel Sheets with High Water Content for Wound Dressings. *Gels 2023, Vol. 9, Page 459*, *9*(6), 459. https://doi.org/10.3390/GELS9060459

Shao, L., Gao, Q., Xie, C., Fu, J., Xiang, M., & He, Y. (2020). Directly coaxial 3D bioprinting of large-scale vascularized tissue constructs. *Biofabrication*, *12*(3), 035014. https://doi.org/10.1088/1758-5090/AB7E76

Shen, C., Zhang, G., Wang, Q., & Meng, Q. (2015). Fabrication of Collagen Gel Hollow Fibers by Covalent Cross-Linking for Construction of Bioengineering Renal Tubules. *ACS Applied Materials and Interfaces*, *7*(35), 19789-19797. https://doi.org/10.1021/ACSAMI.5B05809

Silva, A. K. A., Richard, C., Bessodes, M., Scherman, D., & Merten, O. W. (2009). Growth factor delivery approaches in hydrogels. *Biomacromolecules*, *10*(1), 9-18. https://doi.org/10.1021/bm801103c

Song, K. H., Highley, C. B., Rouff, A., & Burdick, J. A. (2018). Complex 3D-Printed Microchannels within Cell-Degradable Hydrogels. *Advanced Functional Materials*, *28*(31), 1801331. https://doi.org/10.1002/ADFM.201801331

Su, C., Li, Y., Cao, H., Lu, C., Li, Y., Chang, J., & Duan, F. (2019). Novel PTFE hollow fiber membrane fabricated by emulsion electrospinning and sintering for membrane

distillation. *Journal of Membrane Science*, *583*, 200-208. https://doi.org/10.1016/J.MEMSCI.2019.04.037

Sun, J., & Tan, H. (2013). Alginate-Based Biomaterials for Regenerative Medicine Applications. *Materials 2013, Vol. 6, Pages 1285-1309*, *6*(4), 1285-1309. https://doi.org/10.3390/MA6041285

Tabriz, A. G., Hermida, M. A., Leslie, N. R., & Shu, W. (2015). Three-dimensional bioprinting of complex cell laden alginate hydrogel structures. *Biofabrication*, *7*(4). https://doi.org/10.1088/1758-5090/7/4/045012

Tang, G., Luo, Z., Lian, L., Guo, J., Maharjan, S., Garciamendez-Mijares, C. E., … Zhang, Y. S. (2023). Liquid-embedded (bio)printing of alginate-free, standalone, ultrafine, and ultrathin-walled cannular structures. *Proceedings of the National Academy of Sciences of the United States of America*, *120*(7), e2206762120. https://doi.org/10.1073/PNAS.2206762120

Tang, Y., Lan, X., Liang, C., Zhong, Z., Xie, R., Zhou, Y., … Wang, W. (2019). Honey loaded alginate/PVA nanofibrous membrane as potential bioactive wound dressing. *Carbohydrate Polymers*, *219*, 113-120. https://doi.org/10.1016/J.CARBPOL.2019.05.004

Tanga, S., Aucamp, M., & Ramburrun, P. (2023). Injectable Thermoresponsive Hydrogels for Cancer Therapy: Challenges and Prospects. *Gels 2023, Vol. 9, Page 418*, *9*(5), 418. https://doi.org/10.3390/GELS9050418

Therriault, D., White, S. R., & Lewis, J. A. (2007). Rheological behavior of fugitive organic inks for direct-write assembly. *Applied Rheology*, *17*(1), 10112-1. https://doi.org/10.1515/ARH-2007-0001

Thomas, D., Nath, M. S., Mathew, N., R, R., Philip, E., & Latha, M. S. (2020). Alginate film modified with aloevera gel and cellulose nanocrystals for wound dressing application: Preparation, characterization and in vitro evaluation. *Journal of Drug Delivery Science and Technology*, *59*, 101894. https://doi.org/10.1016/J.JDDST.2020.101894

Tomasina, C., Bodet, T., Mota, C., Moroni, L., & Camarero-Espinosa, S. (2019). Bioprinting Vasculature: Materials, Cells and Emergent Techniques. *Materials*, *12*(17), 2701. https://doi.org/10.3390/MA12172701

Ullah, F., Othman, M. B. H., Javed, F., Ahmad, Z., & Akil, H. M. (2015). Classification, processing and application of hydrogels: A review. *Materials Science and Engineering: C*, *57*, 414-433. https://doi.org/10.1016/J.MSEC.2015.07.053

Unagolla, J. M., & Jayasuriya, A. C. (2020). Hydrogel-based 3D bioprinting: A comprehensive review on cell-laden hydrogels, bioink formulations, and future perspectives. *Applied Materials Today*, *18*, 100479. https://doi.org/10.1016/J.APMT.2019.100479

Vowden, K., & Vowden, P. (2017). Wound dressings: principles and practice. *Surgery (Oxford)*, *35*(9), 489-494. https://doi.org/10.1016/J.MPSUR.2017.06.005

Wahyudiono, Machmudah, S., Kanda, H., Okubayashi, S., & Goto, M. (2014). Formation of PVP hollow fibers by electrospinning in one-step process at sub and supercritical CO2. *Chemical Engineering and Processing: Process Intensification*, *77*, 1-6. https://doi.org/10.1016/J.CEP.2013.12.007

Wang, Z., Liu, C., Chen, B., & Luo, Y. (2021). Magnetically-driven drug and cell on demand release system using 3D printed alginate based hollow fiber scaffolds. *International Journal of Biological Macromolecules*, *168*, 38-45. https://doi.org/10.1016/J.IJBIOMAC.2020.12.023

Wen, Y., Yu, B., Zhu, Z., Yang, Z., & Shao, W. (2020). Synthesis of Antibacterial Gelatin/Sodium Alginate Sponges and Their Antibacterial Activity. *Polymers 2020, Vol. 12, Page 1926*, *12*(9), 1926. https://doi.org/10.3390/POLYM12091926

Weng, P., Liu, K., Yuan, M., Huang, G.-Q., Wu, K., Yang, X., … Yang, X. (2023). Development of a ZIF-91-Porous-Liquid-Based Composite Hydrogel Dressing System for Diabetic Wound Healing. *Small*, 2301012. https://doi.org/10.1002/SMLL.202301012

Wu, W., Deconinck, A., & Lewis, J. A. (2011). Omnidirectional Printing of 3D Microvascular Networks. *Advanced Materials*, *23*(24), H178-H183. https://doi.org/10.1002/ADMA.201004625

Wu, X., Black, L., Santacana-Laffitte, G., & Patrick, C. W. (2007). Preparation and assessment of glutaraldehyde-crosslinked collagen–chitosan hydrogels for adipose tissue engineering. *Journal of Biomedical Materials Research Part A*, *81A*(1), 59-65. https://doi.org/10.1002/JBM.A.31003

Xu, F., Dawson, C., Lamb, M., Mueller, E., Stefanek, E., Akbari, M., & Hoare, T. (2022). Hydrogels for Tissue Engineering: Addressing Key Design Needs Toward Clinical Translation. *Frontiers in Bioengineering and Biotechnology*, *10*, 696. https://doi.org/10.3389/FBIOE.2022.849831

Yadav, S., Shire, S. J., & Kalonia, D. S. (2011). Viscosity analysis of high concentration bovine serum albumin aqueous solutions. *Pharmaceutical Research*, *28*(8), 1973-1983. https://doi.org/10.1007/S11095-011-0424-7

Yang, Y., Liang, Y., Chen, J., Duan, X., & Guo, B. (2022). Mussel-inspired adhesive antioxidant antibacterial hemostatic composite hydrogel wound dressing via photo-polymerization for infected skin wound healing. *Bioactive Materials*, *8*, 341-354. https://doi.org/10.1016/J.BIOACTMAT.2021.06.014

Yeo, M. G., Lee, J. S., Chun, W., & Kim, G. H. (2016). An Innovative Collagen-Based Cell-Printing Method for Obtaining Human Adipose Stem Cell-Laden Structures Consisting of Core-Sheath Structures for Tissue Engineering. *Biomacromolecules*, *17*(4), 1365-1375. https://doi.org/10.1021/ACS.BIOMAC.5B01764

Ying, H., Zhou, J., Wang, M., Su, D., Ma, Q., Lv, G., & Chen, J. (2019). In situ formed collagen-hyaluronic acid hydrogel as biomimetic dressing for promoting spontaneous wound healing. *Materials Science and Engineering: C*, *101*, 487-498. https://doi.org/10.1016/J.MSEC.2019.03.093

Zhang, K., Feng, W., & Jin, C. (2020). Protocol efficiently measuring the swelling rate of hydrogels. *MethodsX*, *7*, 100779. https://doi.org/10.1016/J.MEX.2019.100779

Zhang, R., Hummelgrd, M., Lv, G., & Olin, H. (2011). Real time monitoring of the drug release of rhodamine B on graphene oxide. *Carbon*, *49*(4), 1126-1132. https://doi.org/10.1016/J.CARBON.2010.11.026

Zhang, X., Sun, Z., Zeng, Q., Jin, H., Wang, S., Jin, Y., … Cai, Z. (2023). Utilization of ovalbumin-propylene glycol alginate complex system for superior foam: The effect of pH-driven phase behavior. *Food Hydrocolloids*, *135*, 108169. https://doi.org/10.1016/J.FOODHYD.2022.108169

Zhang, Y. S., Haghiashtiani, G., Hübscher, T., Kelly, D. J., Lee, J. M., Lutolf, M., … Malda, J. (2021). 3D extrusion bioprinting. *Nature Reviews Methods Primers*, *1*(1), 1-20. https://doi.org/10.1038/s43586-021-00073-8

Zhou, K., Sun, Y., Yang, J., Mao, H., & Gu, Z. (2022). Hydrogels for 3D embedded bioprinting: a focused review on bioinks and support baths. *Journal of Materials Chemistry B*, *10*(12), 1897-1907. https://doi.org/10.1039/D1TB02554F